

P
2 miy

**NASA TECHNICAL
MEMORANDUM**

NASA TM X-62,281

NASA TM X-62,281

(NASA-TM-X-62281) AERODYNAMIC
CHARACTERISTICS OF A LARGE-SCALE MODEL
WITH A SWEEP WING AND A JET FLAP HAVING
AN EXPANDABLE DUCT (NASA) 96 p HC \$7.00

N74-11826

CSCL 01C G3/02
Unclas
22576

**AERODYNAMIC CHARACTERISTICS OF A LARGE-SCALE MODEL WITH A
SWEEP WING AND A JET FLAP HAVING AN EXPANDABLE DUCT**

Thomas N. Aiken, Kiyoshi Aoyagi, and Michael D. Falarski

Ames Research Center
and
U.S. Army Air Mobility R&D Laboratory
Moffett Field, Calif. 94035

September 1973

NOTATION

AR	wing aspect ratio, $\frac{b^2}{S}$
b	wing span, m (ft)
BLC	boundary layer control
c	chord (streamwise), m (ft)
\bar{c}	mean aerodynamic chord, m (ft)
$C_{D,CD}$	drag coefficient, $\frac{\text{drag}}{qS}$ (see data reduction section)
C_{D_R}	momentum drag coefficient due to engine inlet flow
C_{J_I}	total isentropic thrust coefficient, $C_{J_{JF}} + C_{\mu_{BLC_1}} + C_{\mu_{BLC_2}} + C_{\mu_a}$
$C_{J_{JF}}$	isentropic jet thrust coefficient of main blowing slot, $\frac{\text{isentropic thrust}}{qS}$
$C_{l,CR}$	rolling moment coefficient, $\frac{\text{rolling moment}}{qSb}$
$C_{L,CL}$	lift coefficient, $\frac{\text{lift}}{qS}$
$C_{m,CM}$	pitching moment coefficient, $\frac{\text{pitching moment}}{qS\bar{c}}$
$C_{n,CN}$	yawing moment coefficient, $\frac{\text{yawing moment}}{qSb}$
C_p	local pressure coefficient, $\frac{P-P_\infty}{q}$
C_T	tailpipe thrust coefficient, $\frac{\text{tailpipe thrust}}{qS}$
C_Y,CY	side force coefficient, $\frac{\text{side force}}{qS}$
C_{μ_a}	isentropic jet thrust coefficient of aileron, $\frac{\text{isentropic thrust}}{qS}$
$C_{\mu_{BLC_1}}$	isentropic jet thrust coefficient of flap BLC blowing slot, $\frac{\text{isentropic thrust}}{qS}$

$C_{\mu_{BLC_2}}$	isentropic jet thrust coefficient of aft BLC blowing slot, $\frac{\text{isentropic thrust}}{qS}$
h	blowing nozzle slot height, cm (in)
i_t	horizontal tail incidence, positive with trailing edge down, deg
m	mass rate of flow, Kg/sec (lbm/sec)
P	local pressure, N/sq m (lb/sq ft)
q	freestream dynamic pressure, N/sq m (lb/sq ft)
S	wing planform area, sq m (sq ft)
t	airfoil thickness, m (ft)
x	chordwise station, m (ft)
y	spanwise station, m (ft)
z	vertical distance from wing chord plane, m (ft)
α, AL	model angle of attack, deg
$\beta, BETA$	angle of sideslip of plane of symmetry, deg
δ_a	aileron deflection ($\delta_a = 30/0$ denotes left aileron at 30° , right aileron at 0°) positive with trailing edge down, deg
δ_c	control flap deflection ($\delta_c = 0/20$ denotes left control flap at 0° , right control flap at 20° ; control flaps are not deflected on ailerons) positive with trailing edge down, deg; see figure 2(d)
δ_f	flap deflection ($\delta_f = 60/30$ denotes inboard flap at 60° and outboard flap (no aileron) at 30° ; $\delta_f = 60$ denotes inboard flap at 60° and no outboard flap) positive with trailing edge down, deg
δ_s	slat deflection, positive with leading edge down, deg

n spanwise position, $\frac{2y}{b}$

Subscripts

a aileron
BLC₁ aft BLC blowing slot
BLC₂ flap BLC blowing slot
e elevator
f flap
JF main blowing slot
s slat
t horizontal tail
T total conditions
u uncorrected
vt vertical tail
1 original slat geometry (T-415)
2 modified slat geometry (T-418)
∞ freestream conditions

AERODYNAMIC CHARACTERISTICS OF A LARGE-SCALE MODEL
WITH A SWEEP WING AND A JET FLAP
HAVING AN EXPANDABLE DUCT

Thomas N. Aiken, Kiyoshi Aoyagi, and
Michael D. Falarski

Ames Research Center
and
U.S. Army Air Mobility R&D Laboratory
Moffett Field, Calif., 94035

SUMMARY

This report presents the data from an investigation of the aerodynamic characteristics of the expandable duct-jet flap concept. The investigation was made using a large-scale model in the Ames 40- by 80-foot Wind Tunnel.

The expandable duct-jet flap concept uses a lower surface, split flap and an upper surface, Fowler flap to form an internal, variable area cavity for the blowing air. Small amounts of blowing are used on the knee of the upper surface flap and the knee of a short-chord, trailing edge control flap. The bulk of the blowing is at the trailing edge. The flap could extend the full span of the model wing or over the inboard part only, with blown ailerons outboard.

Primary configurations tested were two flap angles, typical of takeoff and landing; symmetric control flap deflections, primarily for improved landing performance; and asymmetric aileron and control flap deflections, for lateral control. The tests were made with and without the horizontal tail at wind tunnel dynamic pressures from 1144 Newtons per square meter (23.9 pounds per square foot) to 158 Newtons per square meter (3.3 pounds per square foot). These correspond to Reynolds numbers from 5.35 million to 1.99 million, based on the wing mean aerodynamic chord. The range of jet thrust coefficients was 0 to 2.31.

INTRODUCTION

The expandable duct-jet flap concept is being studied as a means of attaining STOL performance in a turbofan powered aircraft. The concept is a derivative of a basic jet flap and has the principal jet located at the flap trailing edge.

The basic jet flap concept has been extensively considered as a propulsive high lift device on many types of aircraft. Integration of this concept into high wing-loading aircraft has been difficult because of the problem of providing sufficient duct area needed for high thrust from the wing jet. Additionally, it is difficult to achieve the proper values of lift to drag ratios needed for STOL descent without high flap deflections and subsequent flow separation and buffet problems.

The expandable duct-jet flap is an attempt to provide solutions to these problems while maintaining the inherent characteristics of the basic jet flap. It has a cavity formed by a lower surface of the expanding flap, the rear wing spar, and the upper surface of the flap system. The resulting cavity increases with flap deflection and is used for the ducting of compressor air to the blowing system. The blowing system primarily consists of the main jet near the flap trailing edge and a BLC slot at the knee of the flap. In addition, a short-chord, control flap is available at the trailing edge to provide additional deflection of the main jet. The control flap's purpose is to control the lift to drag ratio without adverse separation and buffet problems.

A large-scale model was built and tested in the Ames 40- by 80-foot Wind Tunnel to determine the aerodynamic characteristics of the expandable duct-jet flap concept. The wing planform of the model was geometrically similar to that of the augmentor wing model discussed in reference 1, 2 and 3. The flap system extended either the full span or 70 percent of the span with the remainder used as a blown aileron. The compressed air for the blowing nozzles was provided by the cold air from two turbofan engines mounted in the fuselage. Tests at forward speed, out of ground effect, were made for flap angles of 30° and 60° and various deflections of the control flap. The investigation also included the effects of a high-position horizontal tail, sideslip, and differential aileron and control flap deflection.

The tests were performed in cooperation with the Lockheed-Georgia Company and the Flight Dynamics Laboratory of the Department of the Air Force.

MODEL AND APPARATUS

Figures 1(a) through 1(e) show the model installed in the Ames 40- by 80-foot Wind Tunnel. The wing chord plane is in the approximate center of the test section.

Basic Model

Tables I and II give geometric data for the model. Sketches of the model are shown in figure 2. A three-view of the model and a typical wing section are shown in figures 2(a) and 2(b) respectively.

The wing was equipped with a full-span, leading edge slat. The slat position was modified midway through the investigation (see figure 2(c)). The flap system could be configured either as a full span flap or with the outboard 30 percent as a blown aileron.

The horizontal tail was equipped with a fixed, leading edge slat (see figure 2(d)). The elevator and rudder deflection were 0° throughout the test. When the horizontal tail was not installed, a rake having five directional probes was used in its place. A nose fairing was installed during

part of the test (see figure 2(a)). The model was equipped with sound suppressors on the engine inlet and the tailpipe exit.

Blowing System

Supply — The model was equipped with a separate blowing system for each wing. The blowing system is shown schematically in Figure 2(e). The compressed air was the cold or bypass air of two JT15D-1 turbofan engines.

The hot gas from the engine core exhausted out tailpipes in the rear of the fuselage. Tailpipe cooling air was brought into the fuselage through the inlet on the underside of the fuselage (see figure 2(a)) and ejected through an annular ejector at the tailpipe exit. The cold air was ducted to the wing blowing slots through the wing box spar.

Main jet — The blowing slot dimensions for the main jet and the BLC jets are shown in figure 3 while typical spanwise total pressure distributions for C_{J_1} 's less than and greater than 0.4 are given in figure 4. The main jet

slot dimensions are controlled by the movable segment on the trailing edge of the lower surface of the flap system (see figure 2(f)). The dimensions did not change with changes in control flap deflection. The overall dimensions did differ for 30° and 60° flap deflection (see figure 3). Where the outboard 30 percent of the flap system was used as a blown aileron, the main jet slot was blocked.

BLC jets — The flap BLC slot was located on the knee of the upper surface of the flap as shown in figure 2(f). The overall dimension differed for 30° and 60° flap deflections (see figure 3). The flap BLC slot was used for the blowing slot on the blown aileron. The aft BLC slot was located on the upper knee of the control flap as shown in figure 2(f). The dimensions were fixed as shown in figure 3. The aft BLC slot was blocked on the blown aileron.

Instrumentation

The instrumentation used to measure the flow conditions in the blowing system is shown schematically in figure 5. Surface static pressure orifices were located at three spanwise stations on the right wing ($\eta = .195, .467, .816$).

TESTS

Table III is an index to the investigation. The investigation was done in two phases (T-415 and T-418). The only change in configuration between the two phases was a change in the wing slat from position 1 to position 2. The tests were primarily done by increasing angle of attack at constant air-speed and duct pressure. The angle of attack range was -8° to 24°. Sideslip was varied from -18° to 4° at constant angle of attack. The wind tunnel dynamic

pressure range was from 1144 N/sq m (23.9 lb/sq ft) to 158 N/sq m (3.3 lb/sq ft) giving a Reynolds number range from 5.35 million to 1.99 million.

Two basic flap deflections were used; 30° representing a takeoff configuration; and 60° representing a landing configuration. The model was tested with both a full-span flap and with the outboard 30 percent span configured as a blown aileron and set at 30° or 10°. Several values of symmetric control flap deflection were tested for each flap configuration. Asymmetric control flap and aileron deflections were tested for lateral control. The range of the jet thrust coefficient, C_{J_I} , was from 0 to 2.31.

The division of C_{J_I} into its components; $C_{J_{JF}}$, $C_{\mu_{BLC}}$, $C_{\mu_{BLC_2}}$, C_{μ_a} is shown in figure 6 for the various configurations.

The horizontal tail was installed during part of the investigation and tested at several values of incidence. For two power-off runs, the nose fairing was installed and the model tested at two flap deflections; 0° and 60°.

DATA ACQUISITION AND REDUCTION

Data Acquisition

Six-component force data were obtained from the wind tunnel balance system. The moment center was located at the .35 \bar{c} point and .20 \bar{c} below the wing chord plane.

Total temperature and pressure within the duct were recorded for the locations shown in figure 5. The tailpipe mass flow and thrust were measured with a total pressure and temperature rake installed during a wind-off test prior to model assembly. These measurements were used to evaluate the tailpipe thrust and mass flow as functions of tailpipe total pressure and temperature which were recorded during the wind tunnel tests.

Other data obtained during the test included surface static pressures at three spanwise stations on the right wing ($\eta = .195, .467, .816$), directional probe measurements of the downwash at the horizontal tail location, and photographs of wing surface tufts.

Data Reduction

Blowing parameters — The thrusts for the three blowing slots on each wing were computed from the measured duct total pressures and temperatures and the measured areas for each slot. No correction was made for nozzle discharge or velocity efficiencies. Results of several wind-off tests indicated that the nozzle thrust coefficient (actual thrust/isentropic thrust) is approximately 0.85.

Force and moment data -- The forces and moments due to the inlet momentum drag and the tailpipe thrust have been subtracted from all force and moment data presented. The inlet momentum drag was computed using the calibrations of the tailpipe for the core mass flow and the computed, isentropic mass flow from the blowing slots for the fan flow. The forces are resolved with respect to the wind axes while the moments are resolved with respect to the stability axes. The corrections for inlet momentum drag and tailpipe thrust are as follows:

$$C_L = C_{L_u} - C_T \sin \alpha$$

$$C_{D_c} = C_{D_u} + C_T \cos \alpha - C_{D_R}$$

$$C_{m_c} = C_{m_u} - .134 C_T + C_{D_R} (.347 \cos \alpha - 2.816 \sin \alpha)$$

$$C_y = C_{y_u}$$

$$C_n = C_{n_u}$$

$$C_i = C_{i_u}$$

where C_{L_u} , C_{D_u} , C_{m_u} , C_{y_u} , C_{n_u} , C_{i_u} are based on measured forces and moments and α is the corrected angle of attack.

Wind tunnel wall corrections -- All of the data presented have been corrected for wind tunnel wall constraints. Conventional corrections are used, but the lift coefficient is replaced by the effective circulation lift coefficient, $C_{L_{aero}}$, defined as:

$$C_{L_{aero}} = C_L - \left(C_{J_{JF}} + C_{\mu_{BLC_1}} + C_{\mu_{BLC_2}} \right) \sin (\Delta f + \alpha)$$

(full-span flap)

$$C_{L_{aero}} = C_L - \left(C_{J_{JF}} + C_{\mu_{BLC_1}} + C_{\mu_{BLC_2}} + C_{\mu_a} \right) \sin (\Delta f + \alpha)$$

(part-span flap plus aileron)

where Δf is a jet angle determined from wind-off tests.

The wind tunnel wall corrections are, therefore:

$$\alpha = \alpha_u + .453 C_{L_{aero}}$$

$$C_D = C_{D_C} + .00793 C_{L_{aero}}^2$$

and with the horizontal tail on,

$$C_m = C_{m_c} + .0326 C_{L_{aero}}$$

DATA PRESENTATION

The data are presented in figures 7 to 24. Table IV is an index to the data figures. The jet coefficients and dynamic pressures listed are nominal values.

REFERENCES

1. Falarski, M. D.; Koenig, D. G.: Aerodynamic Characteristics of a Large-Scale Model with a Swept Wing and Augmented Jet Flap. NASA TM X-62,029, July, 1971.
2. Falarski, M. D.; Koenig, D. G.: Longitudinal and Lateral Stability and Control Characteristics of a Large-Scale Model with a Swept Wing and Augmented Jet Flap. NASA TM X-62,145, April, 1972.
3. Falarski, M. D.; Koenig, D. G.: Longitudinal Aerodynamic Characteristics of a Large-Scale Model with a Swept Wing and Augmented Jet-Flap in Ground Effect. NASA TM X-62,174, October, 1972.

TABLE I. — MODEL REFERENCE DIMENSIONS

Wing

Area, sq m (sq ft)		21.37 (230.0)
Aspect ratio		8.00
Taper ratio		0.30
Span, m (ft)		13.080 (42.895)
Root chord, m (ft)		2.510 (8.250)
Tip chord, m (ft)		.750 (2.475)
Mean aerodynamic chord, m (ft)		1.790 (5.881)
Sweep at 1/4 chord, deg		27.5
Airfoil section (see Table II)	NACA	65A - 4 XX
	root t/c =	.125
	tip t/c =	.105
Incidence, twist		0

Vertical Tail

Area, sq m (sq ft)		6.32 (68.0)
Aspect ratio		1.20
Taper ratio		.74
Span, m (ft)		2.760 (9.04)
Root chord, m (ft)		2.630 (8.65)
Tip chord, m (ft)		1.950 (6.40)
Mean aerodynamic chord, m (ft)		2.310 (7.58)
Sweep at 1/4 chord, deg		38.5
Airfoil section	NACA	0012
Volume coefficient		.114

Horizontal Tail

Area, sq m (sq ft)		6.72 (72.3)
Aspect ratio		4.00
Taper ratio		.49
Span, m (ft)		2.590 (8.50)
Root chord, m (ft)		1.740 (5.71)
Tip chord, m (ft)		.850 (2.80)
Mean aerodynamic chord, m (ft)		1.350 (4.42)
Sweep at 1/4 chord, deg		25
Airfoil section (inverted)	NACA	64-012
Volume coefficient		1.038

TABLE II. - WING AIRFOIL COORDINATES, $\eta = .1945$

<u>Basic Airfoil</u> x/c (100)	Z upper/c	Z lower/c
0	0	0
.0625	.0054	-.0023
.125	.0071	-.0033
.25	.0093	-.0048
.375	.0109	-.0059
.50	.0123	-.0069
.625	.0134	-.0077
.75	.0146	-.0085
1.0	.0166	-.0099
1.25	.0184	-.0110
1.50	.0200	-.0120
1.75	.0215	-.0129
2.00	.0228	-.0137
2.50	.0253	-.0150
5.00	.0350	-.0192
7.50	.0432	-.0224
10.00	.0501	-.0252
15.00	.0613	-.0293
20.00	.0700	-.0322
25.00	.0767	-.0343
30.00	.0817	-.0356
35.00	.0853	-.0362
36.25	.0859	-.0363
40.00	.0873	-.0361
45.00	.0878	-.0353
50.00	.0866	-.0334
55.00	.0836	-.0305
57.50	.0815	-.0288
60.00	.0791	-.0269
65.00	.0732	-.0227
69.50	.0667	-.0188
69.831	.0662	-.0185
70.00	.0660	-.0183
75.00	.0576	-.0139
80.00	.0478	-.0099
85.00	.0365	-.0070
90.00	.0246	-.0046
92.50	.0185	-.0035
95.00	.0125	-.0024
97.00	.0076	-.0016
98.00	.0052	-.0012
99.00	.0027	-.0007
100.00	.0003	-.0003

TABLE II. — CONCLUDED

Slat Inner Surface

x/c (100)	Z upper/c	Z lower/c
2.50	-.0030	-.0030
2.625	.0028	.0088
2.75	.0052	.0110
3.00	.0086	.0137
3.25	.0112	.0154
3.50	.0134	.0165
3.75	.0154	.0173
4.00	.0172	.0178
4.25	.0189	.0182
4.50	.0204	.0185
4.75	.0219	
5.00	.0233	
5.50	.0260	
6.00	.0285	
6.50	.0308	
7.00	.0330	
7.50	.0352	
8.00	.0373	
9.00	.0412	
10.00	.0450	
11.00	.0487	
12.00	.0522	
13.00	.0556	
14.00	.0590	

Flap Upper Contour

x/c (100)	Z upper/c
58.347	-.0201
58.50	-.0148
58.75	-.0083
59.00	-.0028
60.00	.0139
61.00	.0262
62.00	.0358
63.00	.0435
64.00	.0497
65.00	.0546
66.00	.0585
67.00	.0613
68.00	.0633
69.00	.0644
70.00	.0647
71.00	.0641
71.50	.0635
72.00	.0627

TABLE III. - CONTINUED

T-415

Run	TUNNEL			BLOWING		WING				TAIL				REMARKS	FIGURE
	η psf	α deg	β deg	C_f		δ_t deg	δ_s deg	δ_a deg	δ_c deg	i_t deg	δ_{st} deg	δ_e deg	δ_r deg		
41	13.4	~	0	.58		60	60	30	50	OFF	—	0		POLARS	8g
42	9.9			0											8g
43	4.5			1.73					0						—
44	0	0		—		30								STATIC CALIBRATION	—
45	4.9	~		1.50										POLARS	15a
46	7.5			1.00											15a
47	9.9			.77											15a
48	14.7			.51											15a
49	18.4			.24											15a
50	9.7			0											15a
51	4.9			1.52					30						15c
52	7.4			1.00											15c
53	14.6			.51											15c
54	9.9			0											15c
55	0	0		—										STATIC CALIBRATION	—
56	5.0	~		1.45					50					POLARS	15d
57	7.5			.97											15d
58	14.7			.50											15d
59	10.0			0											15d
60	0	0		—		30/30		—	0					STATIC CALIBRATION	—

TABLE III. - CONTINUED

T-418

Run	TUNNEL			BLOWING	WING				TAIL				REMARKS	FIGURE
	η pst	α deg	β deg	C_T	δ_f deg	δ_s deg	δ_a deg	δ_c deg	δ_e deg	δ_{st} deg	δ_o deg	δ_r deg		
1	0	0	0	-	60/30	60	-	0	off	-	-	0	STATIC CALIBRATION	-
2	3.3	~		.731									BASIC POLARS, LANDING, δ_f	7d
3	4.9			.57										7d
4	6.7			.115										7d
5	10.0			.77										7d
6	0	0		-									NOISE	-
7	0			-	60		30						STATIC CALIBRATION	-
8	4.8	~		.155									POLARS	8b, 20a
9	7.2			.104										8b, 20a
10	14.5			.51										8b, 20a
11	14.5		18	.51									DISTORTION CHECK	-
12	7.2		0	.102				40					POLARS, SYM. δ_c	8f
13	14.7			.51										8f
14	7.3			.104				10						8c
15	14.5			.52										8c
16	7.3			.105				0/40					POLARS, ASYM. δ_c	12b, 20d
17	14.6			.53										12b, 20d
18	7.3			.105				0/20						12a, 20c
19	14.5			.53										12a, 20c
20	9.6			.87				0					POLARS, TWICE CYCLE NORMAL	11

TABLE III. - CONTINUED

T-418

No	TUNNEL			BLOWING	WING				TAIL				REMARKS	FIGURE	
	η psf	α deg	β deg	C_D	δ_f deg	δ_s deg	δ_a deg	δ_c deg	i_t deg	δ_{st} deg	δ_e deg	δ_r deg			
41	5.0	~	0	1.50	30	60	30	0/20	OFF	—	—	0	POLARS, ASYM. δ_c	17b	23c
42	7.4			1.02										17b	23c
43	14.5			.52										17b	23c
44	4.8			1.59				0/40						17c	23d
45	7.2			1.06										17c	23d
46	7.3			1.02				0	0	40	0		BASIC POLARS, TAIL ON	16b	
47	7.3			1.03					-5					16b	
48	7.3			1.03					-15					16a,b	
49	4.9			1.53										16a	
50	14.5			.52										16a	
51	9.6			0										16a	
52	4.9	4	~	1.52									BASIC YAWLERS	24a	
53	7.3			1.02										24a	
54	7.3	12		1.02										24b	
55	14.6			.51										24b	
56	14.6	4		.51										24c	
57	4.9	12		1.52										24b	
58	9.6			0										24b	
59	9.6	4		0										24a	
60	7.1	~	0	1.04	60								BASIC POLARS, TAIL ON	—	

TABLE III. - CONCLUDED

T-418

Run	TUNNEL			BROWING		WING				TAIL				REMARKS	FIGURE
	η psf	α deg	β deg	C_j		δ_4 deg	δ_5 deg	δ_a deg	δ_c deg	δ_t deg	δ_{st} deg	δ_e deg	δ_r deg		
81	14.5	~	0	.53		60	60	30	0	-10	40	0	0	BASIC POLARS	9a
82	21.4			.27											9a
83	7.3	4	~	1.05										YAWLERS	22a
84	7.3	12		1.05											22a
85	9.6	~	0	0										POLARS	9a
86	4.9			1.54					40						9c
87	7.3			1.03											9c
88	9.6			.79											9c
89	14.5			.52											9c
90	7.2	4	~	1.04										YAWLERS	22d
91	7.2	12		1.04											22d
92	21.3	~	0	.27										POLARS	9c
93	4.9			1.28										POLAR; $C_{TEL} = 1.5 C_{TE}$	—
94	9.7			0										POLAR	9c
95	~	0,8		0					0					NOSE FAIRING ON, NOISE	—
96	9.6	-8, ~		0		0		0		~ 0,				L SWEEP, POLAR	—
97	9.6	-8, 0		0						~ 0,	OFF				18,19
98	~	0,8		0						0				NOISE	—
99	~	—		—						—				NOISE, MODEL OUT	—

TABLE IV. - INDEX TO FIGURES

LONGITUDINAL DATA

FIGURE	EFFECT OF	VARIABLES	δ_f	δ_a	δ_c	δ_s	HOR. i_z Tail
7 a	CJE	$\alpha, \delta_f, \delta_s$	60/60	—	0	1-45	OFF
b			60/30				
c						1-60	
d						2-60	
8 a	CJE	α, δ_c	60	30	0	1-60	
b						2-60	
c					10		
d					20		
e					30	1-60	
f					40	2-60	
g					50	1-60	
9 a	CJE	α, δ_c	60	30	0	2-60	-10
b					20		
c					40		
10	CJE	α	60	10	0		OFF
11	CJE	α, C_{MBC}	60	30	0		
12 a	CJE	α, δ_c	60	30	0/-20		
b					0/40		
13	CJE	α	60	30/10	0		
14 a	CJE	α, δ_c	30/30	—	0	1-60	
b					30		
15 a	CJE	α, δ_c	30	30	0		
b						2-60	
c					30	1-60	
d					50		
16 a	CJE	α	30	30	0	2-60	-15
b	i_z						~
17 a	CJE	α, δ_c	30	30	0/-20		OFF
b					0/20		
c					0/40		
18	BASE RUN	α	0	0	0	2-60	0
19	i_z		0	0	0		~

TABLE IV. - CONCLUDED

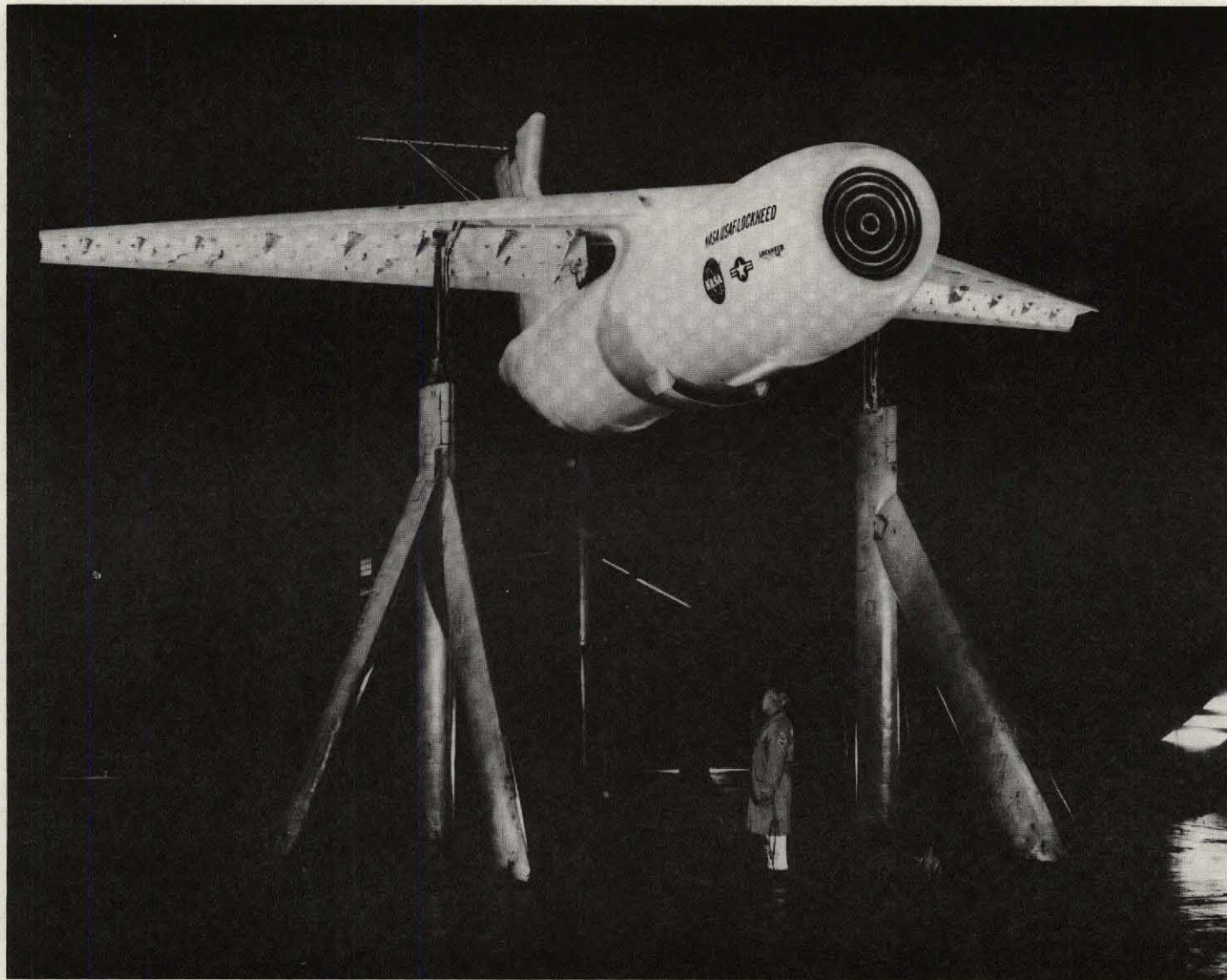
LATERAL - DIRECTIONAL DATA

FIGURE	EFFECT OF	VARIABLE	δ_f	δ_a	δ_c	δ_s	HOR. TAIL
20 a	CJT	α, δ_c	60	30	0	2-60	OFF
b					20		
c					0/-20		
d					0/40		
21	CJT	α	60	30/10	0		
22 a	α	β, α	60	30	0		-10
b	CJT				20		
c							
d	α				40		
23 a	CJT	α, δ_c	30	30	0		OFF
b					0/-20		
c					0/20		
d					0/40		
24 a	CJT	β, α	30	30	0		-15
b							



(a) Top view of model.

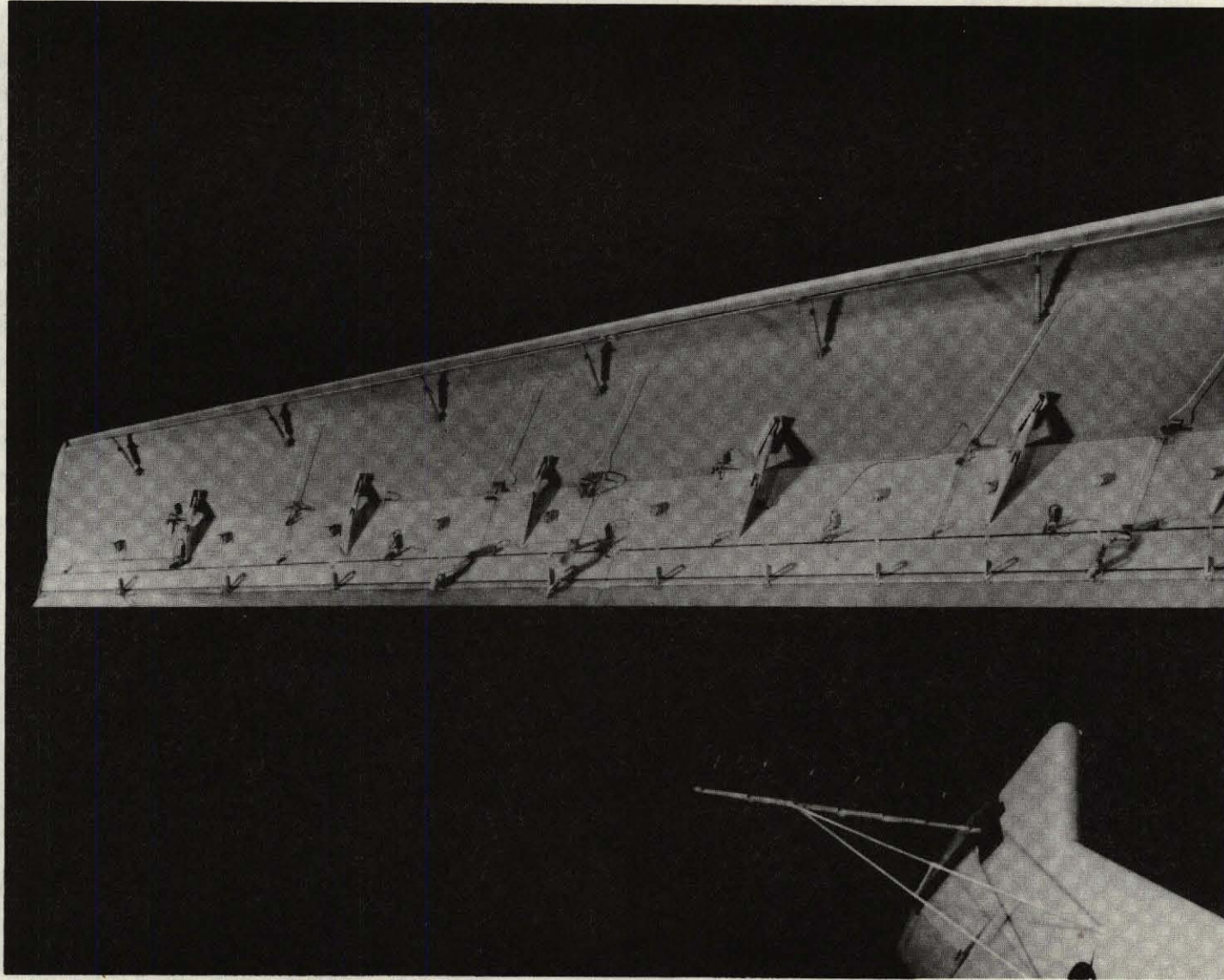
Figure 1. — Views of the model installed in the Ames 40- by 80-foot Wind Tunnel.



(b) Front view of model.
Figure 1. - Continued.

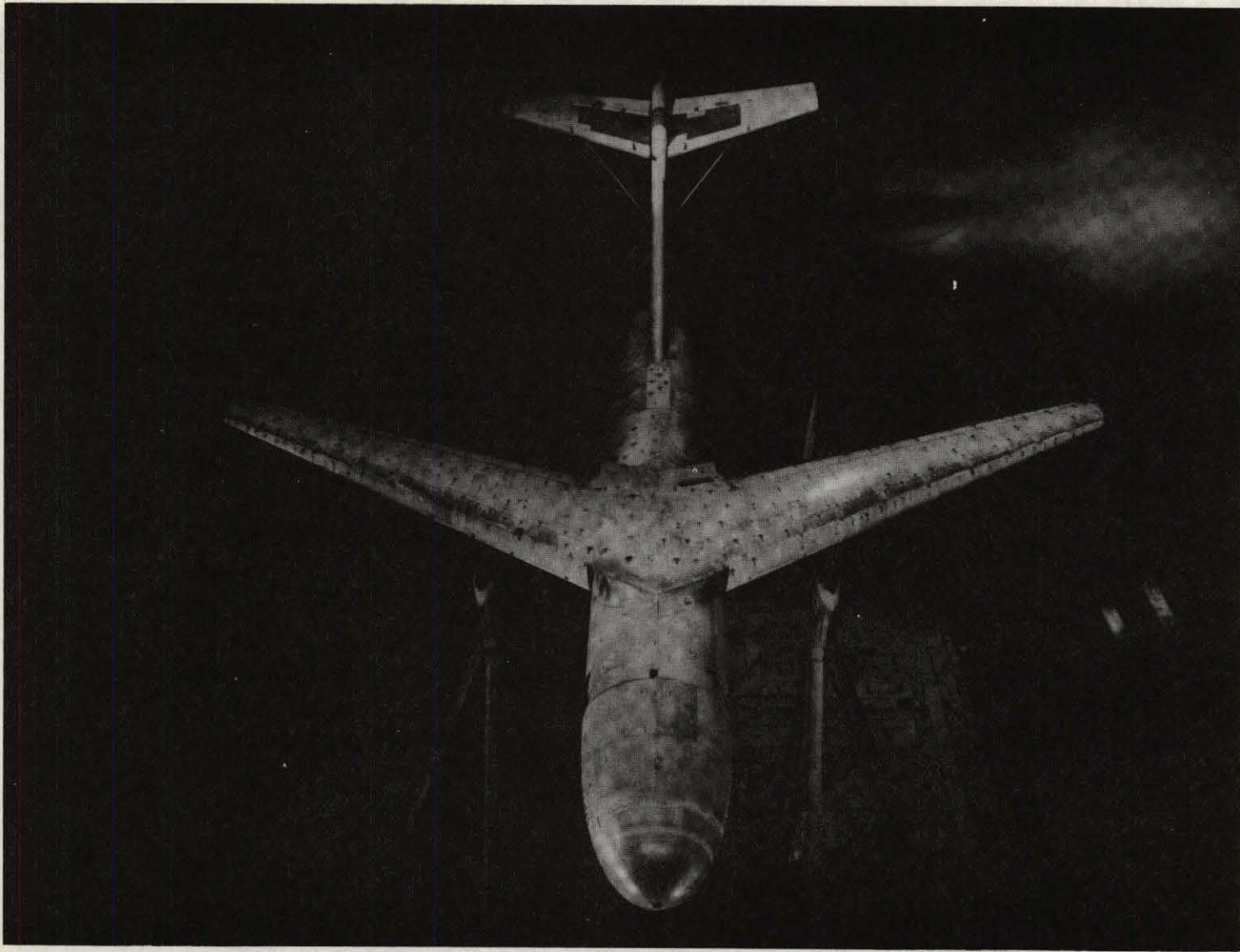


(c) Rear view of model.
Figure 1. - Continued.



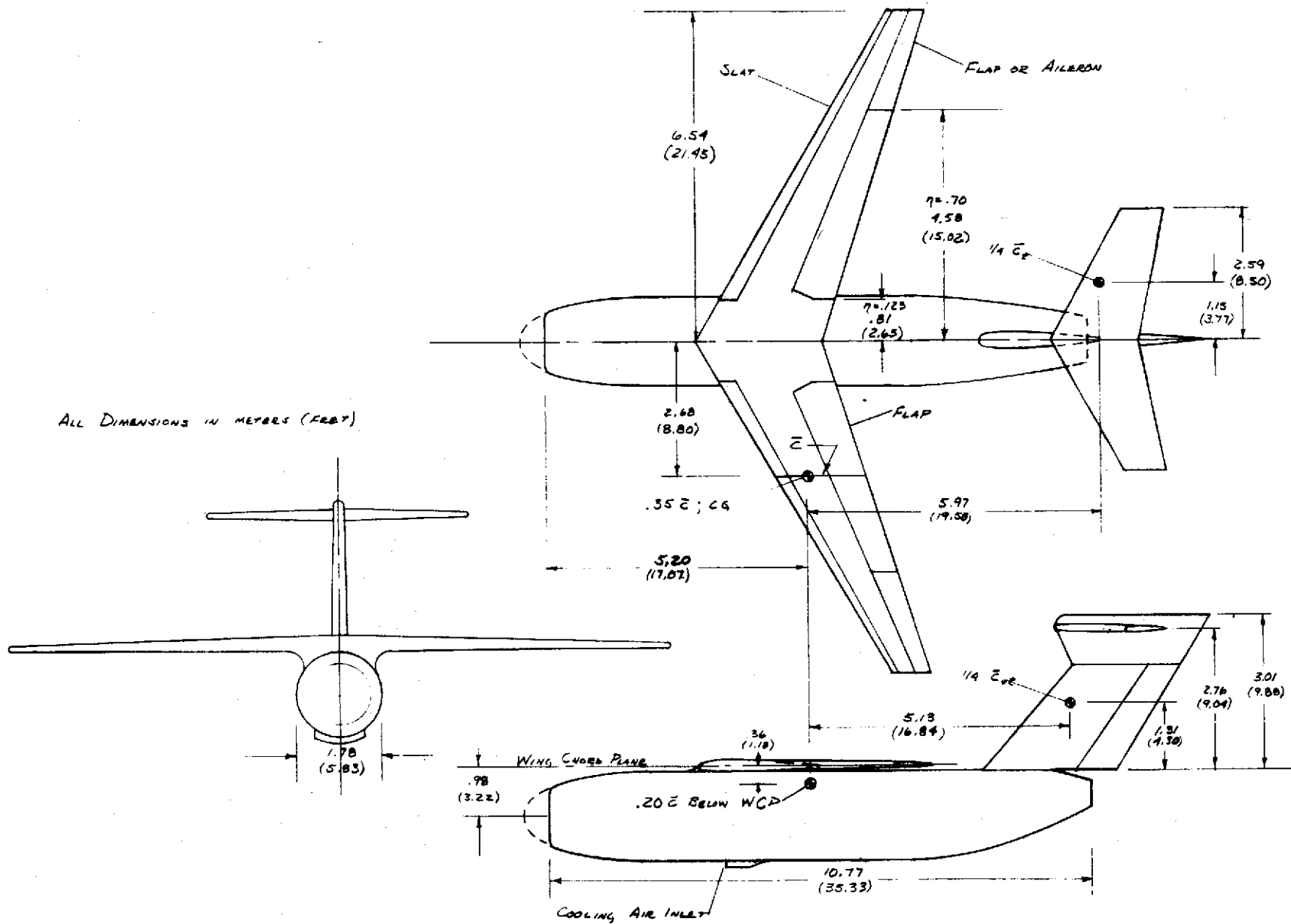
(d) View of the lower wing surface.

Figure 1. — Continued



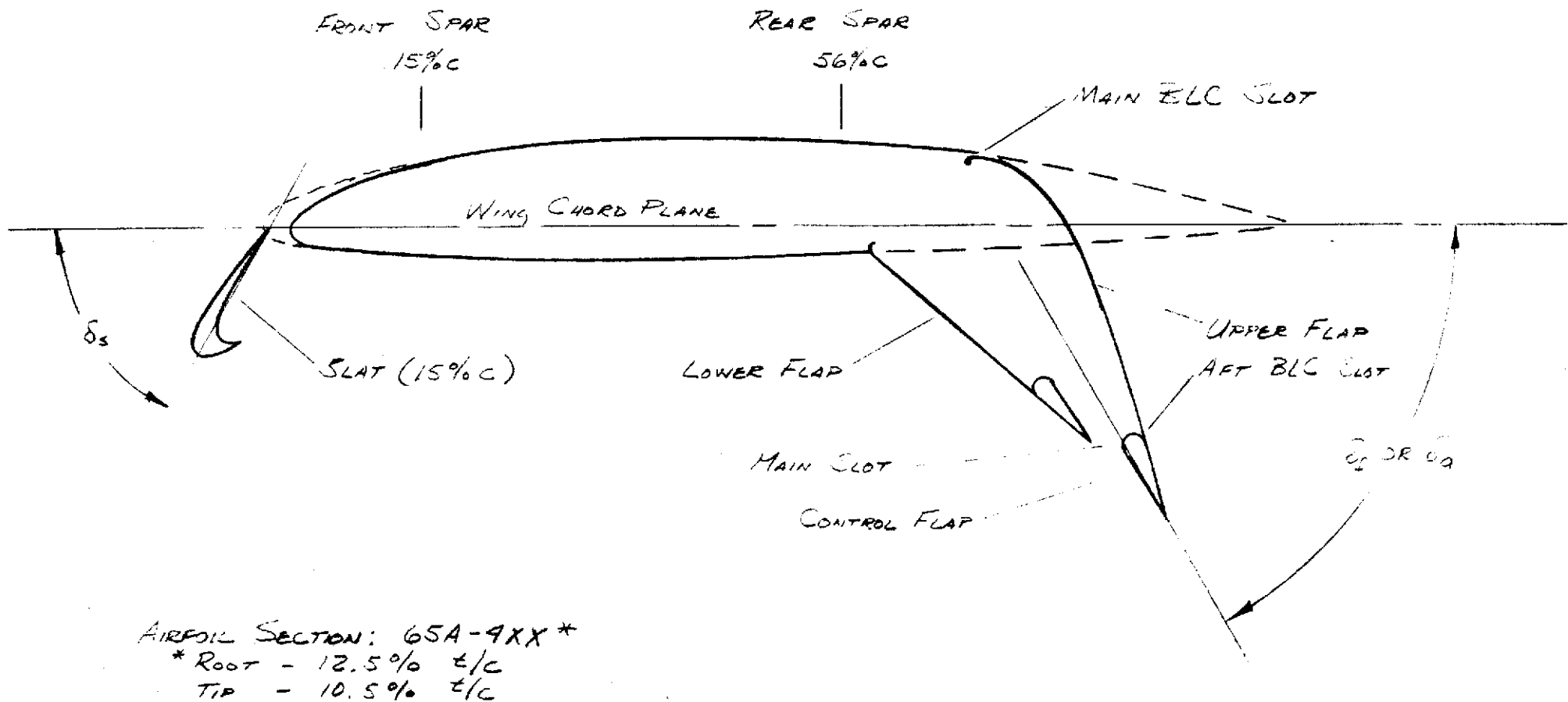
(e) Top view of model with horizontal tail and nose fairing installed.

Figure 1. - Concluded.



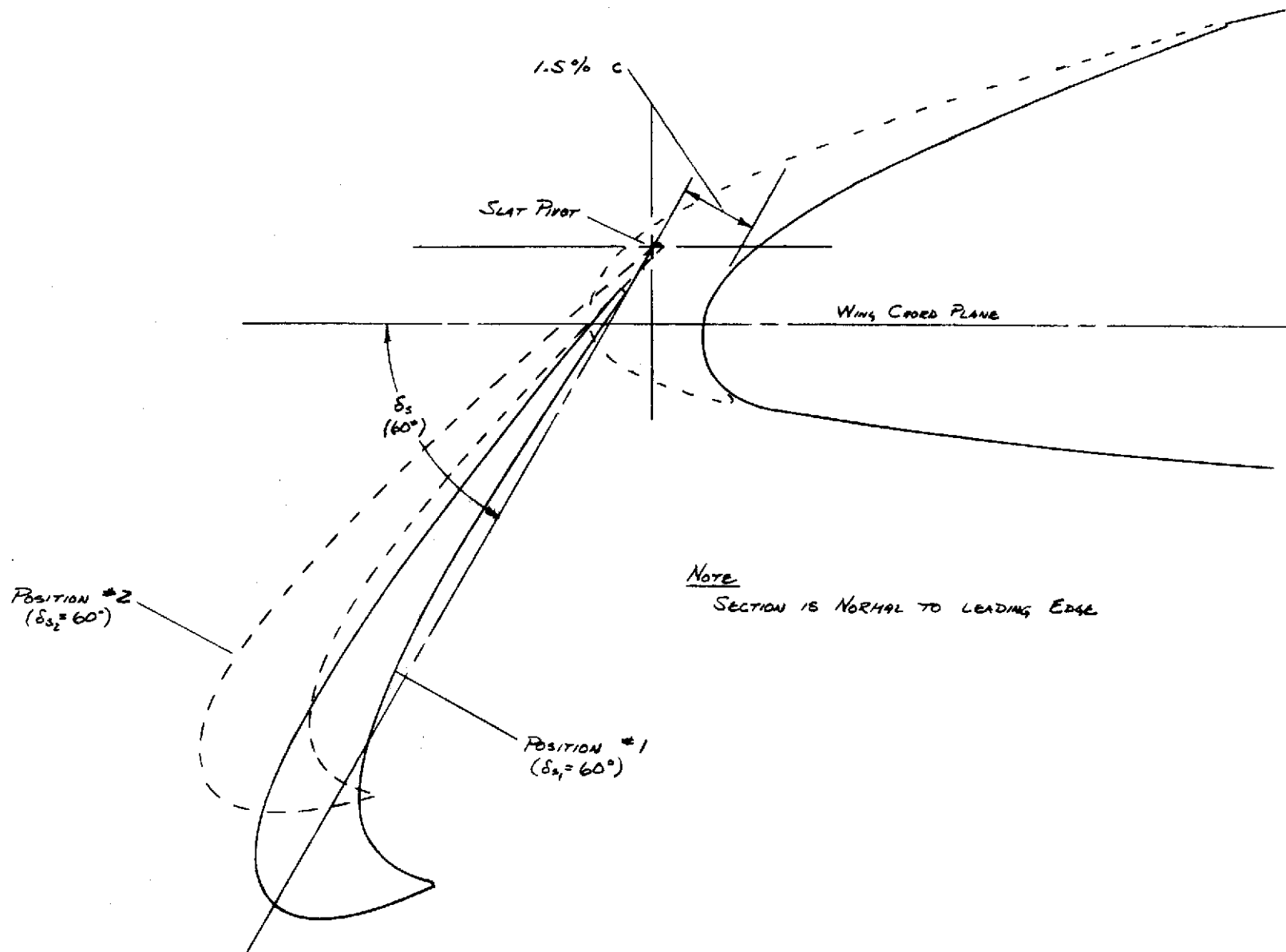
(a) Three-view sketch of the model.

Figure 2. — Geometric details of the model.



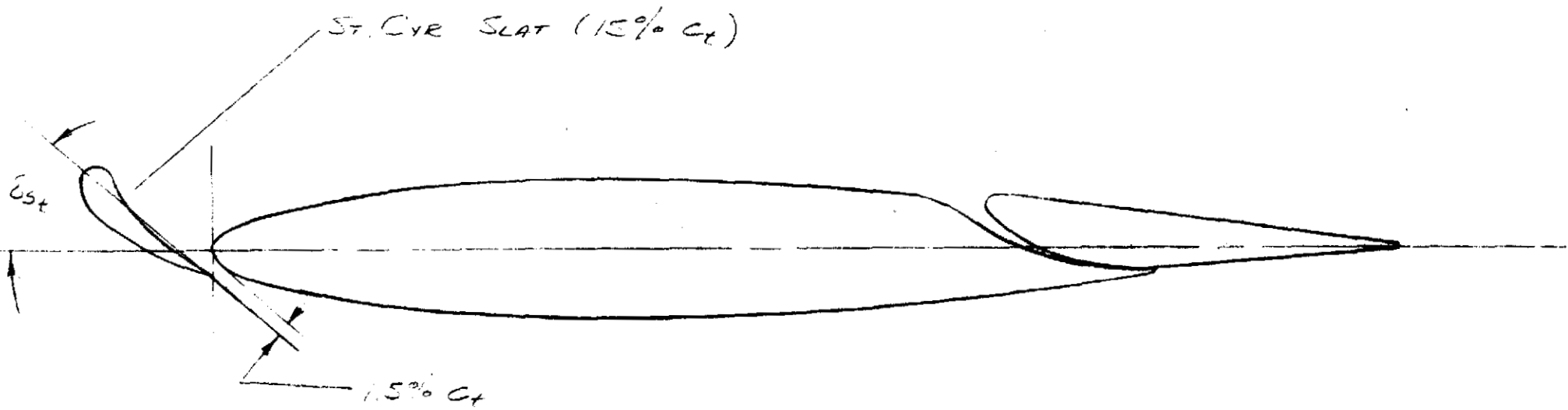
(b) Wing section geometry.

Figure 2. - Continued



(c) Slat section geometry.

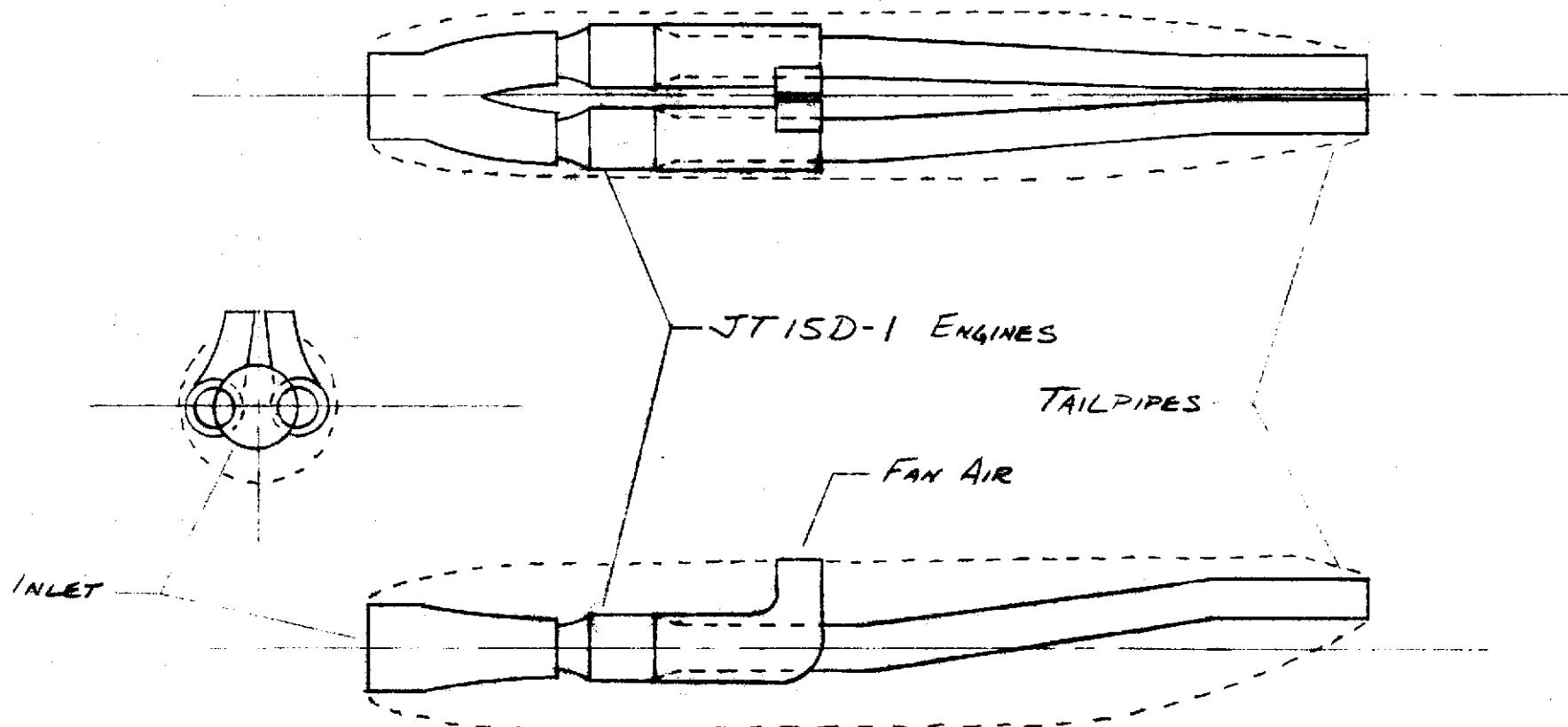
Figure 2. - Continued.



AIRFOIL SECTION : 64-012

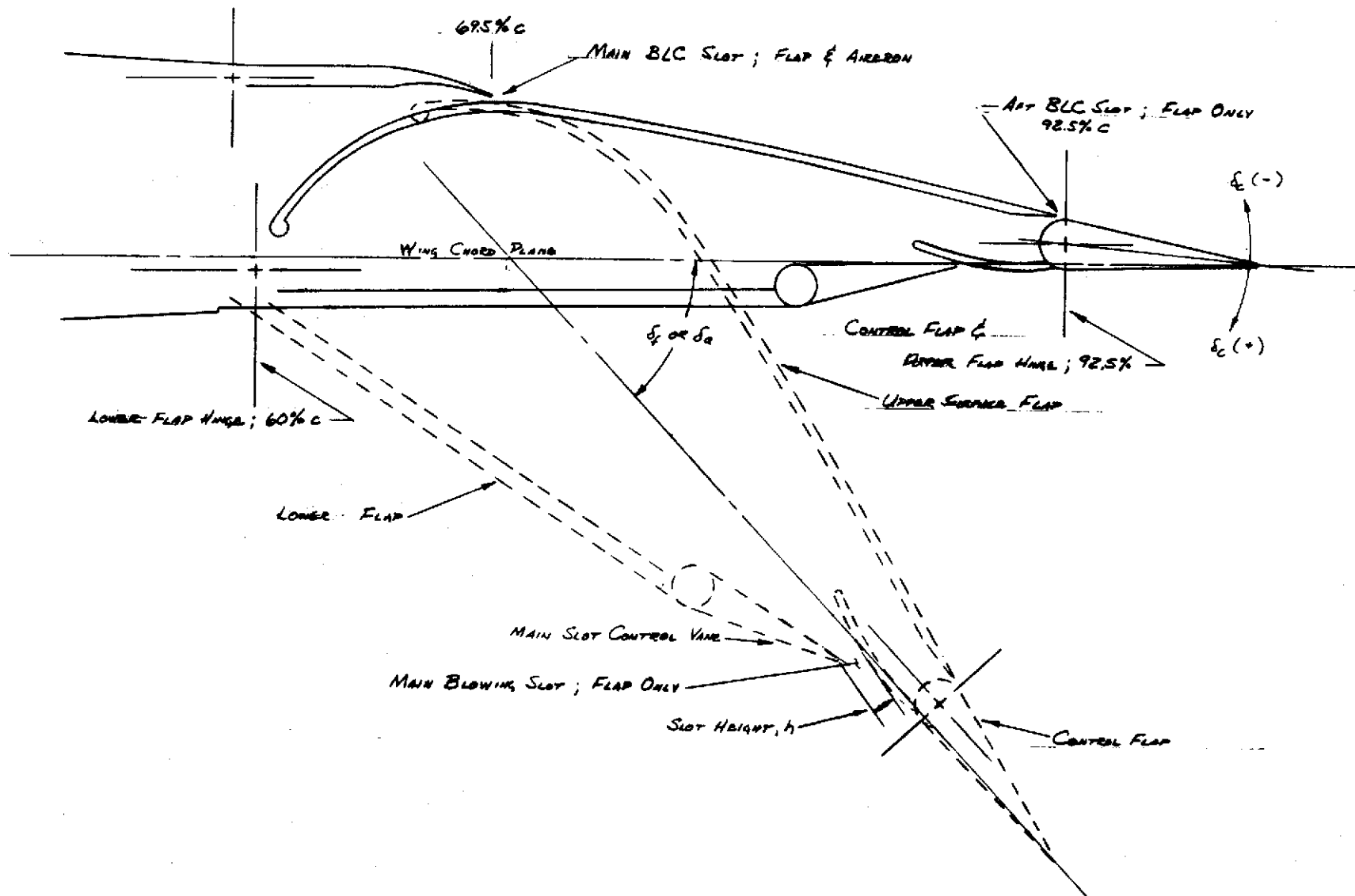
(d) Horizontal tail section geometry.

Figure 2. - Continued.

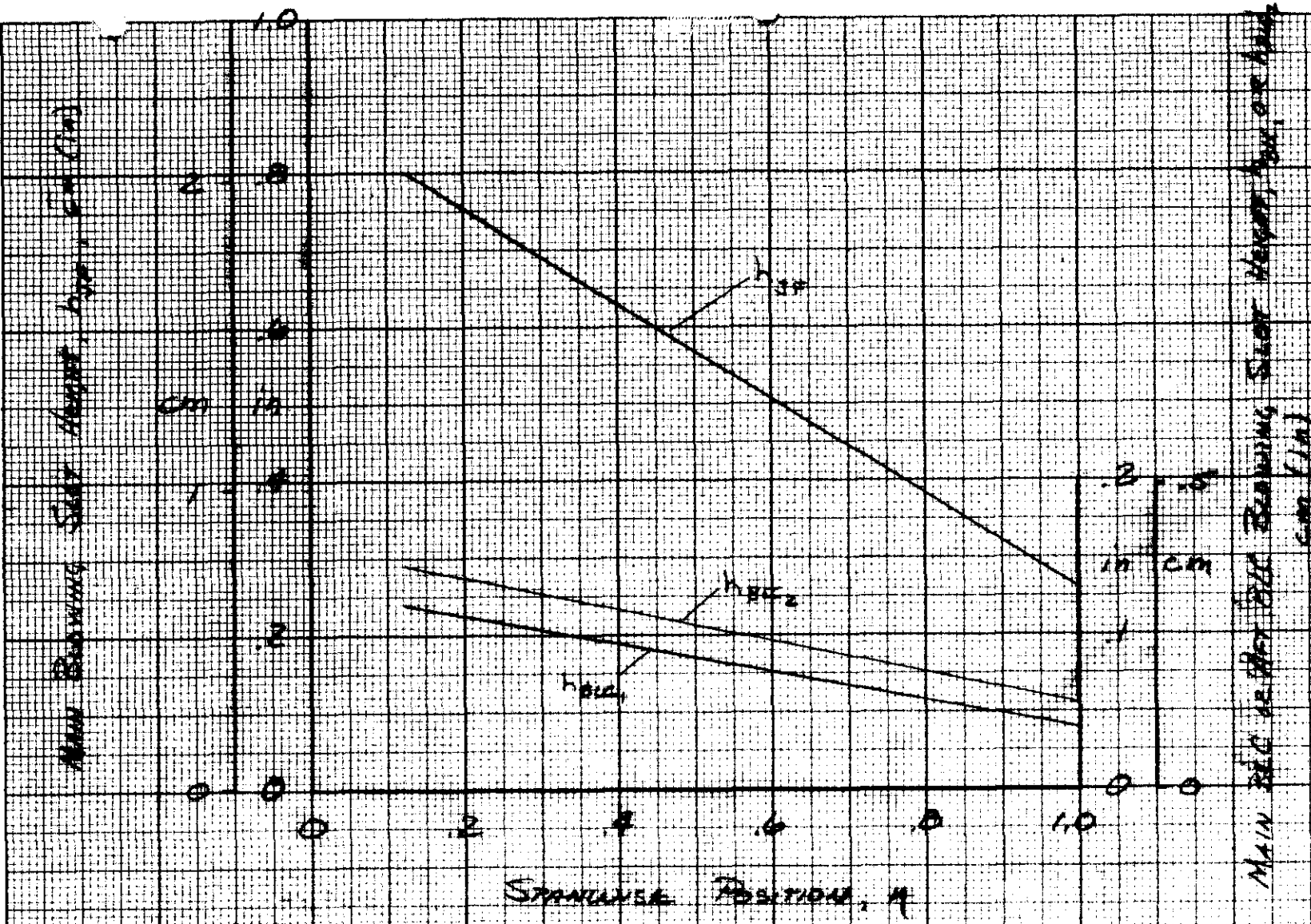


(e) Schematic of the air supply system.

Figure 2. - Continued.

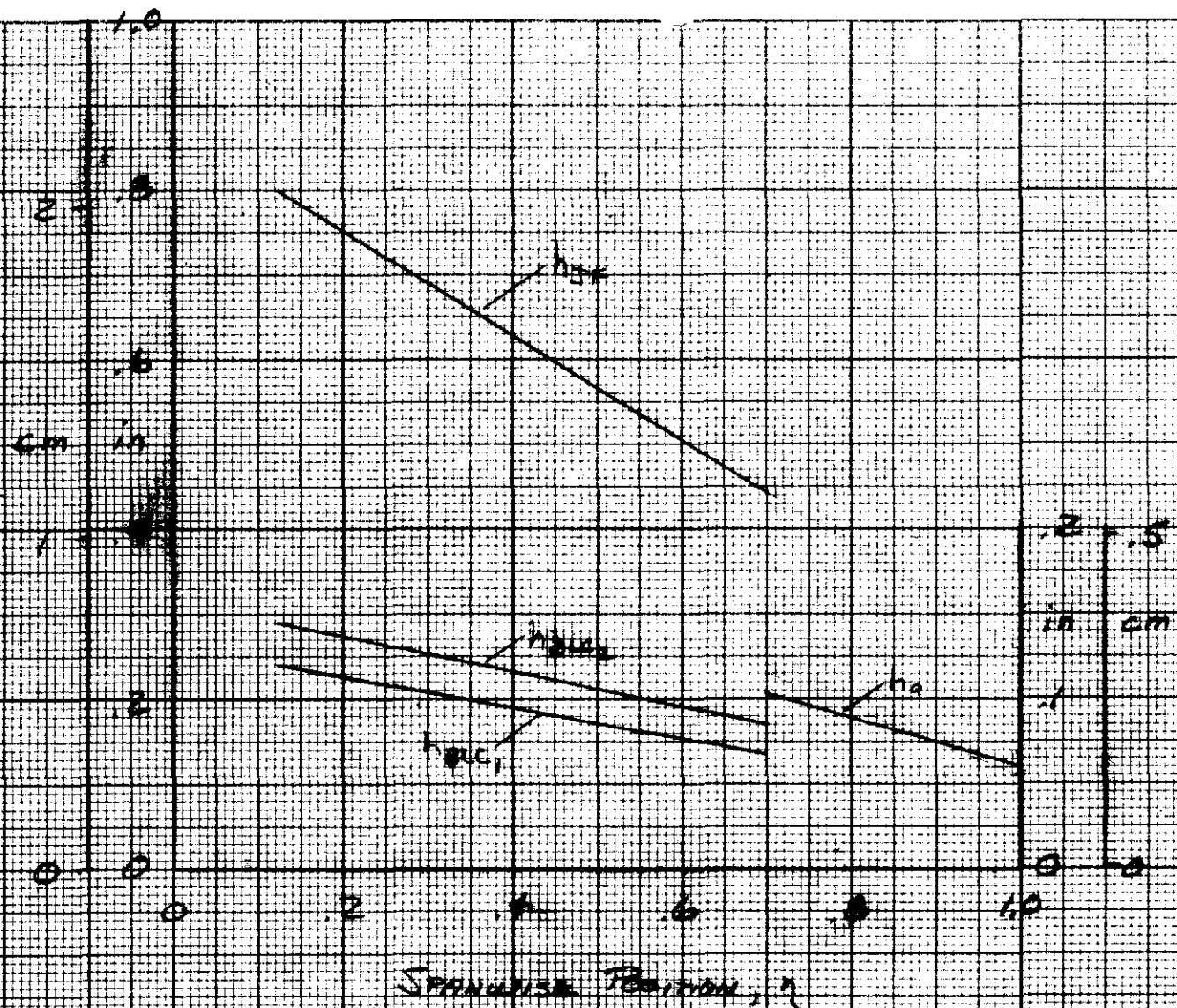


(f) Flap section geometry.
 Figure 2. - Concluded.



(a) $\delta_f = 60^\circ$, full-span flap.
 Figure 3. - Dimensions of model blowing slots.

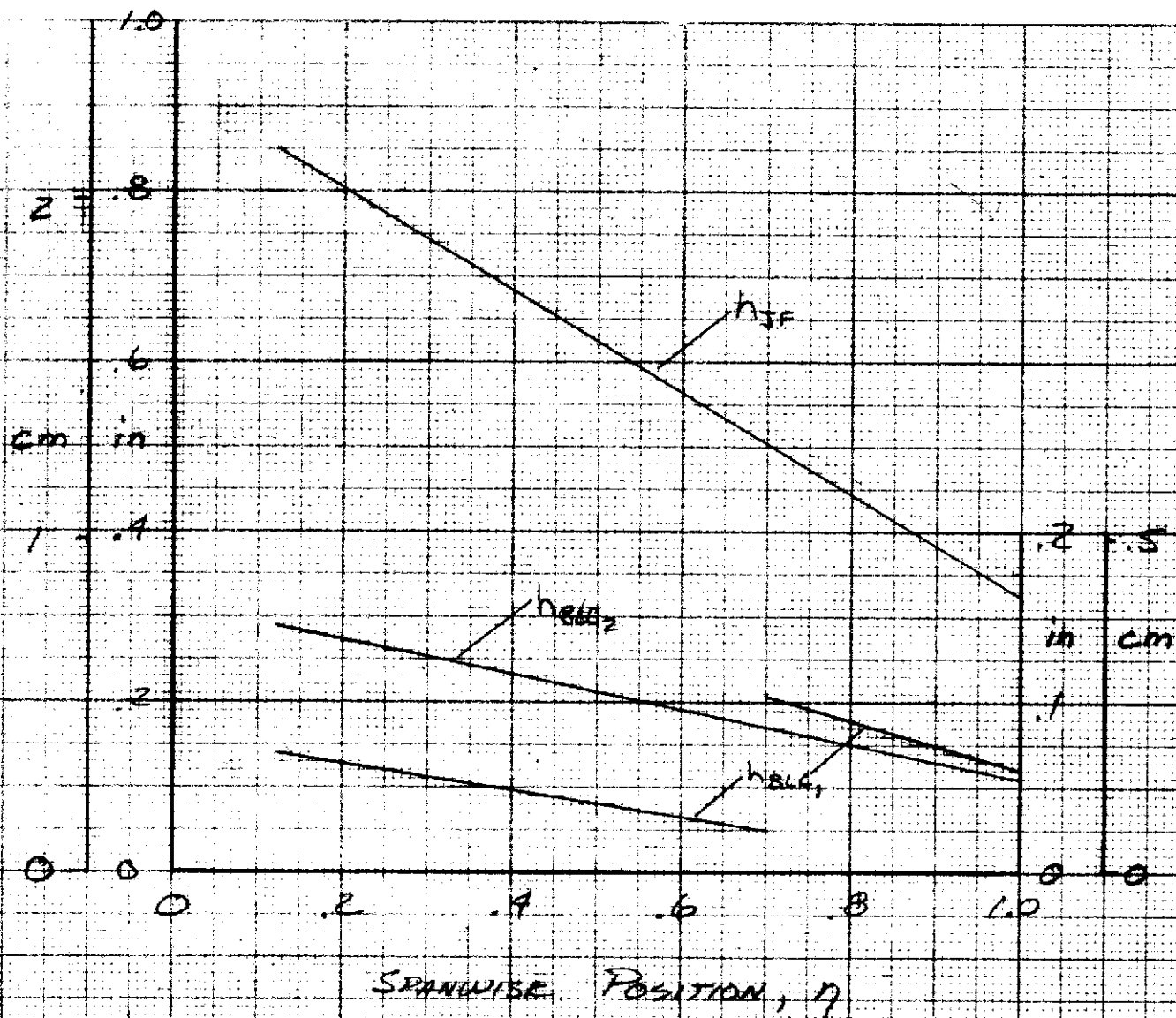
Main Bleeding Slot Height, h_{ms} , cm (in)



Main Bleeding Slot Height, h_{ms} , cm (in)

(b) $\delta_f = 60^\circ$, part-span flap.
Figure 3. - Continued.

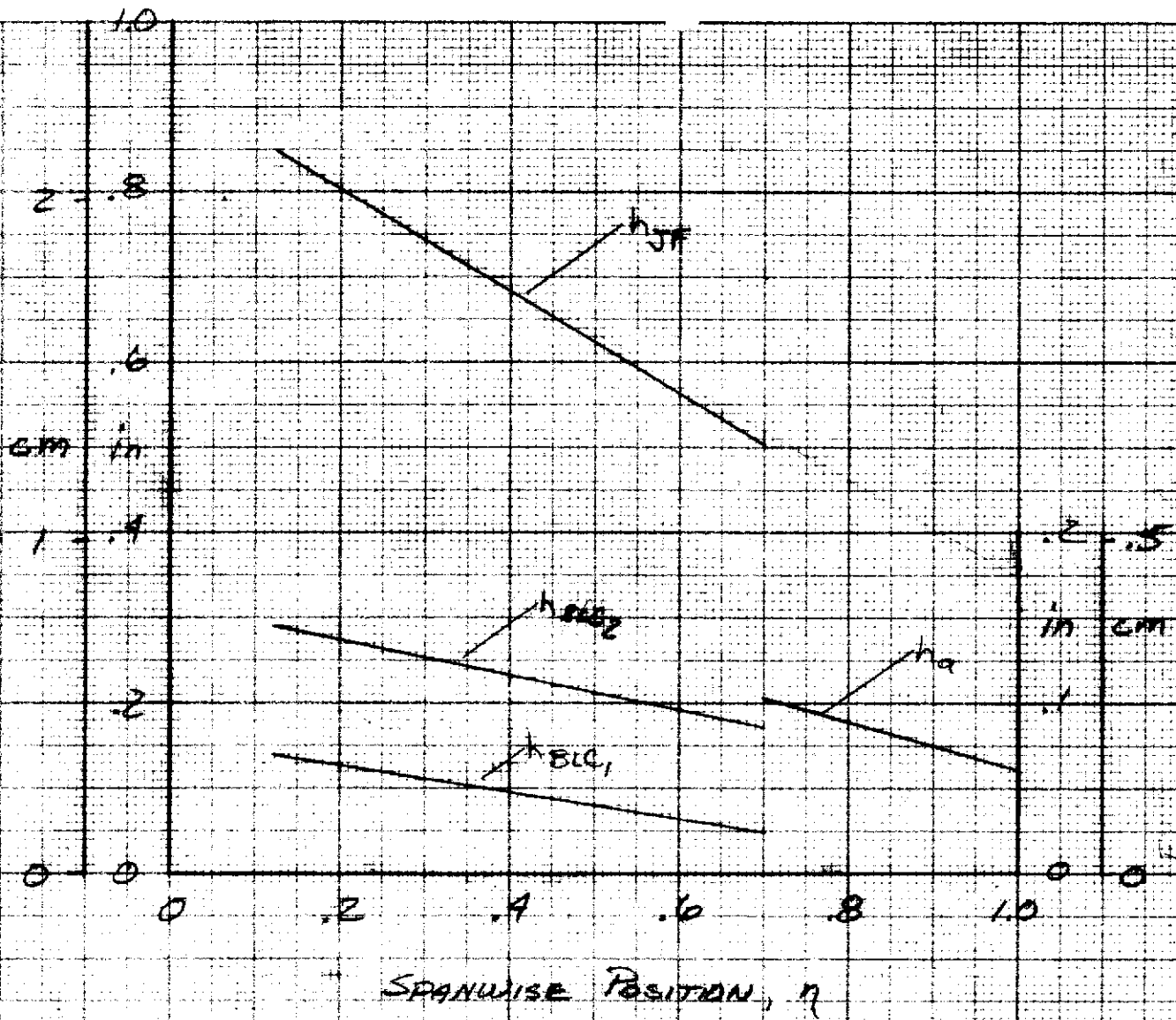
MAIN BLOWING SLOT HEIGHT, h_{BF} , CM (IN)



MAIN BLOWING SLOT HEIGHT, h_{BF} , CM (IN)

(c) $\delta_f = 30^\circ$, full-span flap.
Figure 3. - Continued.

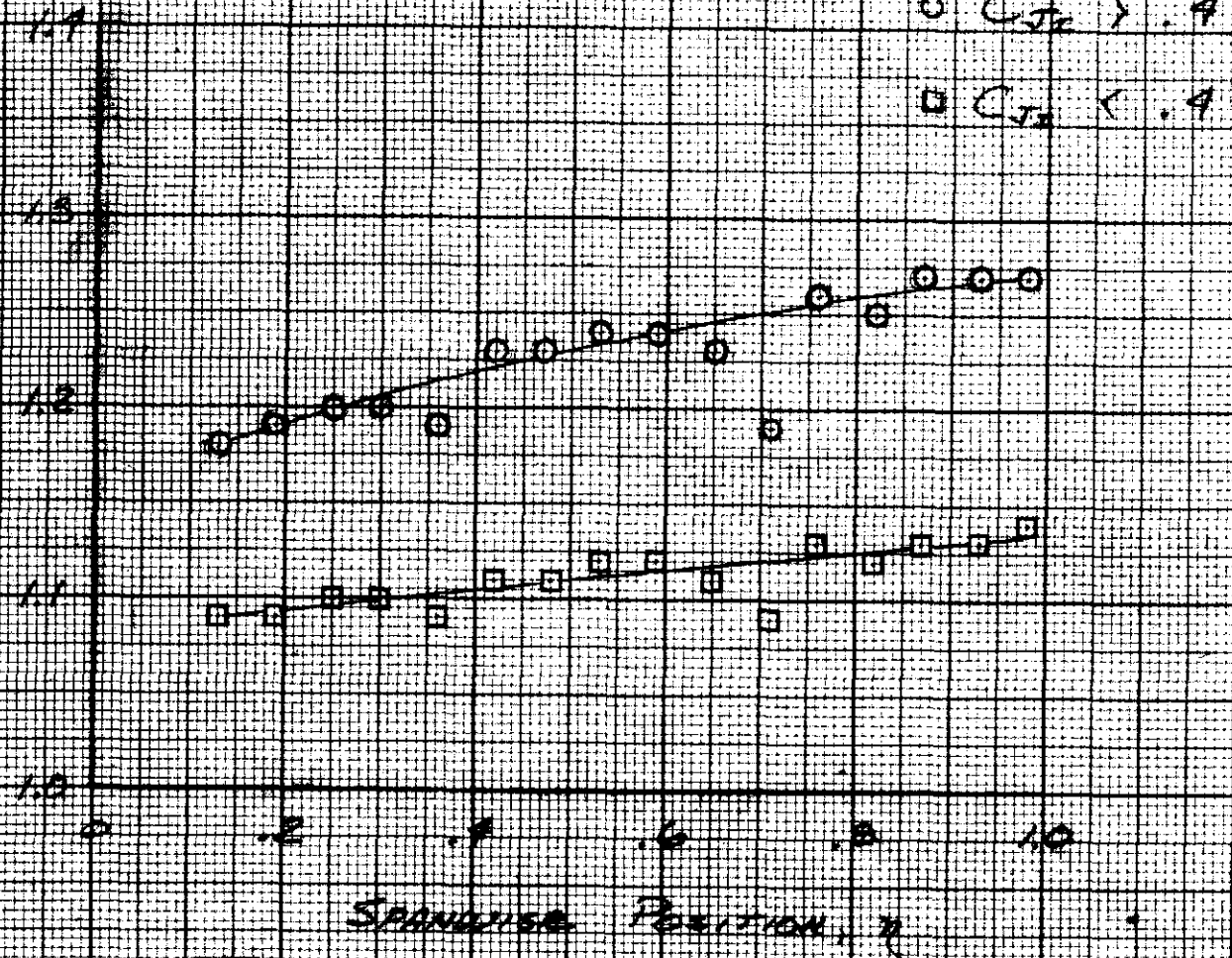
MAIN BLOWING SLOT HEIGHT, h_{BF} , cm (in)



MAIN BLC OR AFT BLC OR AIRFLOW BLOWING SLOT HEIGHT, h_{BLC} OR h_a , cm (in)

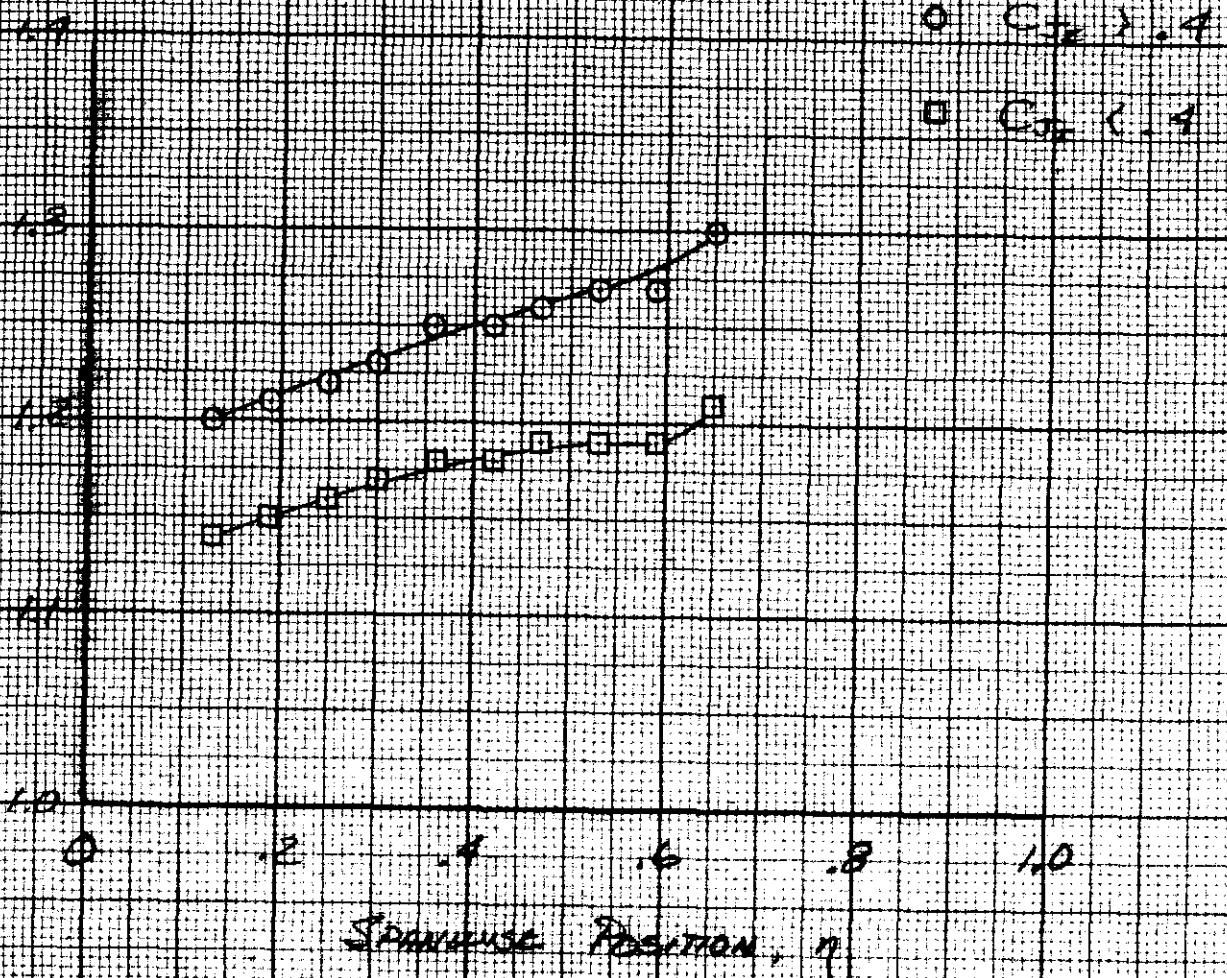
(d) $\delta_f = 30^\circ$, part-span flap.
Figure 3. - Concluded.

MAIN BLOWING SLOT PRESSURE RATIO, P_s/P_a



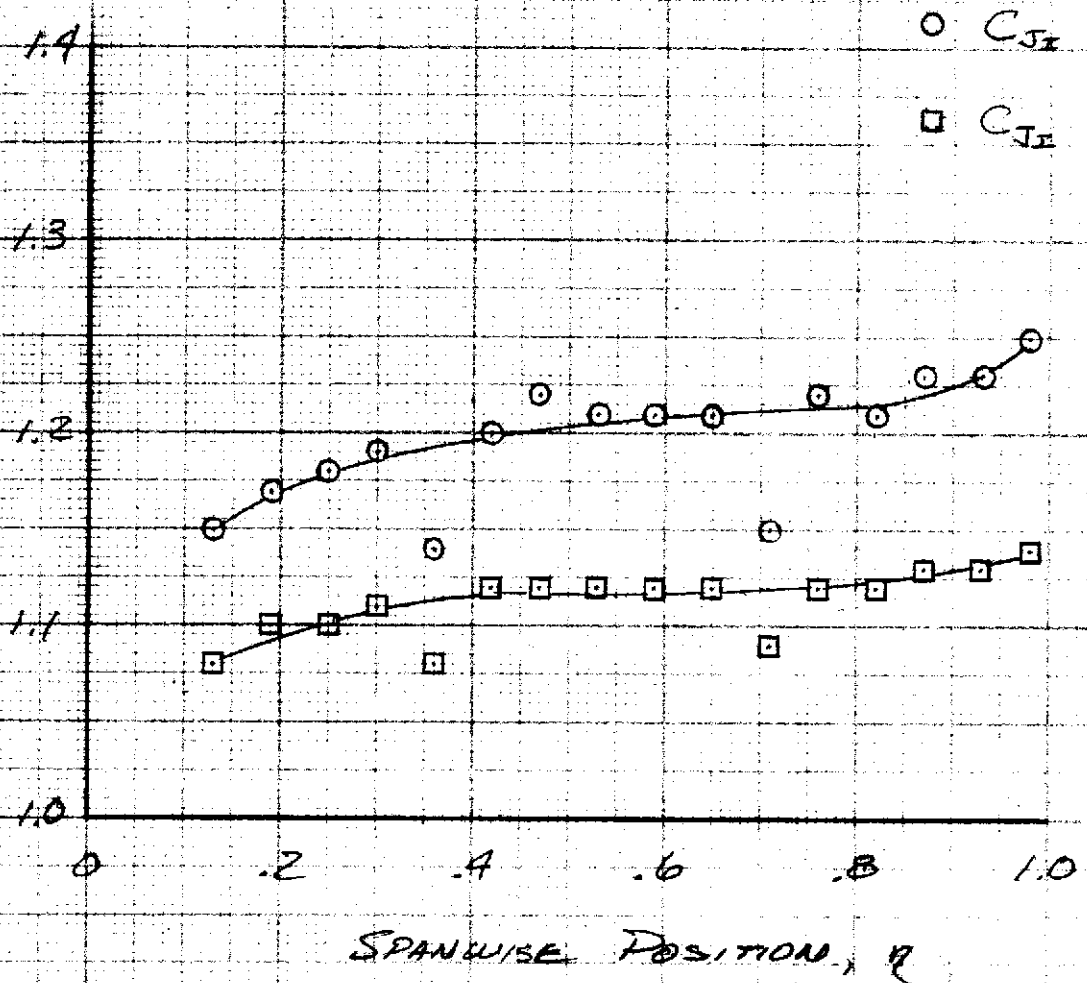
(a) $\delta_f = 60^\circ$, full-span flap.
 Figure 4. - Typical main blowing slot pressure ratio.

MAIN SPOONING SLOT PRESSURE
 RATIO, P_s/P_a



(b) $\delta_f = 60^\circ$, part-span flap.
 Figure 4. - Continued.

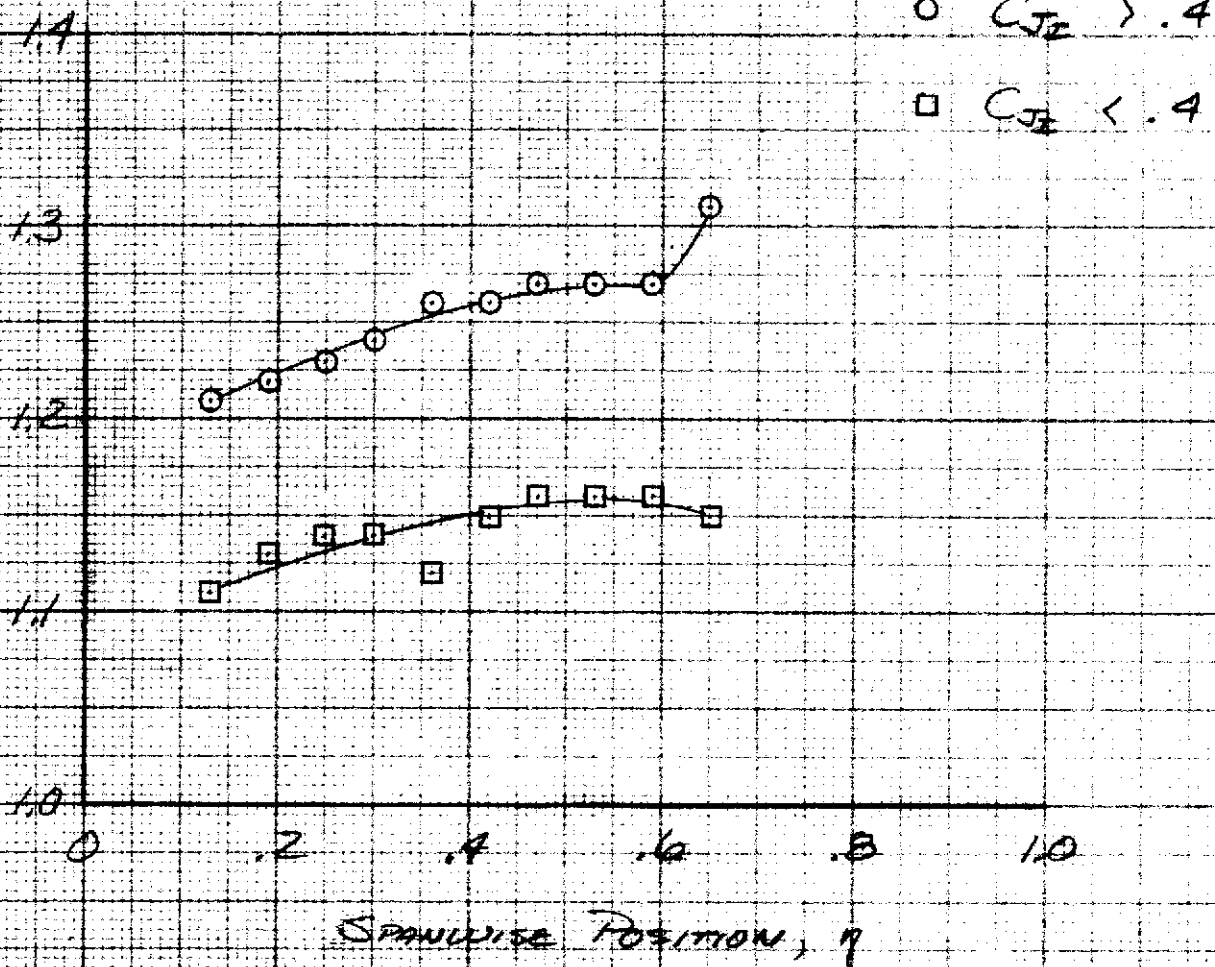
MAIN BLOWING SLOT PRESSURE RATIO, P_1/P_0



○ $C_{JT} > .4$
□ $C_{JT} < .4$

(c) $\delta_f = 30^\circ$, full-span flap.
Figure 4. - Continued.

MAIN BLOWING SLOT PRESSURE
RATIO, P_s/P_0



(d) $\delta_f = 30^\circ$, part-span flap.
Figure 4. - Concluded.

AMM
MEMBER
NO. 2584

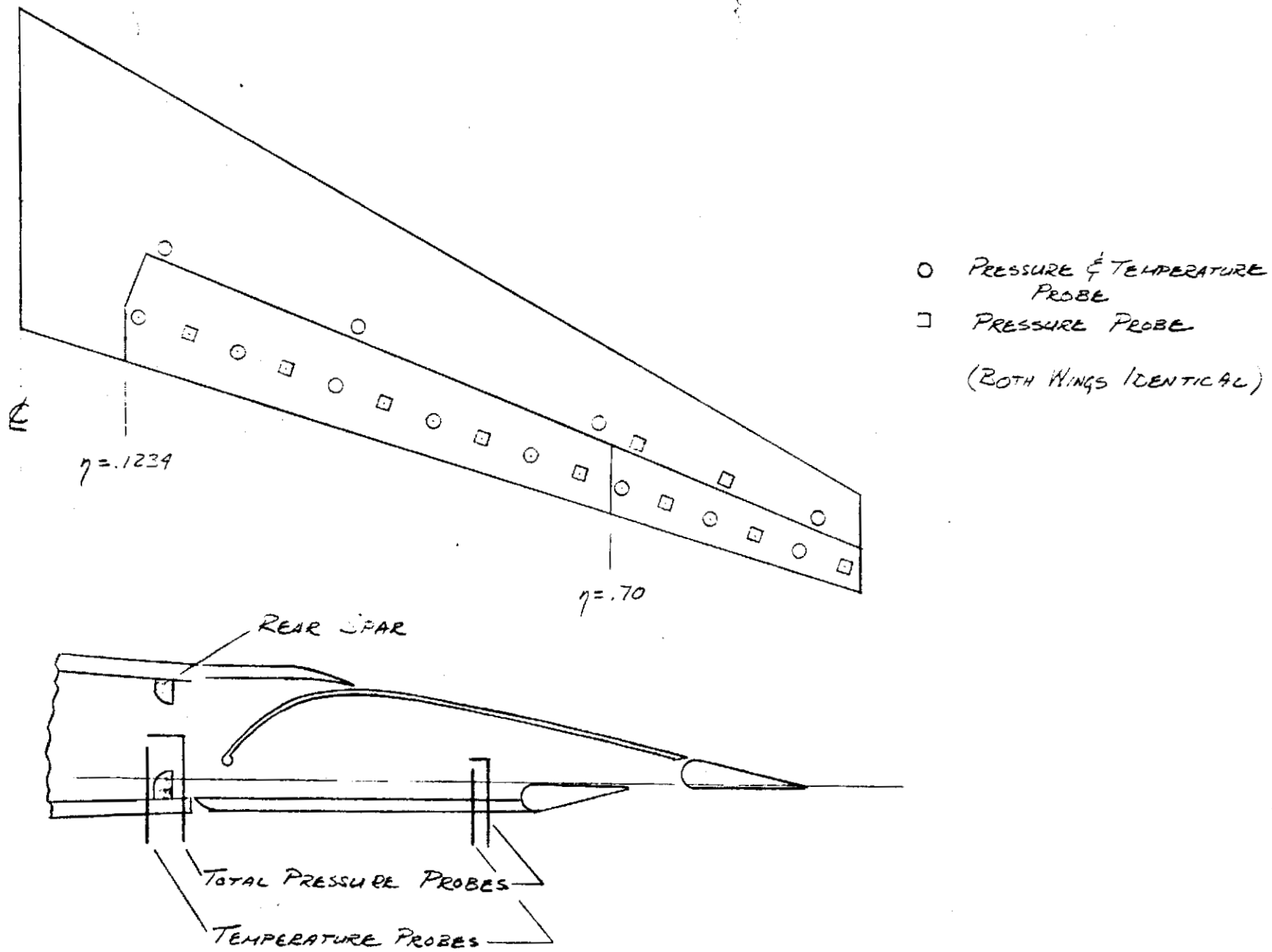
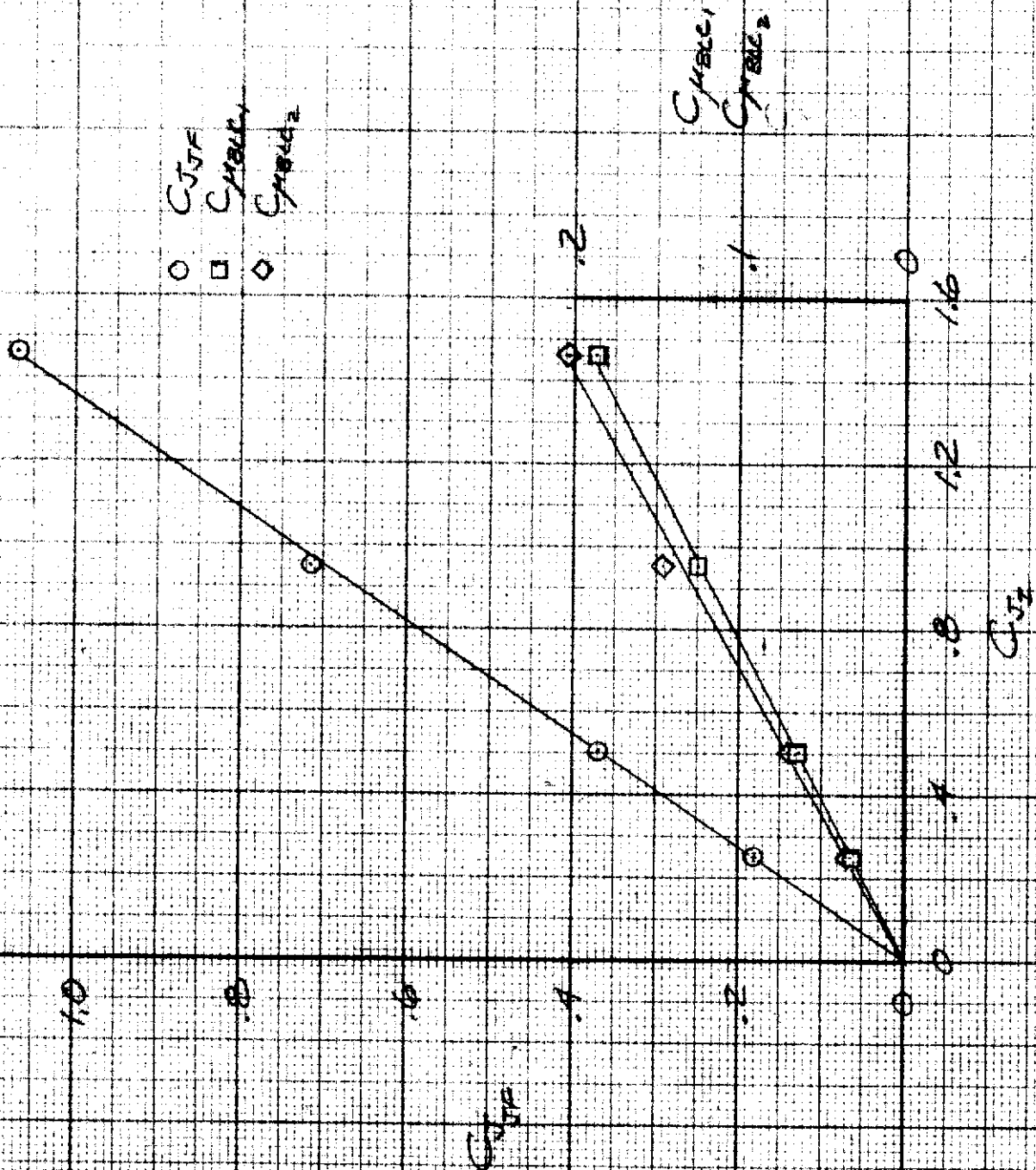


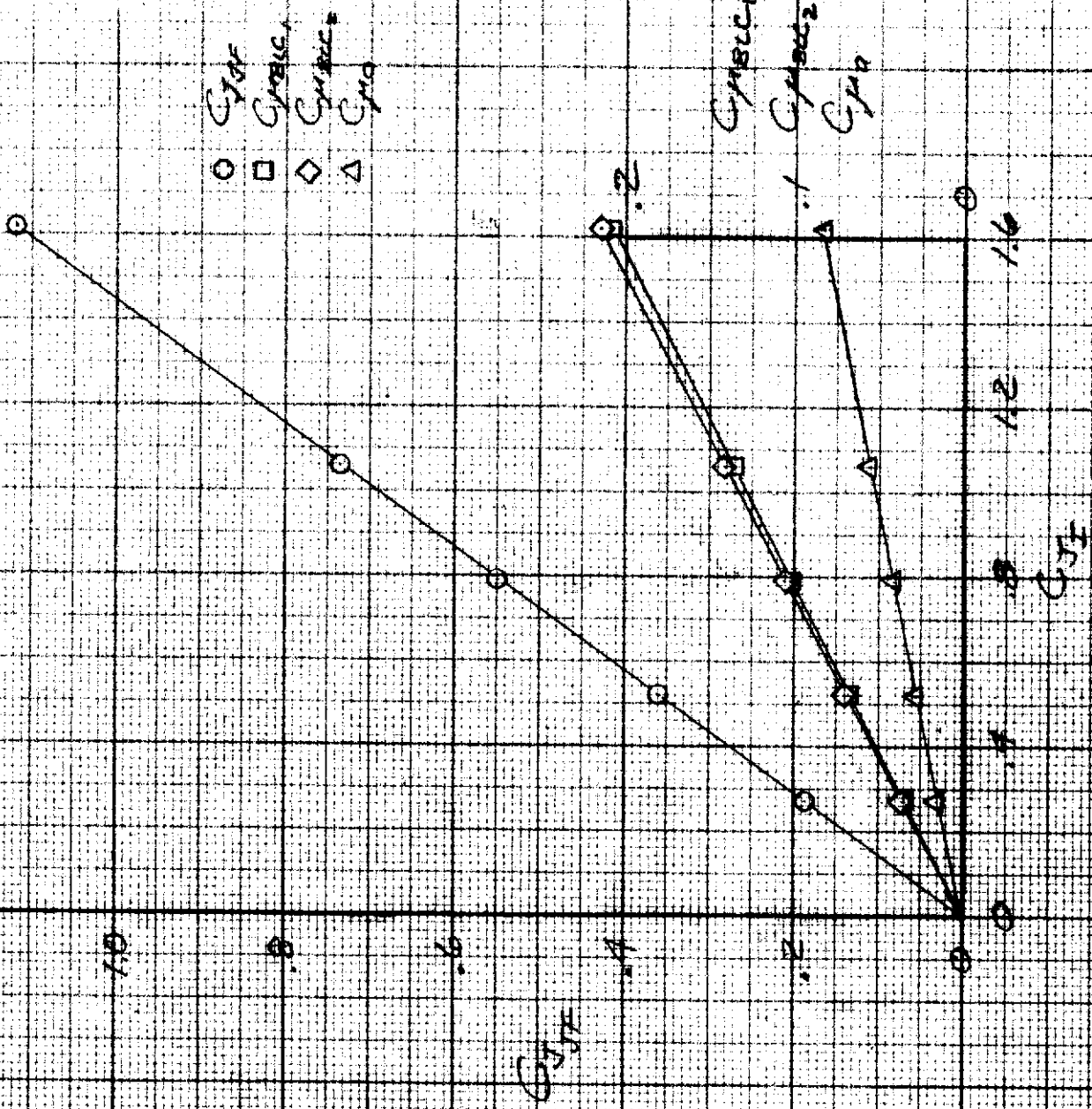
Figure 5. - Schematic of wing duct instrumentation layout.



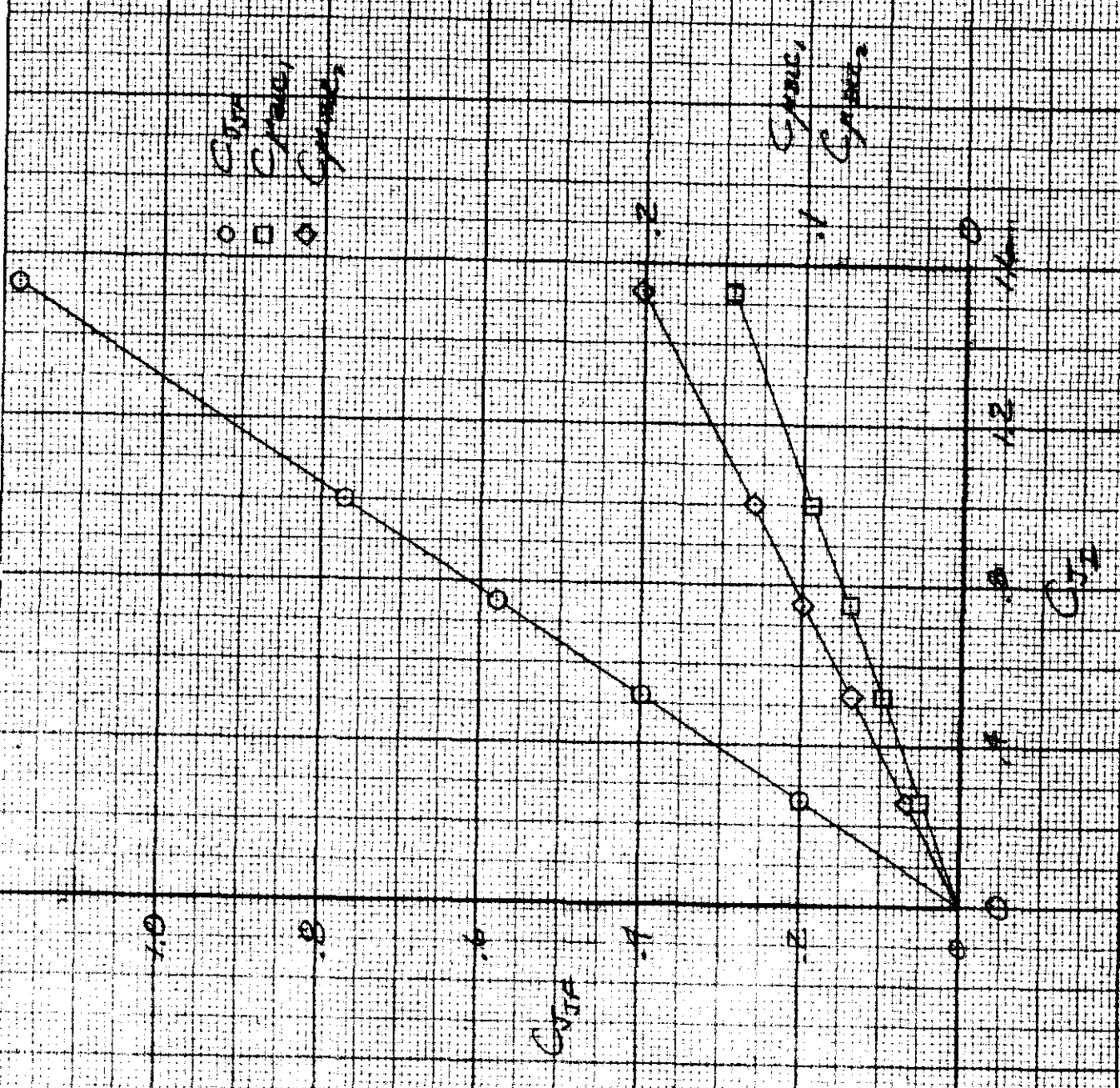
(a) $\delta_f = 60^\circ$, full-span flap.

Figure 6. - The division of C_{J_I} into its components,

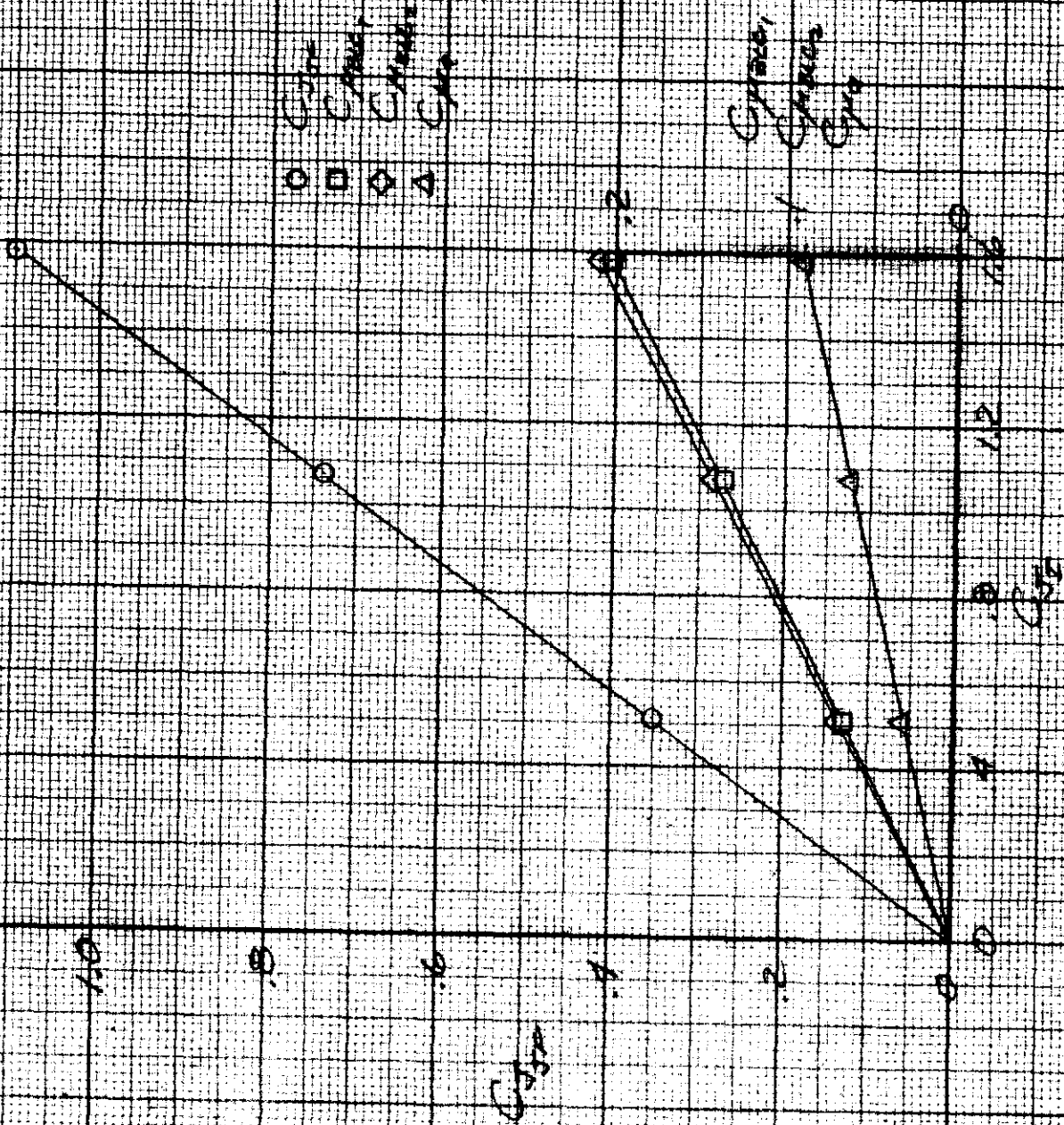
$$C_{J_{JF}}, C_{\mu_{BLC1}}, C_{\mu_{BLC2}}, C_{\mu_a}$$



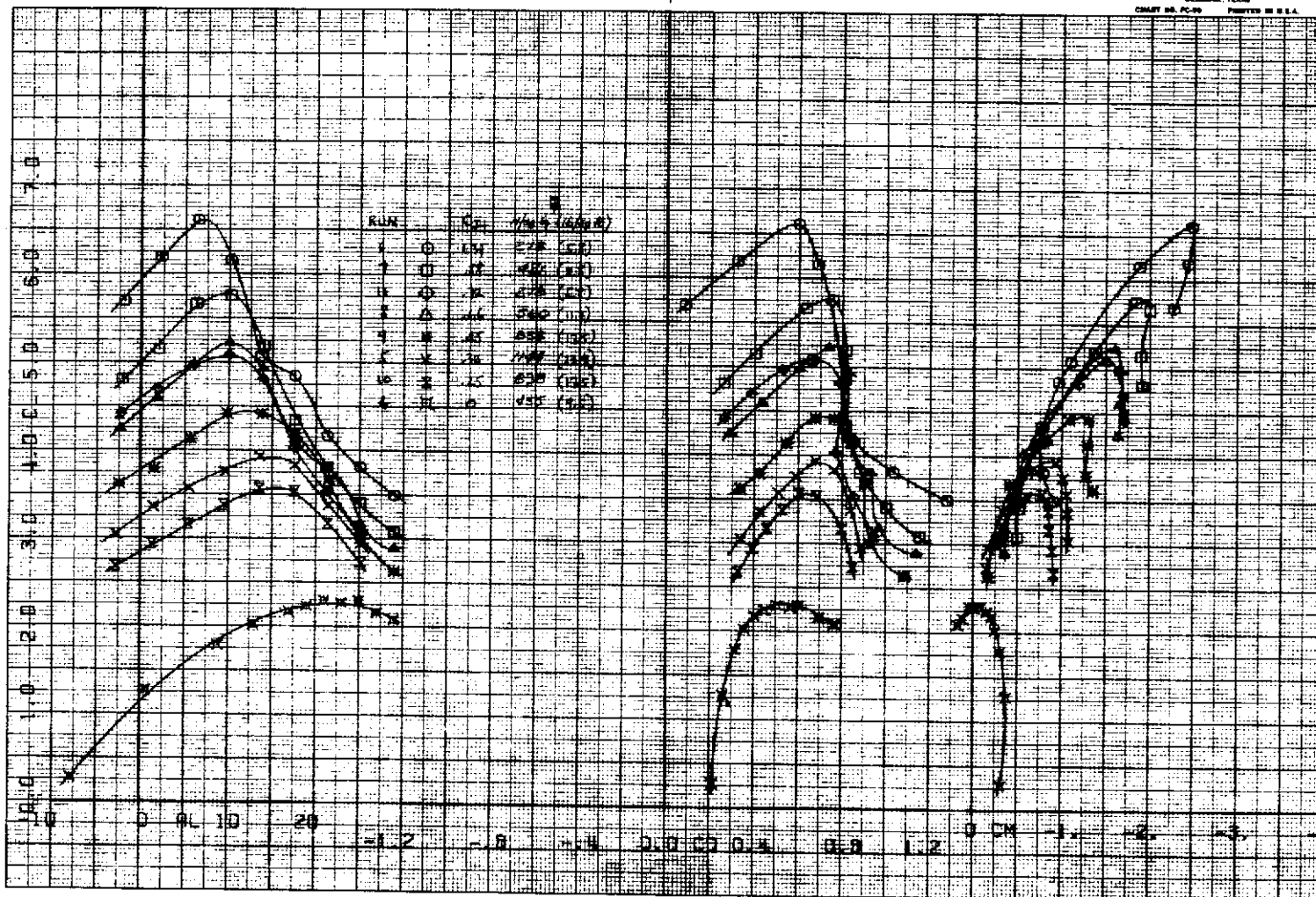
(b) $\delta_f = 60^\circ$, part-span flap.
Figure 6. - Continued.



(c) $\delta_f = 30^\circ$, full-span flap.
Figure 6. - Continued.



(d) $\delta_f = 30^\circ$, part-span flap.
Figure 6. - Concluded.



(a) $\delta_f = 60^\circ/60^\circ$, $\delta_{s1} = 45^\circ$.

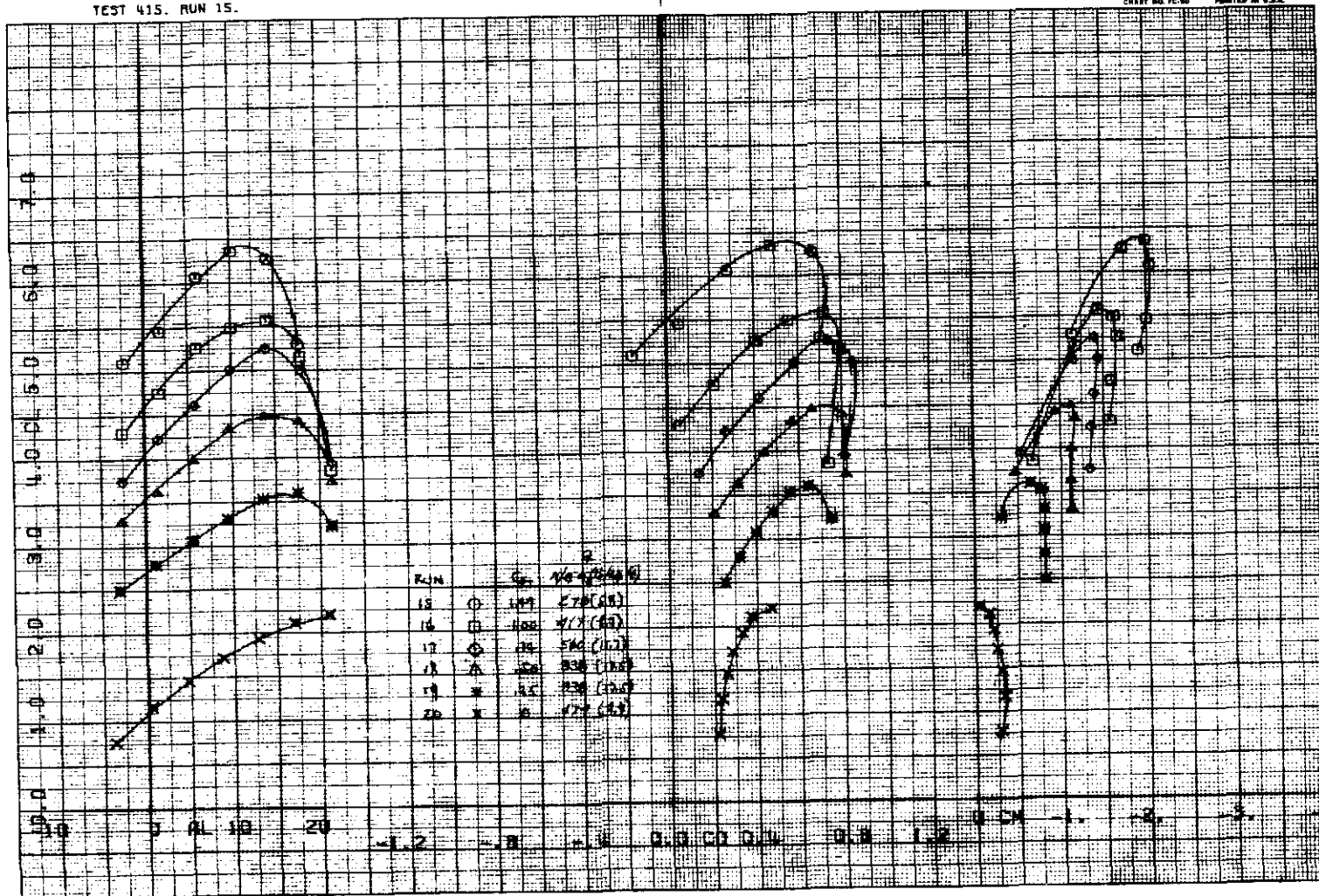
Figure 7. - The affect of C_{jI} on the longitudinal characteristics of the model; full-span flap, $\delta_c = 0^\circ$, horizontal tail off.

TEST 415. RUN 15.

COMPL^oT

OMNIGRAPHIC^o

HOUSTON INSTRUMENT
 DIVISION OF HARRIS CORPORATION
 BELLAMY, TEXAS
 CHART NO. FC-50 PRINTED IN U.S.A.



(b) $\delta_f = 60^\circ/30^\circ$, $\delta_{s_1} = 45^\circ$.

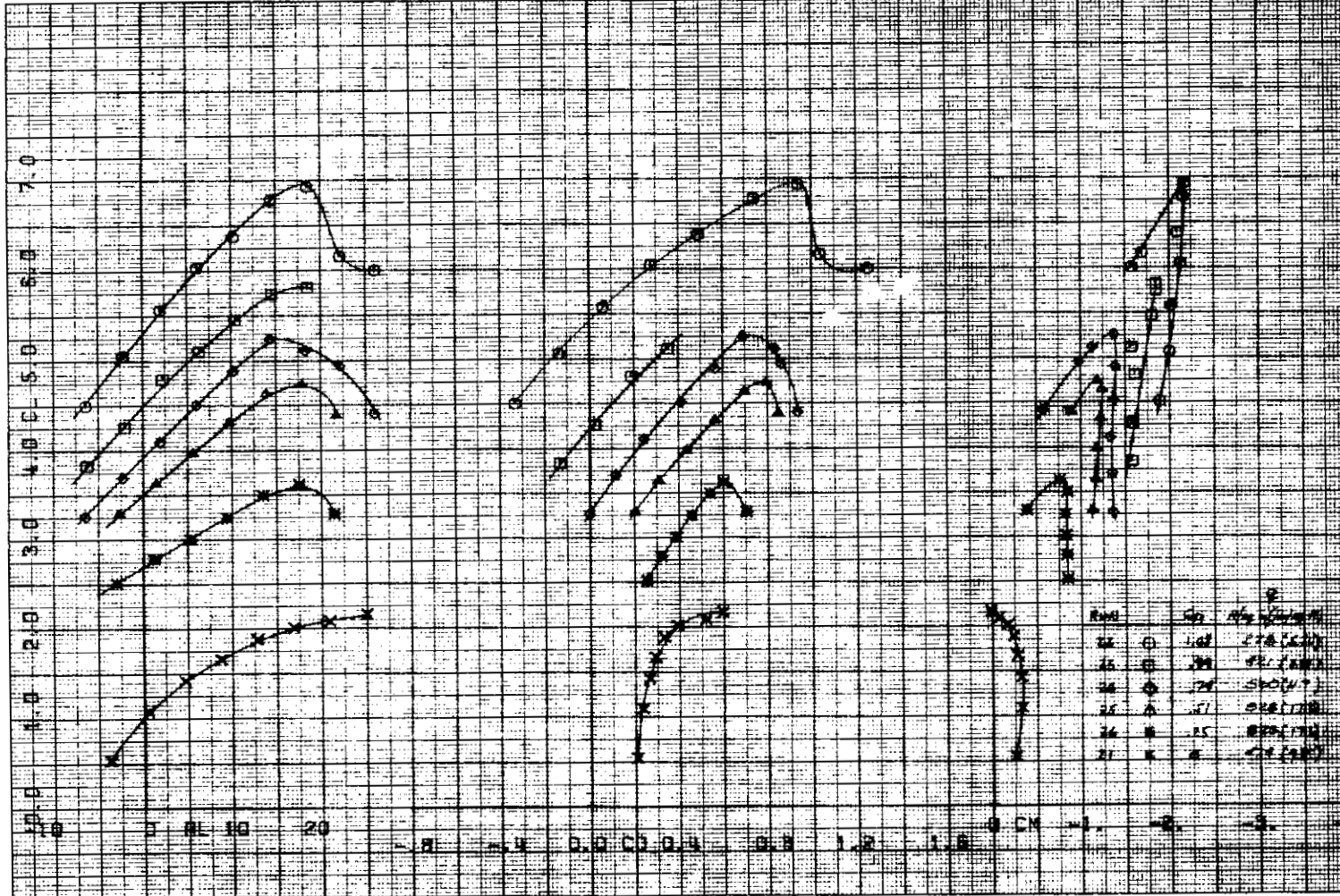
Figure 7. - Continued.

TEST 415. RUN 22. - 26 and 27

COMPLLOT®

OMNIGRAPHIC®

HOUSTON INSTRUMENT
 DIV. OF INTERNATIONAL
 BELLAMY, TEXAS
 CIRCLE 100, P.O. BOX 10000, HOUSTON 20, TEXAS



(c) $\delta_f = 60^\circ/30^\circ$, $\delta_{s1} = 60^\circ$.

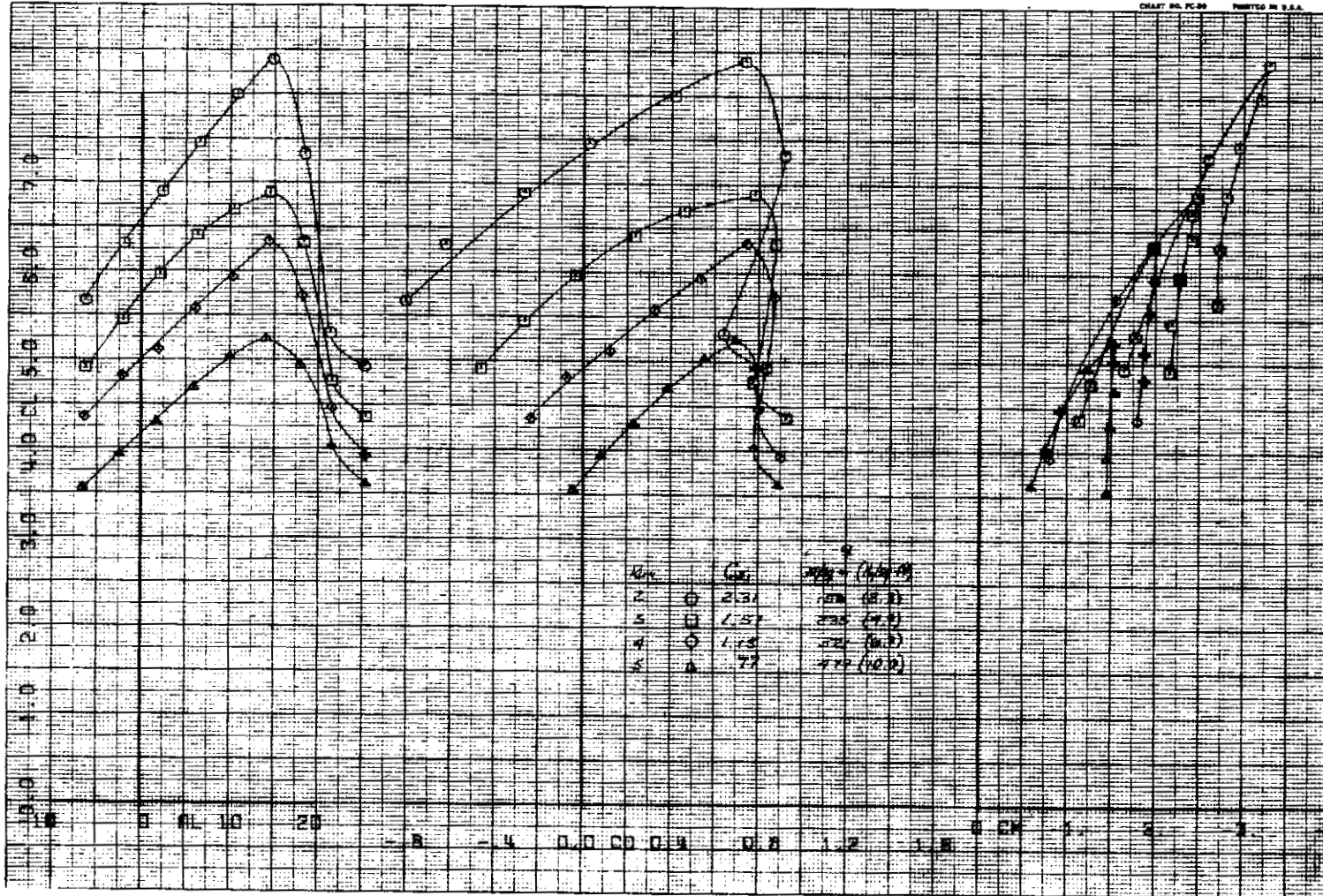
Figure 7. - Continued.

TEST 418. RUN 2.

COMPLLOT

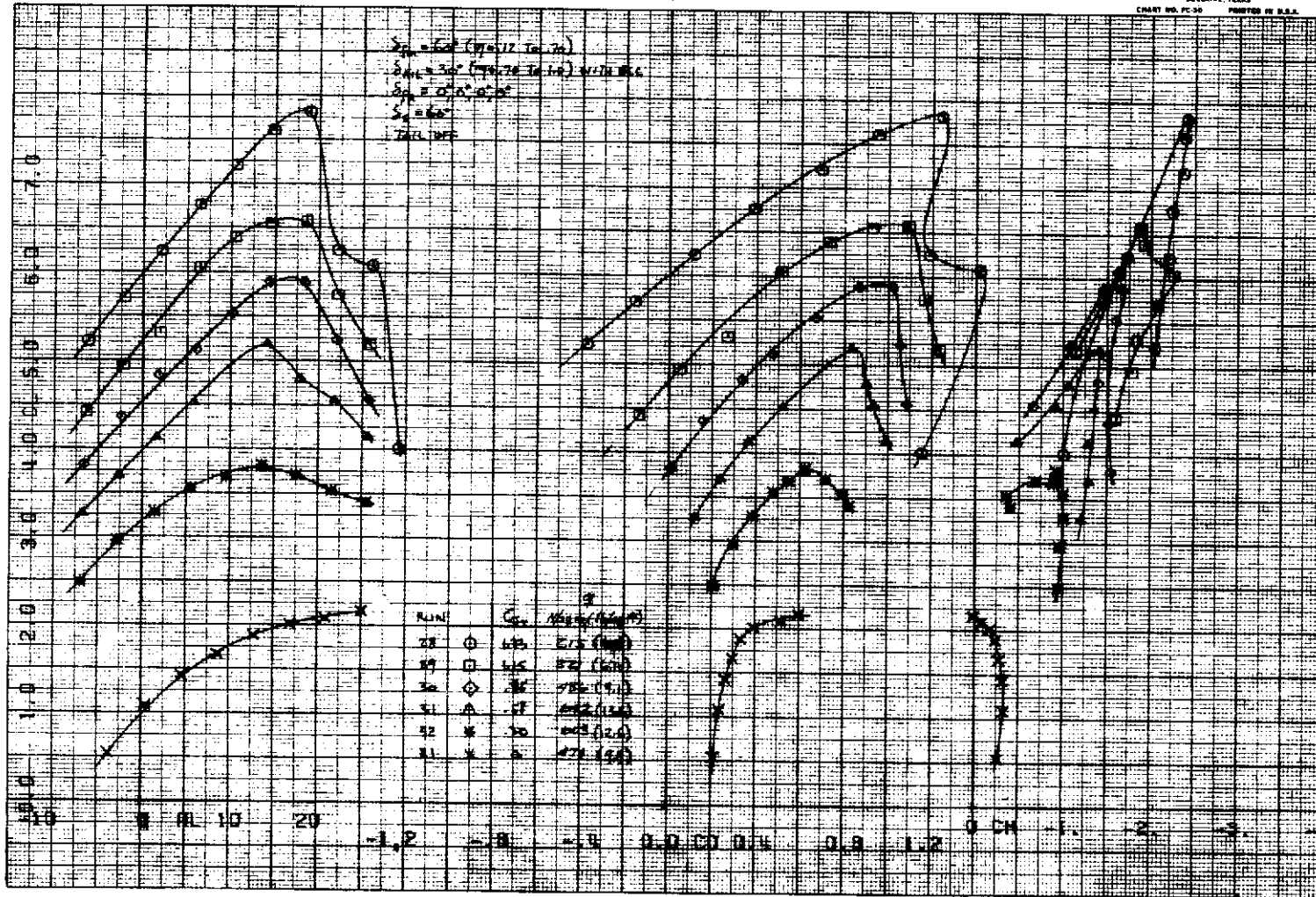
OMNIGRAPHIC

HOUSTON INSTRUMENT
 PELLANDRE TEXAS
 CHART NO. PC-30 PRINTED IN U.S.A.



(d) $\delta_f = 60^\circ/30^\circ$, $\delta_{s_2} = 60^\circ$.

Figure 7. - Concluded.



(a) $\delta_c = 0^\circ$, $\delta_{s1} = 60^\circ$.

Figure 8. — The effect of C_{J1} on the longitudinal characteristics of the model; part-span flap, $\delta_f = 60^\circ$, $\delta_a = 30^\circ$, horizontal tail off.

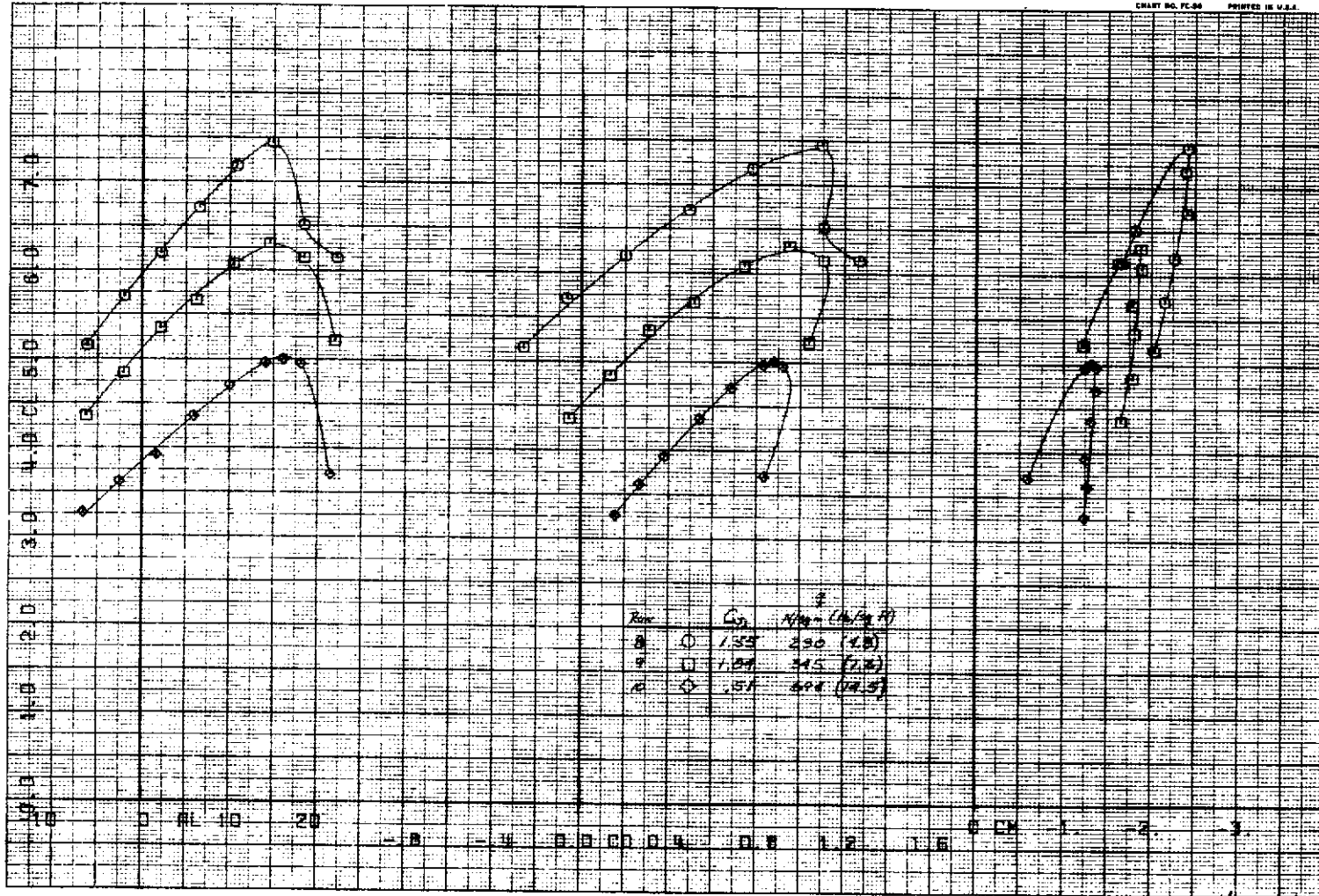
PLOT 2

TEST 418, RUN 8.

COMPLOR

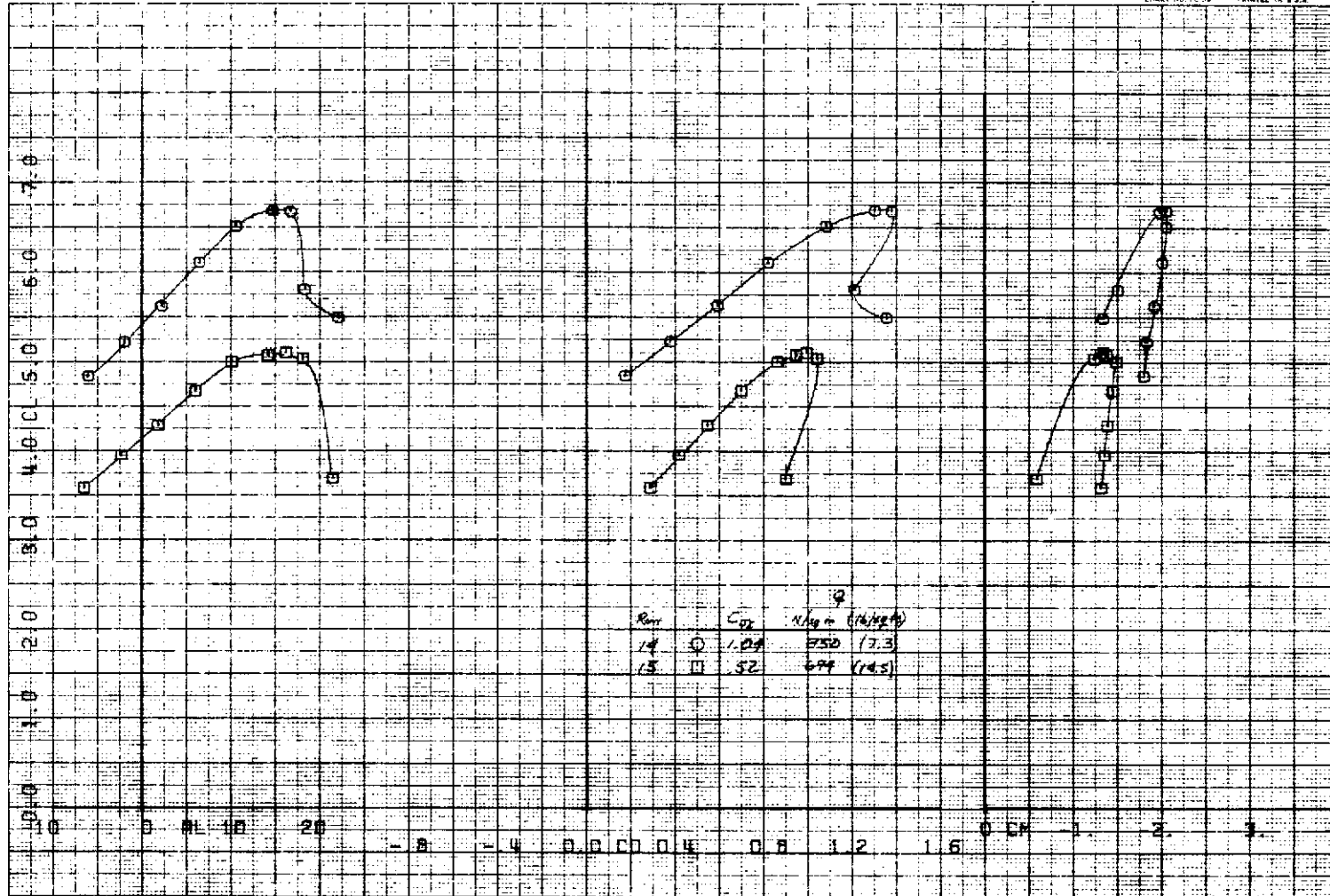
OMNIGRAPHIC

HOUSTON INSTRUMENT
 BELLAIRE TEXAS
 CHART NO. FC-88 PRINTED IN U.S.A.



(b) $\delta_c = 0^\circ$, $\delta_{s_2} = 60^\circ$.

Figure 8. - Continued.



(c) $\delta_c = 10^\circ$, $\delta_{s_2} = 60^\circ$.

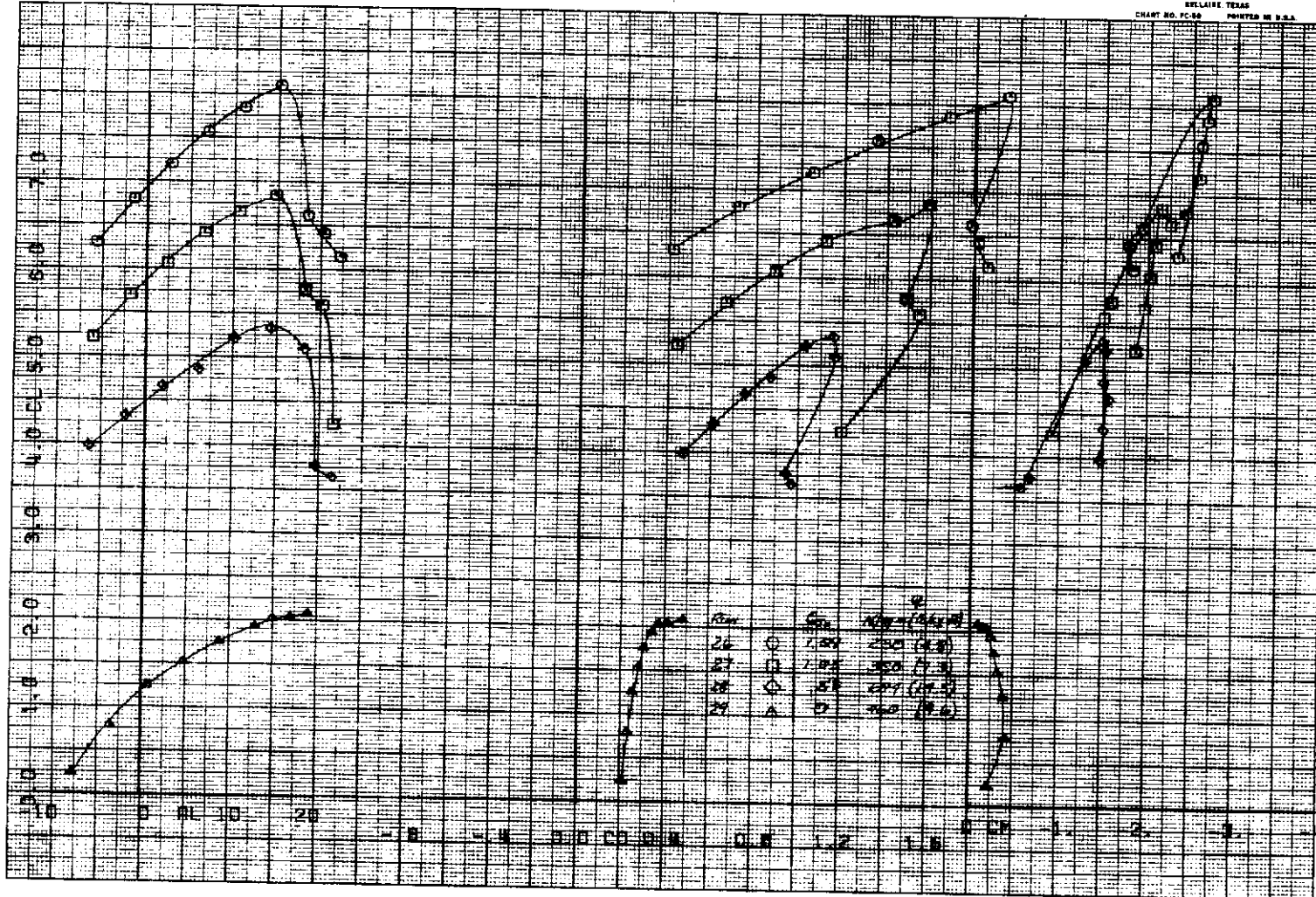
Figure 8. - Continued.

TEST 418. RUN 26.

COMPLLOT

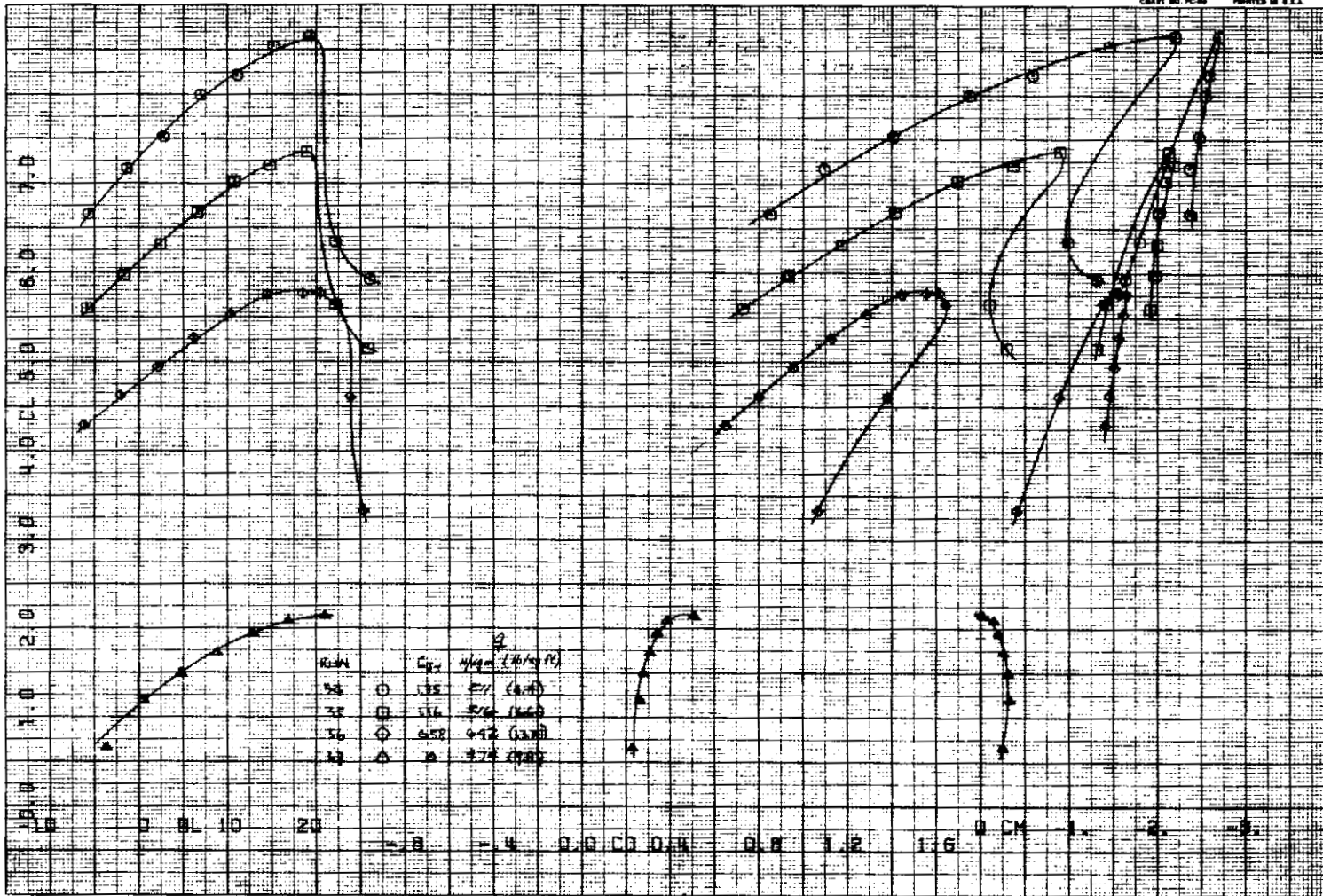
OMNIGRAPHIC

HOUSTON INSTRUMENT
 DIVISION OF
 BELL & HOWELL
 BELLAIRE, TEXAS
 CHART NO. FC-60 PRINTED IN U.S.A.



(d) $\delta_c = 20^\circ$, $\delta_{s_2} = 60^\circ$.

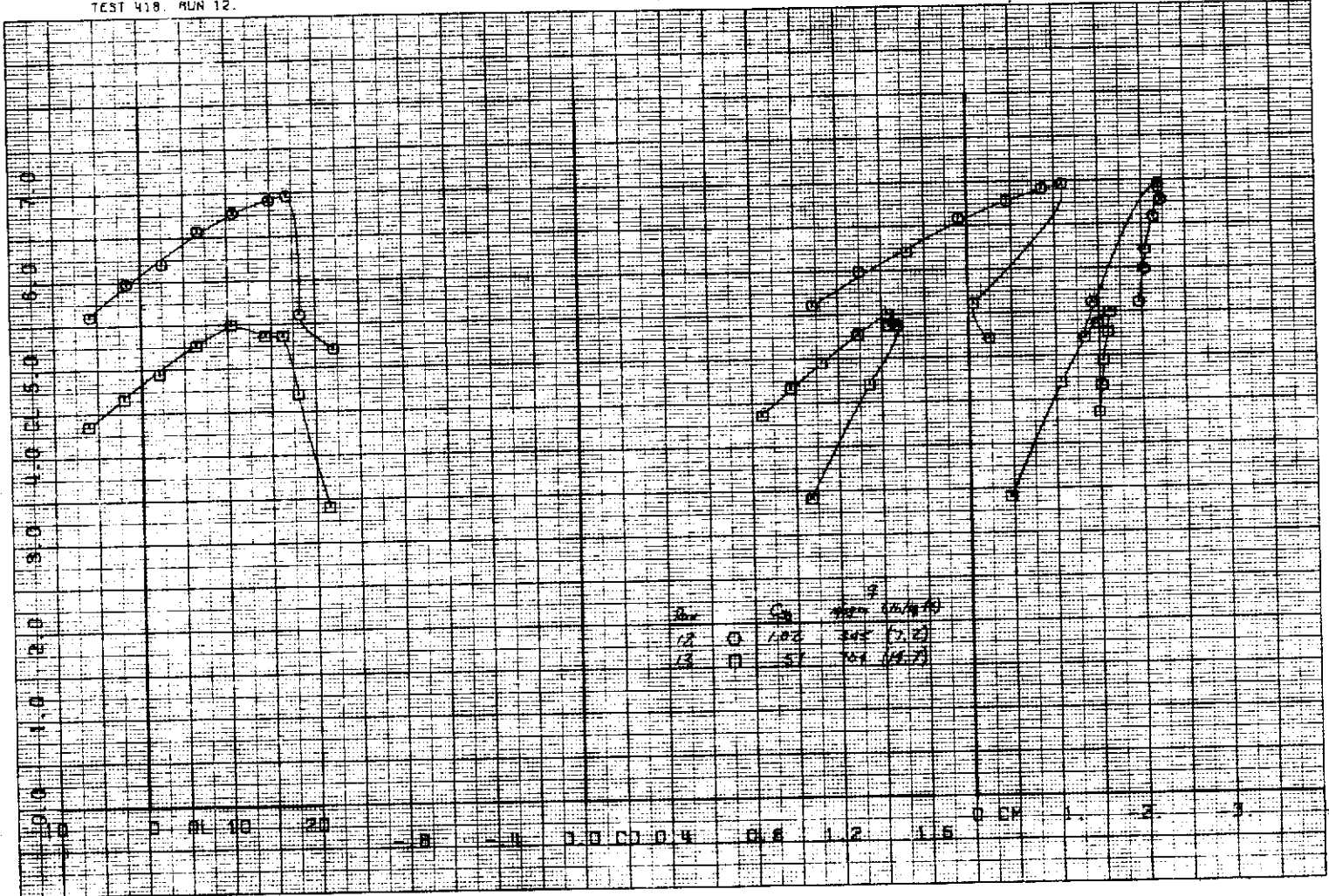
Figure 8. - Continued.



(e) $\delta_c = 30^\circ$, $\delta_{s1} = 60^\circ$.

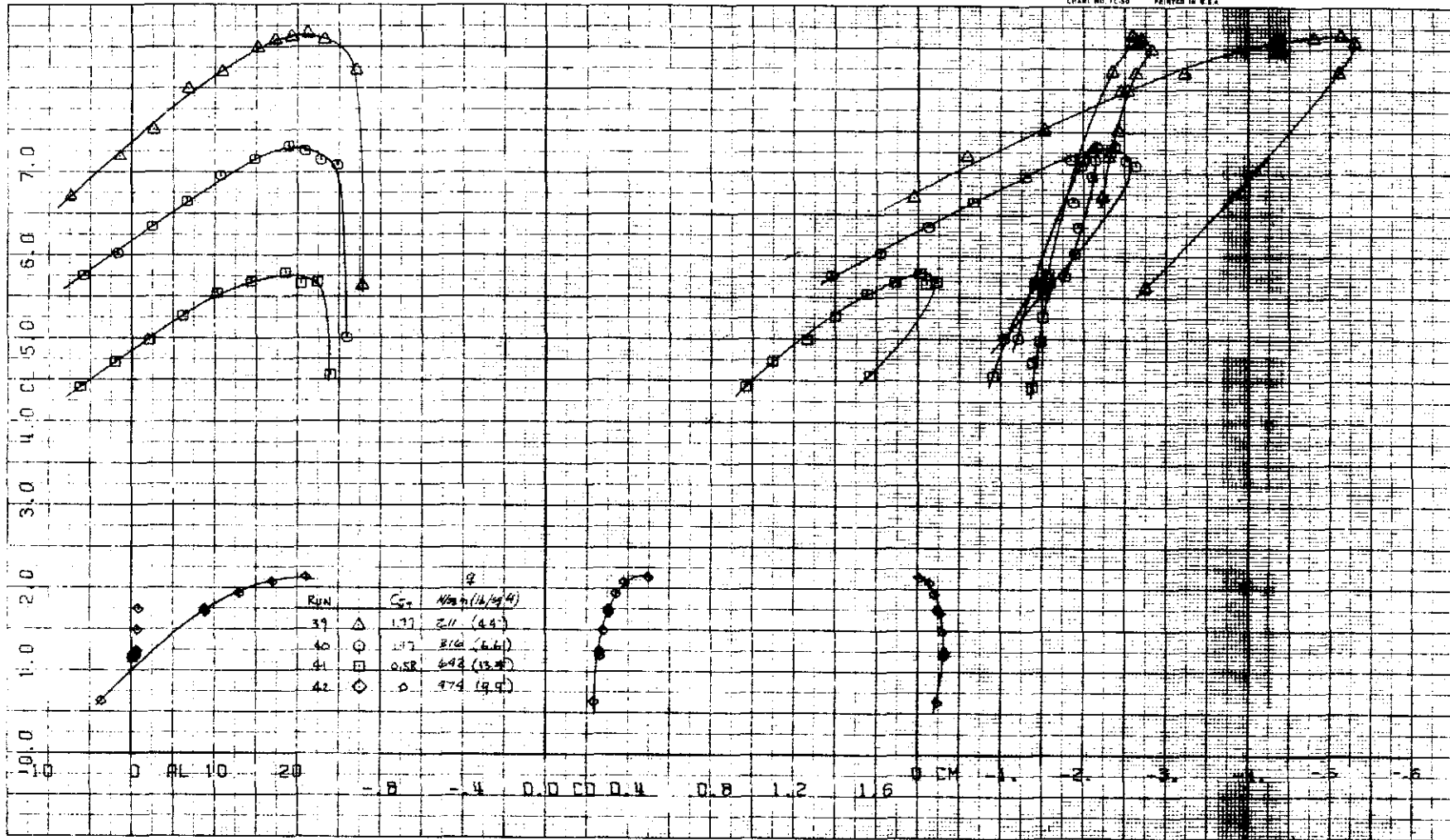
Figure 8. - Continued.

TEST 418. RUN 12.



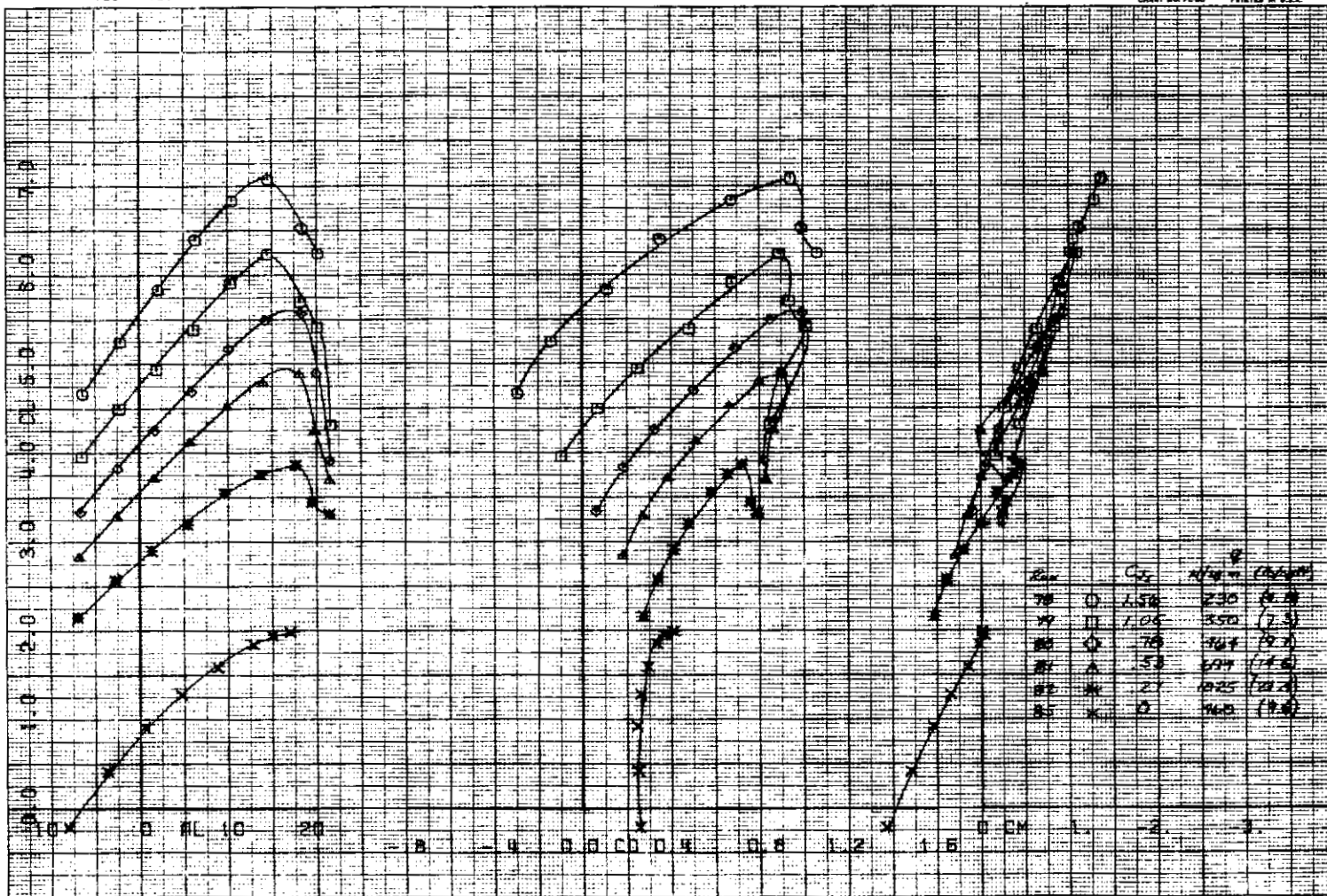
$$(f) \delta_c = 40^\circ, \delta_{s_2} = 60^\circ.$$

Figure 8. - Continued.



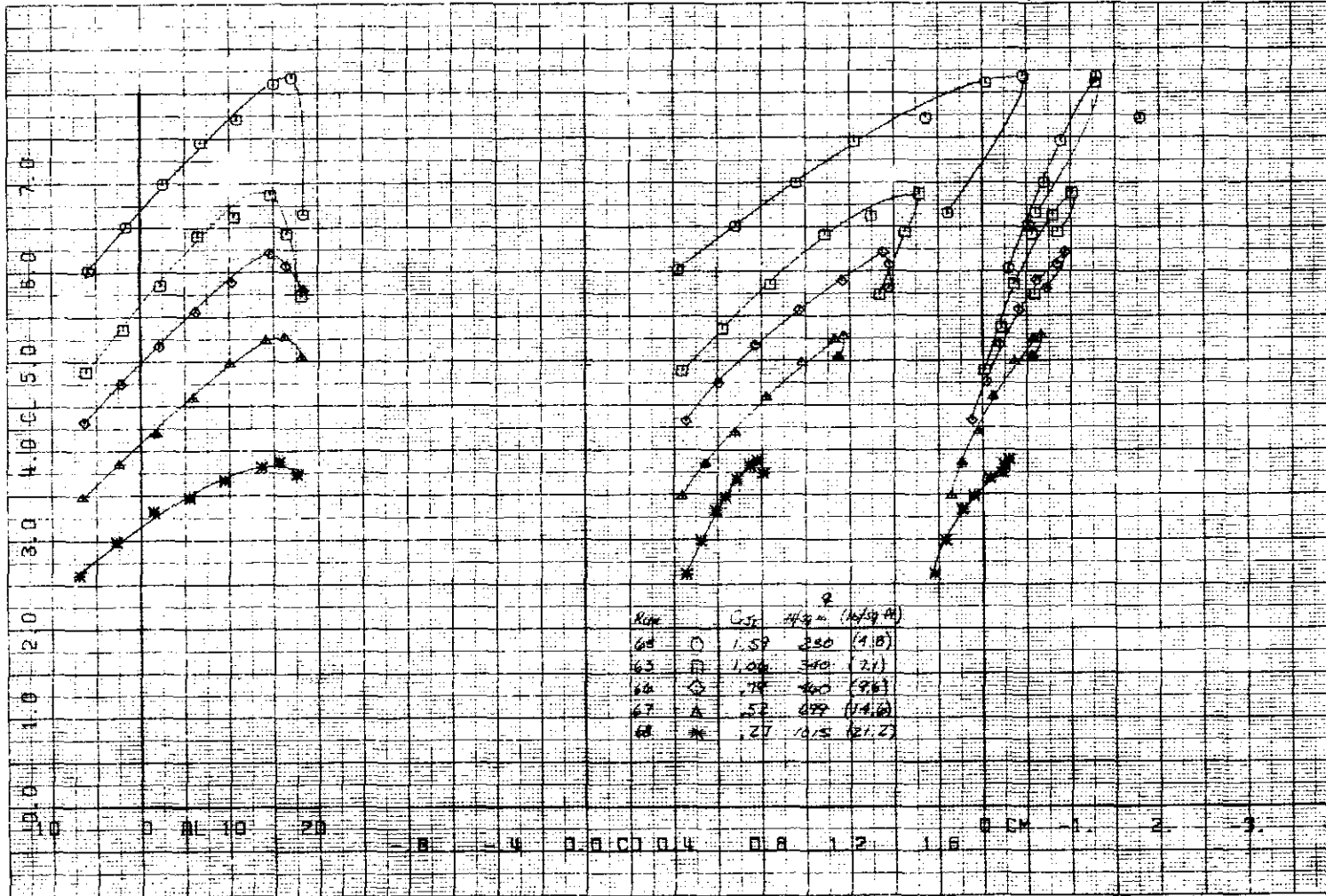
(g) $\delta_c = 50^\circ$, $\delta_{s1} = 60^\circ$.

Figure 8. - Concluded.



(a) $\delta_c = 0^\circ$.

Figure 9. - The effect of C_{J_I} on the longitudinal characteristics of the model; part-span flap, $\delta_f = 60^\circ$, $\delta_a = 30^\circ$, $\delta_{s2} = 60^\circ$, $i_t = -10^\circ$.



(b) $\delta_c = 20^\circ$.

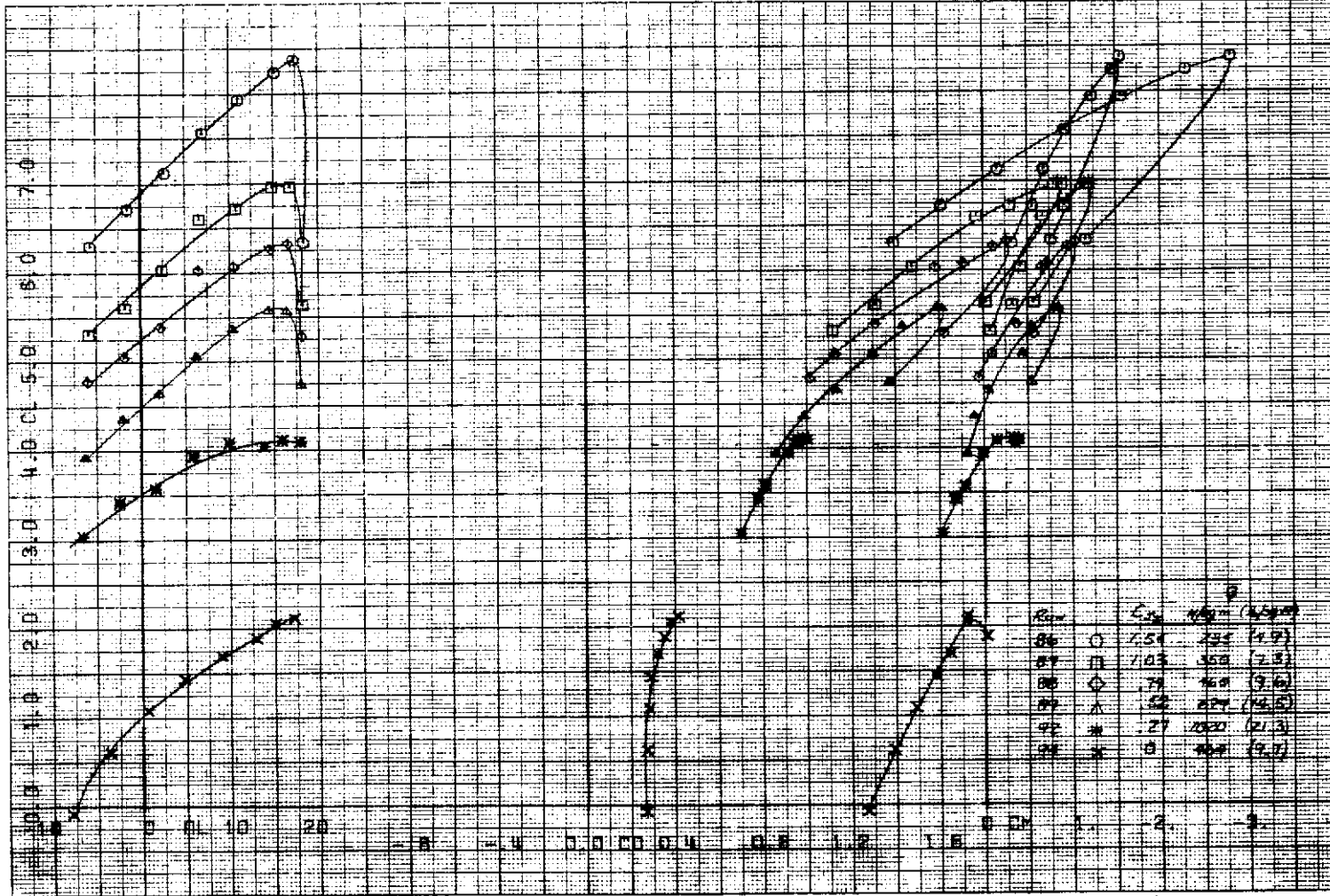
Figure 9. - Continued.

TEST 419. RUN 86

COMPL0T

OMNIGRAPHIC

HOUSTON INSTRUMENT
HOUSTON, TEXAS
 ELLIOTT 1944
 CHART NO. FC 80 PRINTED IN U.S.A.



(c) $\delta_c = 40^\circ$.

Figure 9. - Concluded.

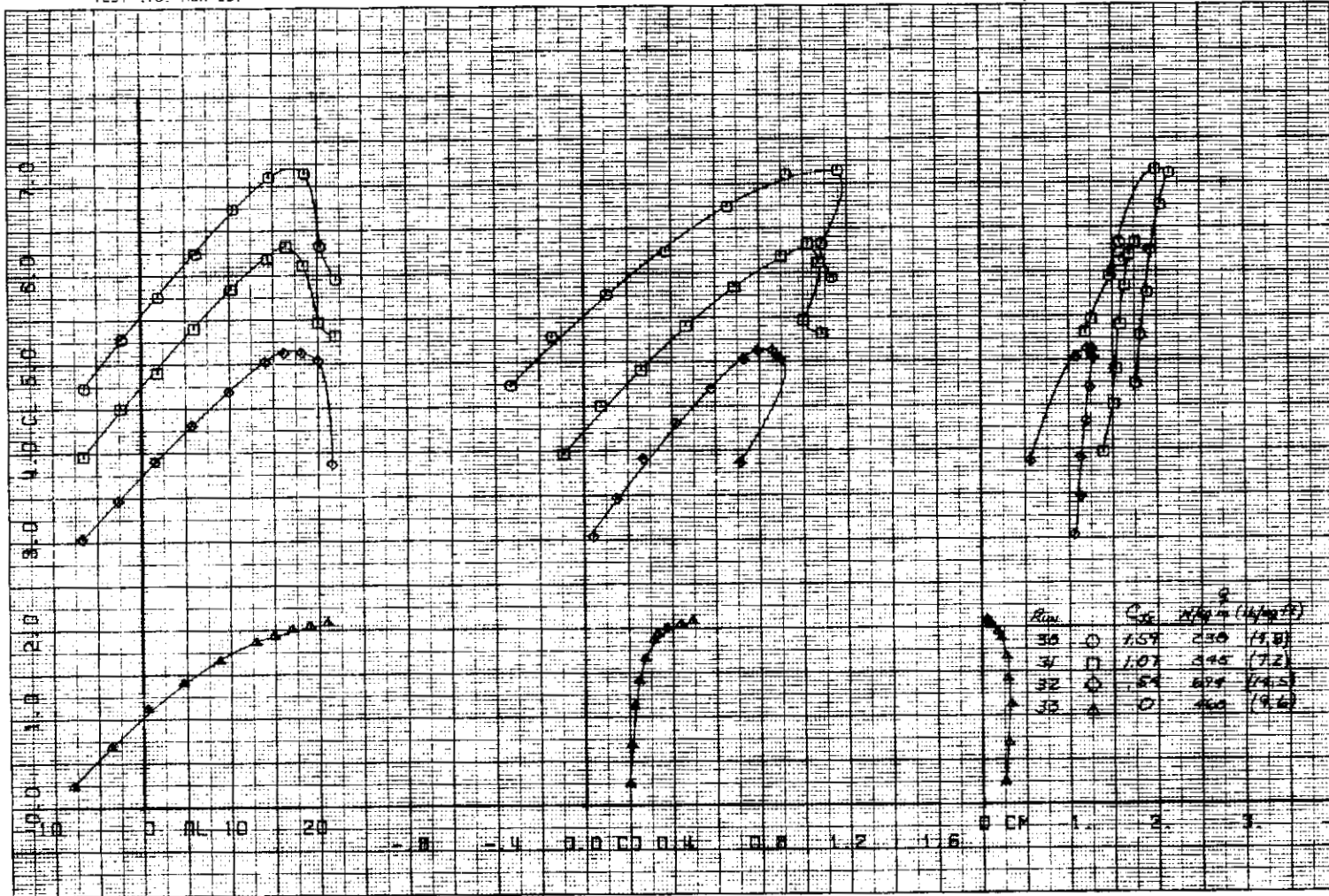


Figure 10. - The effect of C_{J_1} on the longitudinal characteristics of the model; part-span flap, $\delta_f = 60^\circ$, $\delta_a = 10^\circ$, $\delta_{s_2} = 60^\circ$, horizontal tail off.

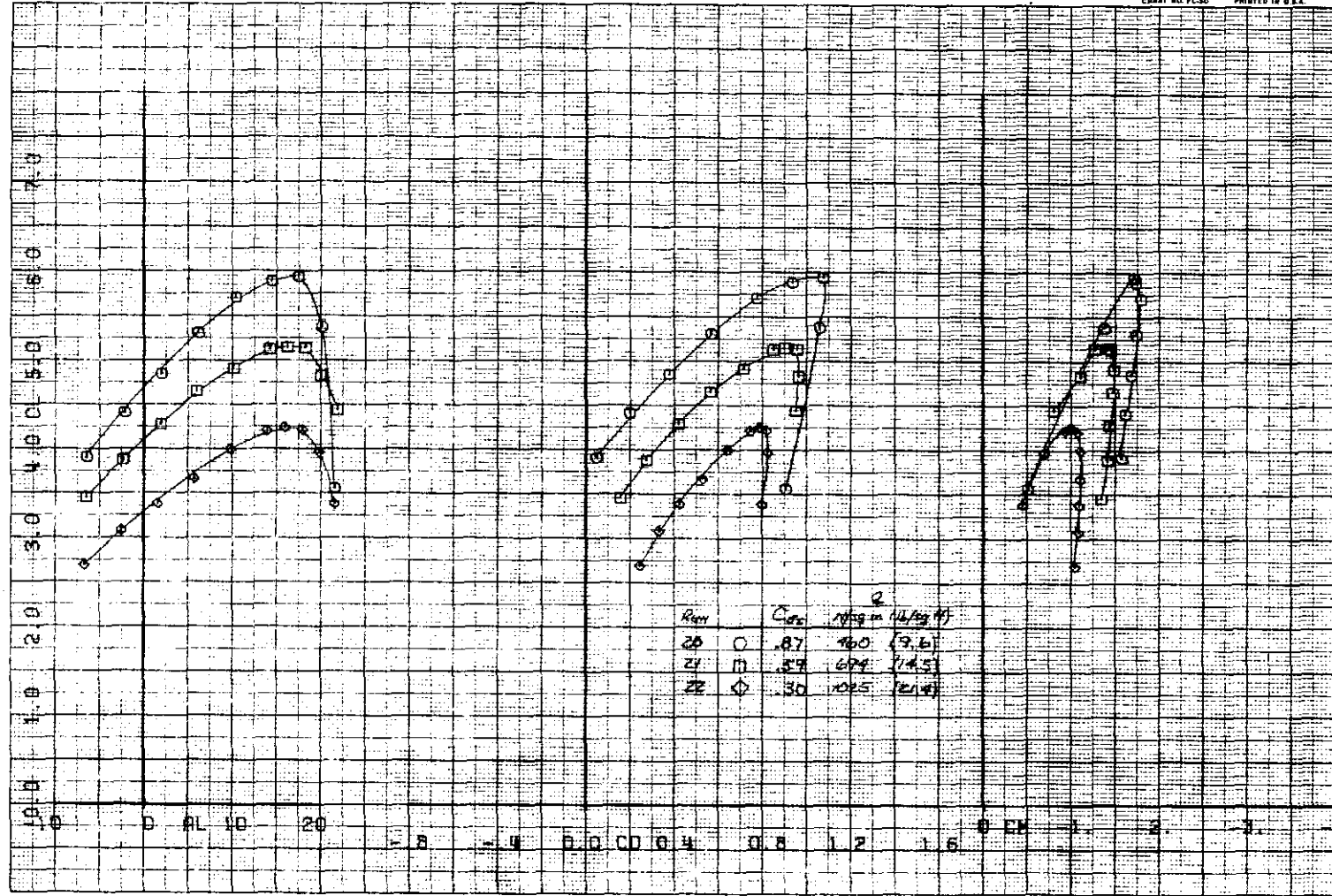


Figure 11. — The effect of C_{J1} on the longitudinal characteristics of the model with twice normal $C_{\mu_{BLC}}$; part-span flap, $\delta_f = 60^\circ$, $\delta_a = 30^\circ$, $\delta_{s2} = 60^\circ$, horizontal tail off.

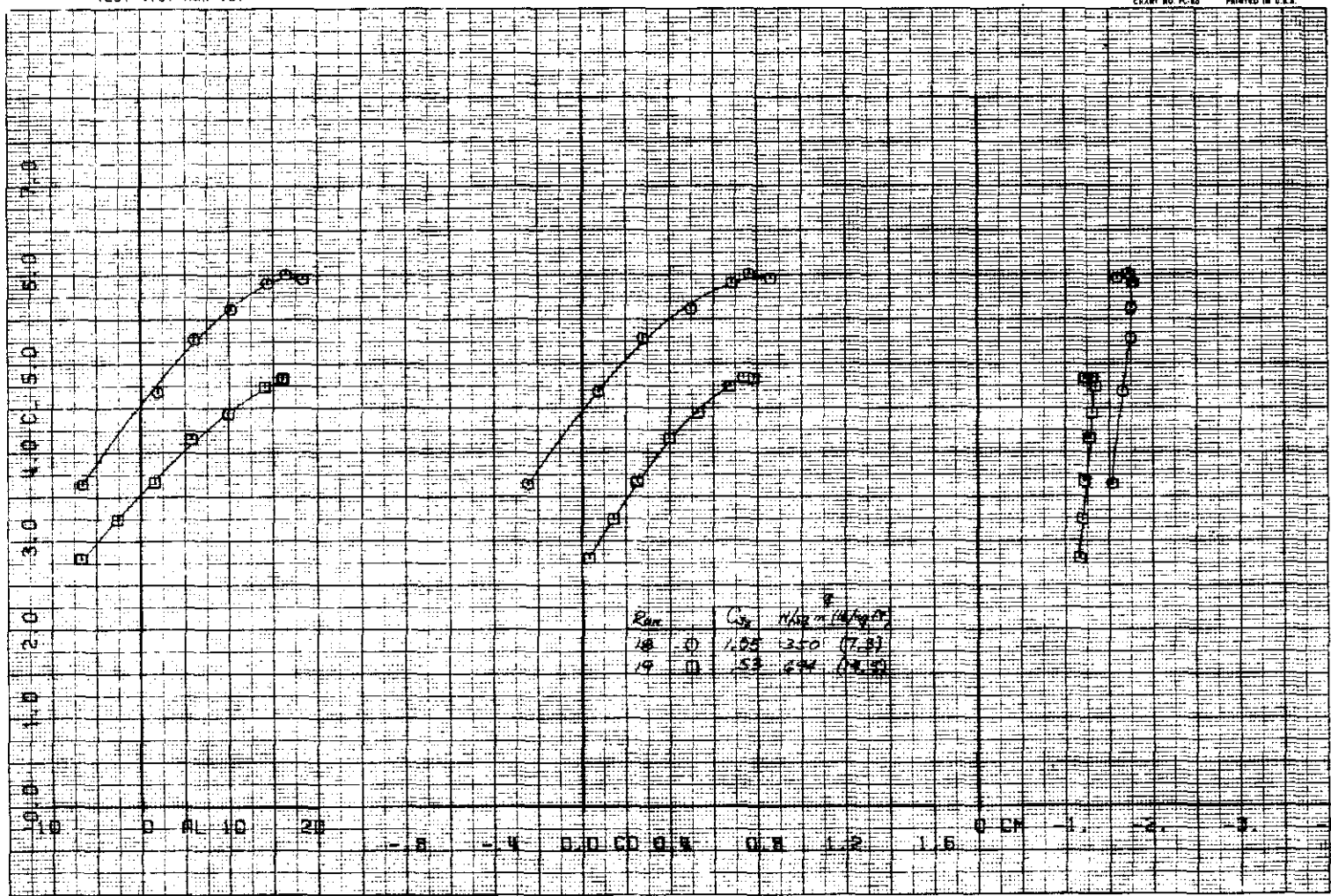
2018

TEST 418. RUN 18.

COMPLOT

OMNIGRAPHIC

HOUSTON INSTRUMENT
DALLAS, TEXAS
CHART NO. FC-80 PRINTED IN U.S.A.



(a) $\delta_c = 0^\circ/-20^\circ$.

Figure 12. - The effect of C_{J_I} on the longitudinal characteristics of the model; part-span flap, $\delta_f = 60^\circ$, $\delta_a = 30^\circ$, $\delta_{s2} = 60^\circ$, horizontal tail off.

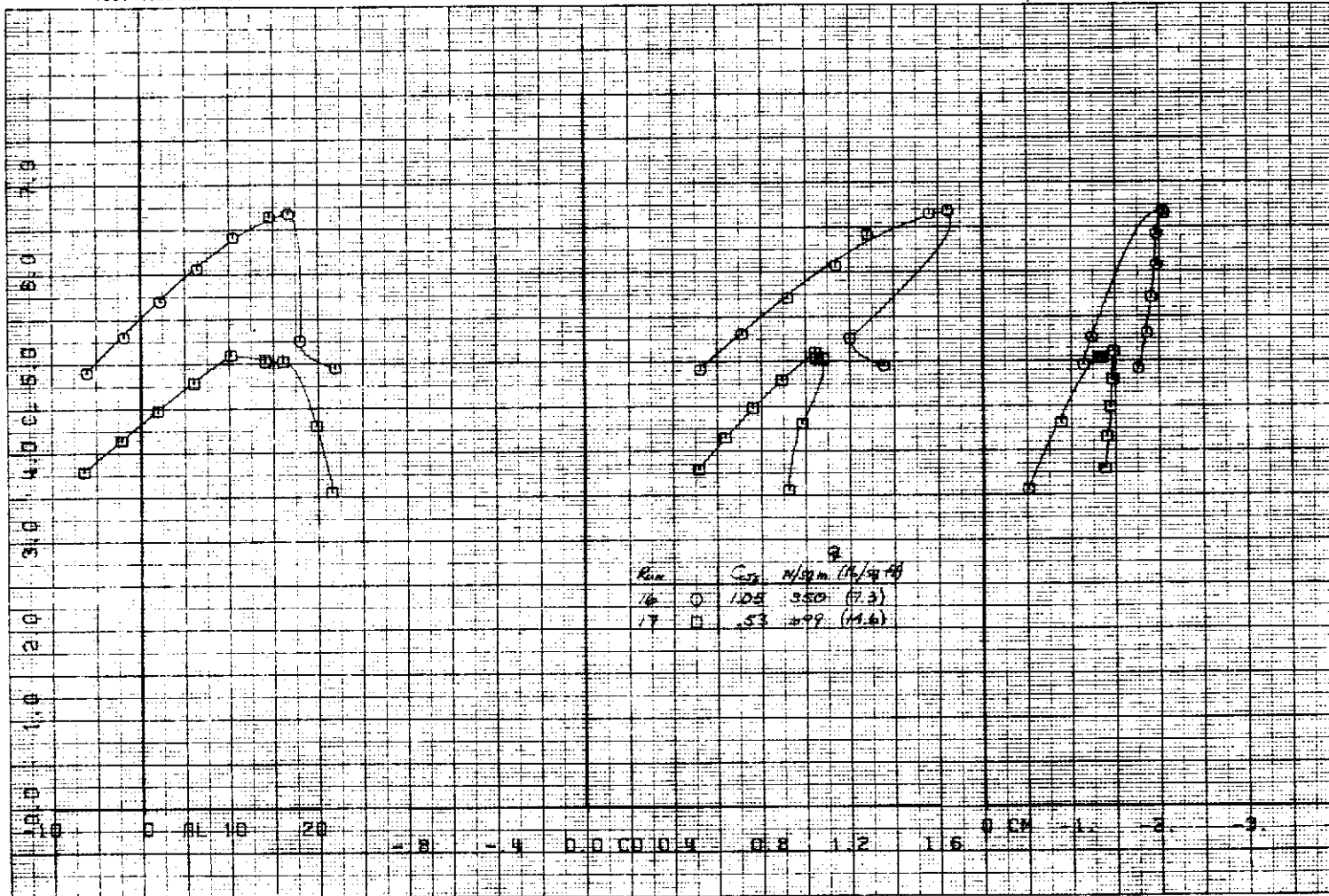
12-14

TEST 418. RUN 16.

COMPLET'

OMNIGRAPHIC'

HOUSTON INSTRUMENT
 1704 N. HOUSTON
 BELLAIRE TEXAS
 CHART NO. FC-80 PRINTED IN U.S.A.



(b) $\delta_c = 0^\circ/40^\circ$.

Figure 12. - Concluded.

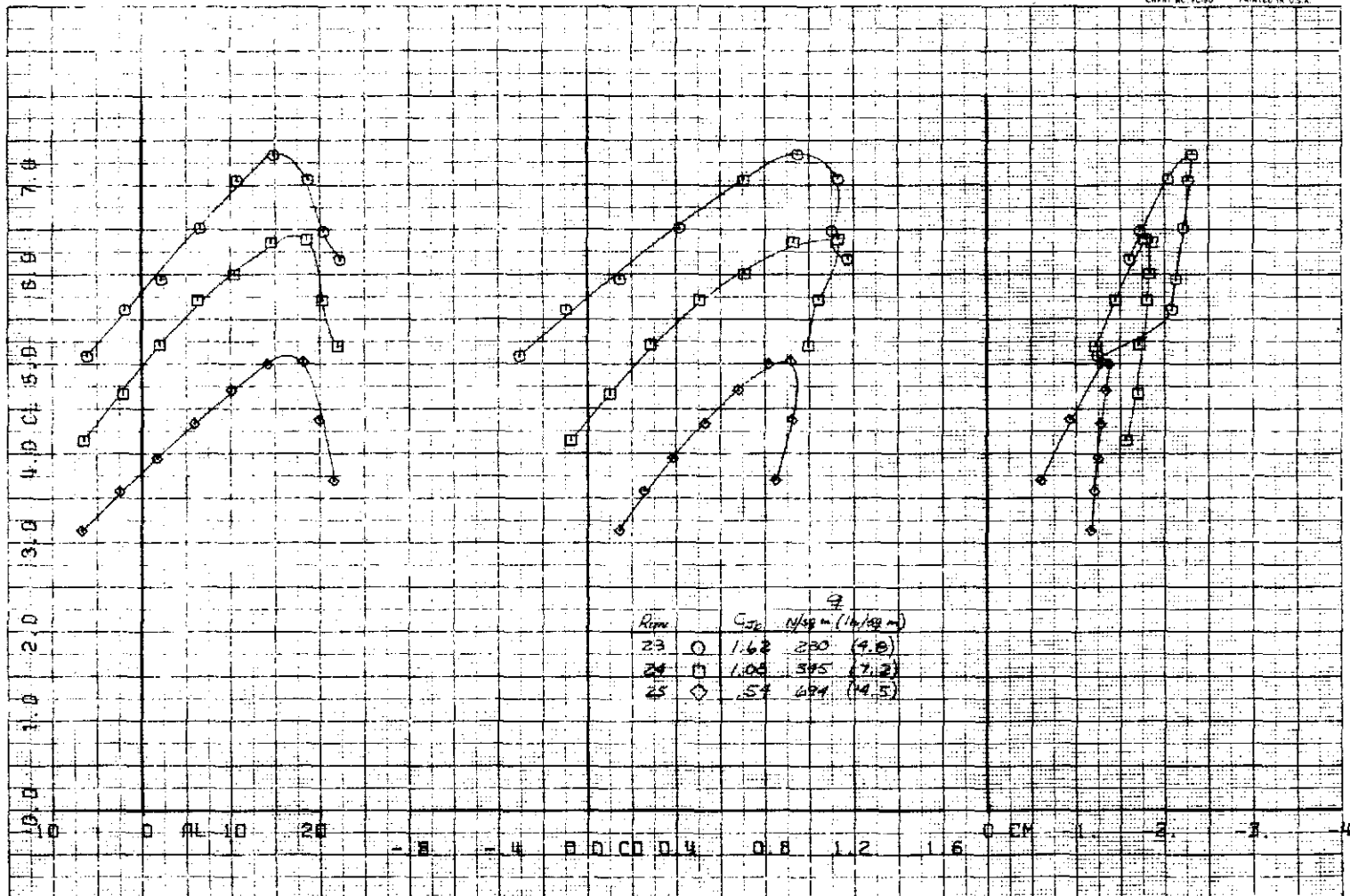
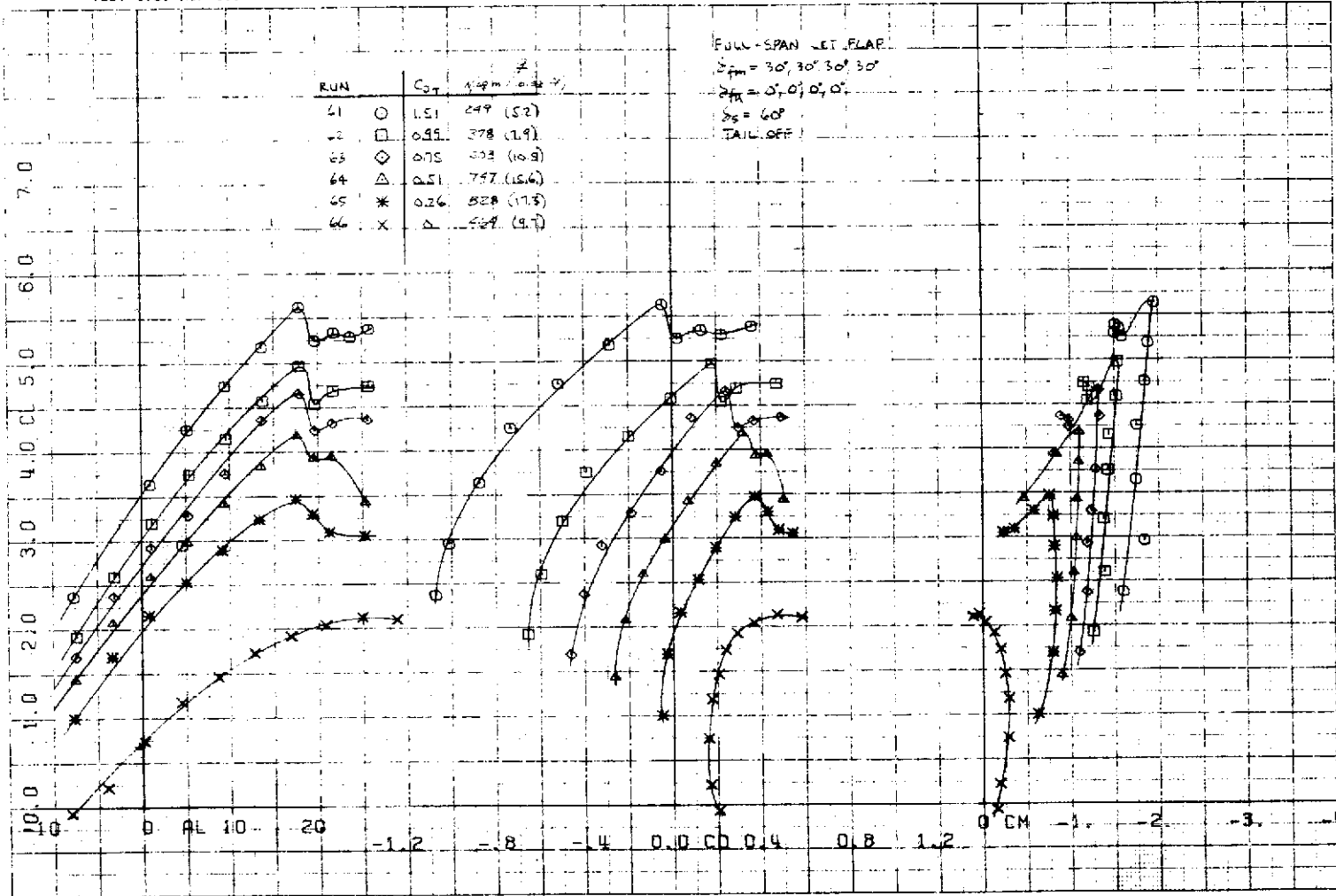


Figure 13. — The effect of C_{J_I} on the longitudinal characteristics of the model; part-span flap, $\delta_f = 60^\circ$, $\delta_a = 30^\circ/10^\circ$, $\delta_c = 0^\circ$, $\delta_{s_2} = 60^\circ$, horizontal tail off.



(a) $\delta_c = 0^\circ$.

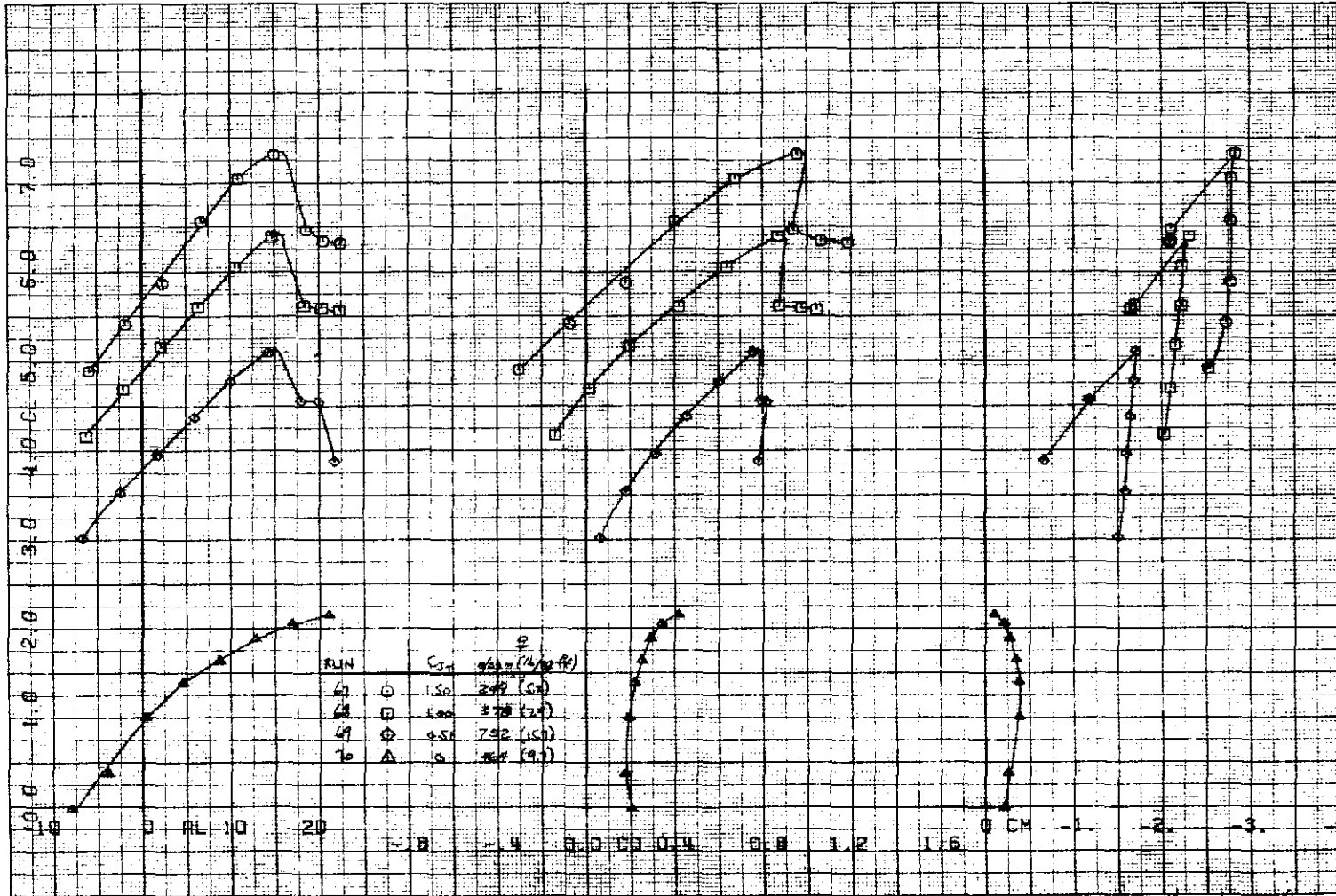
Figure 14. — The effect of C_{J_I} on the longitudinal characteristics of the model; full-span flap, $\delta_f = 30^\circ/30^\circ$, $\delta_{s1} = 60^\circ$, horizontal tail off.

TEST 415. RUN 67.

COMPLET*

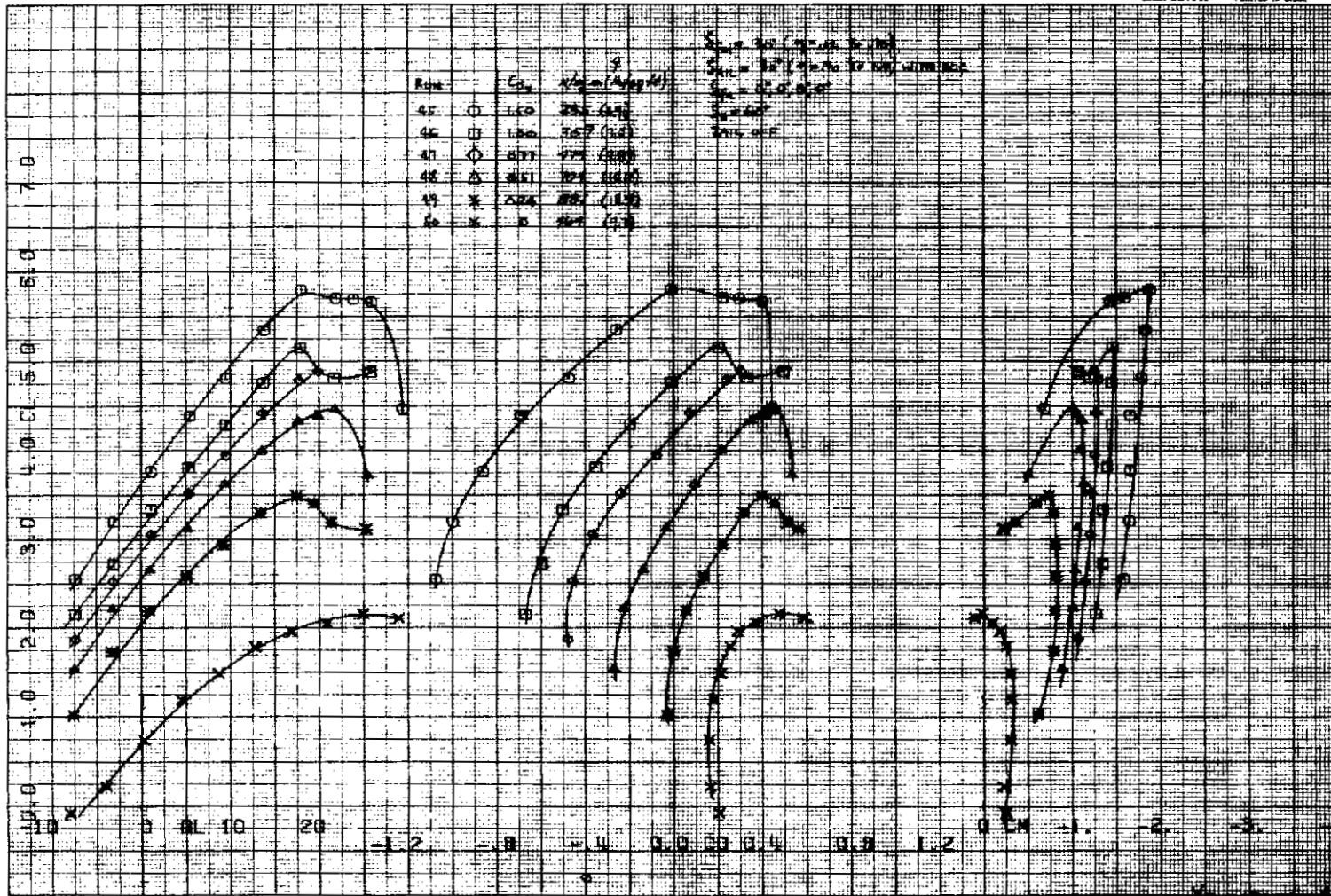
OMNIGRAPHIC*

HOUSTON INSTRUMENT
 BELLEVUE TEXAS
 CHART NO. FC-50 PRINTED IN U.S.A.



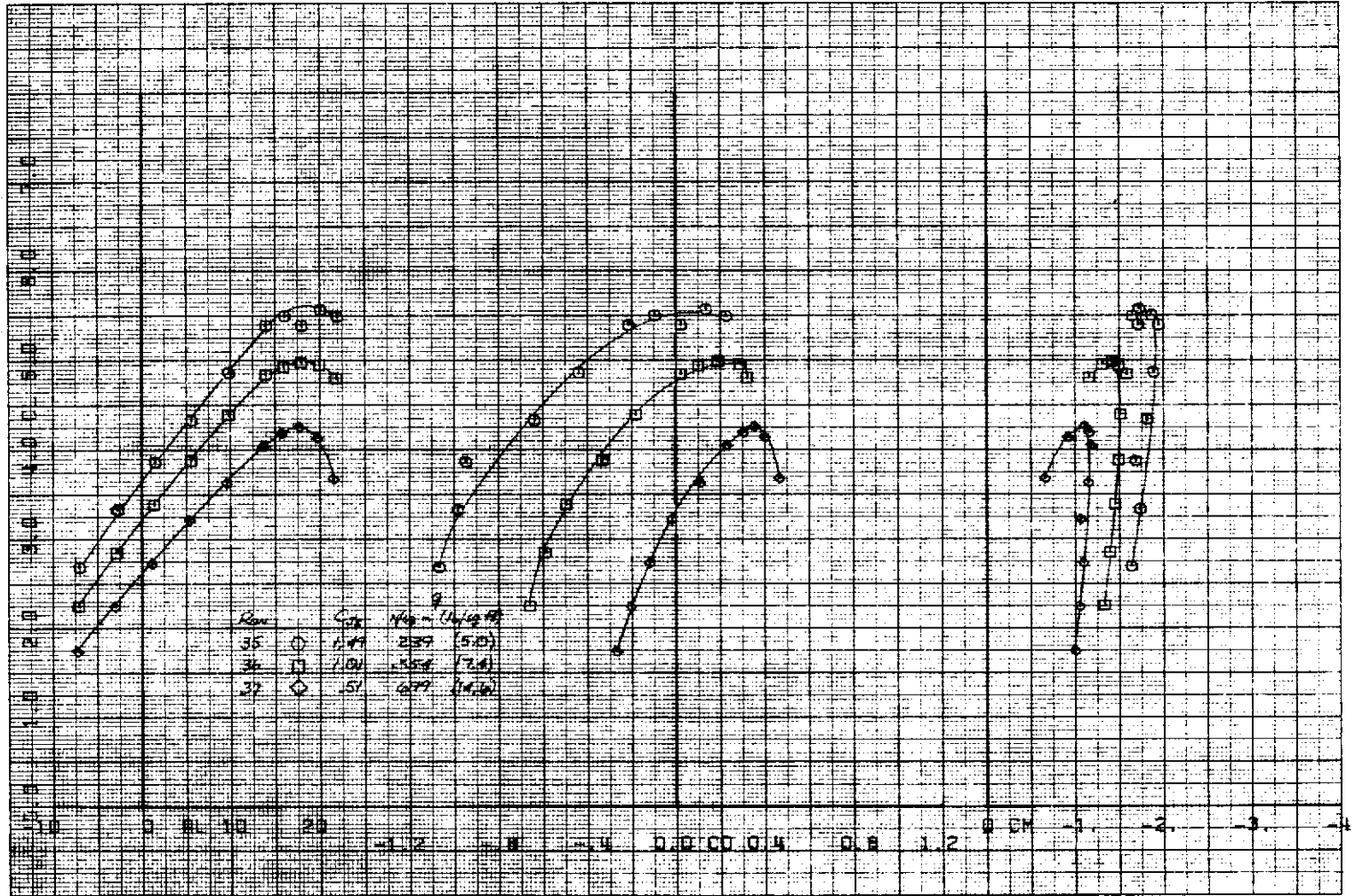
(b) $\delta_c = 30^\circ$.

Figure 14. - Concluded.



(a) $\delta_c = 0^\circ$, $\delta_{s_1} = 60^\circ$.

Figure 15. — The effect of C_{J_I} on the longitudinal characteristics of the model; part-span flap, $\delta_f = 30^\circ$, $\delta_a = 30^\circ$, horizontal tail off.



(b) $\delta_c = 0, \delta_{s_2} = 60^\circ$.

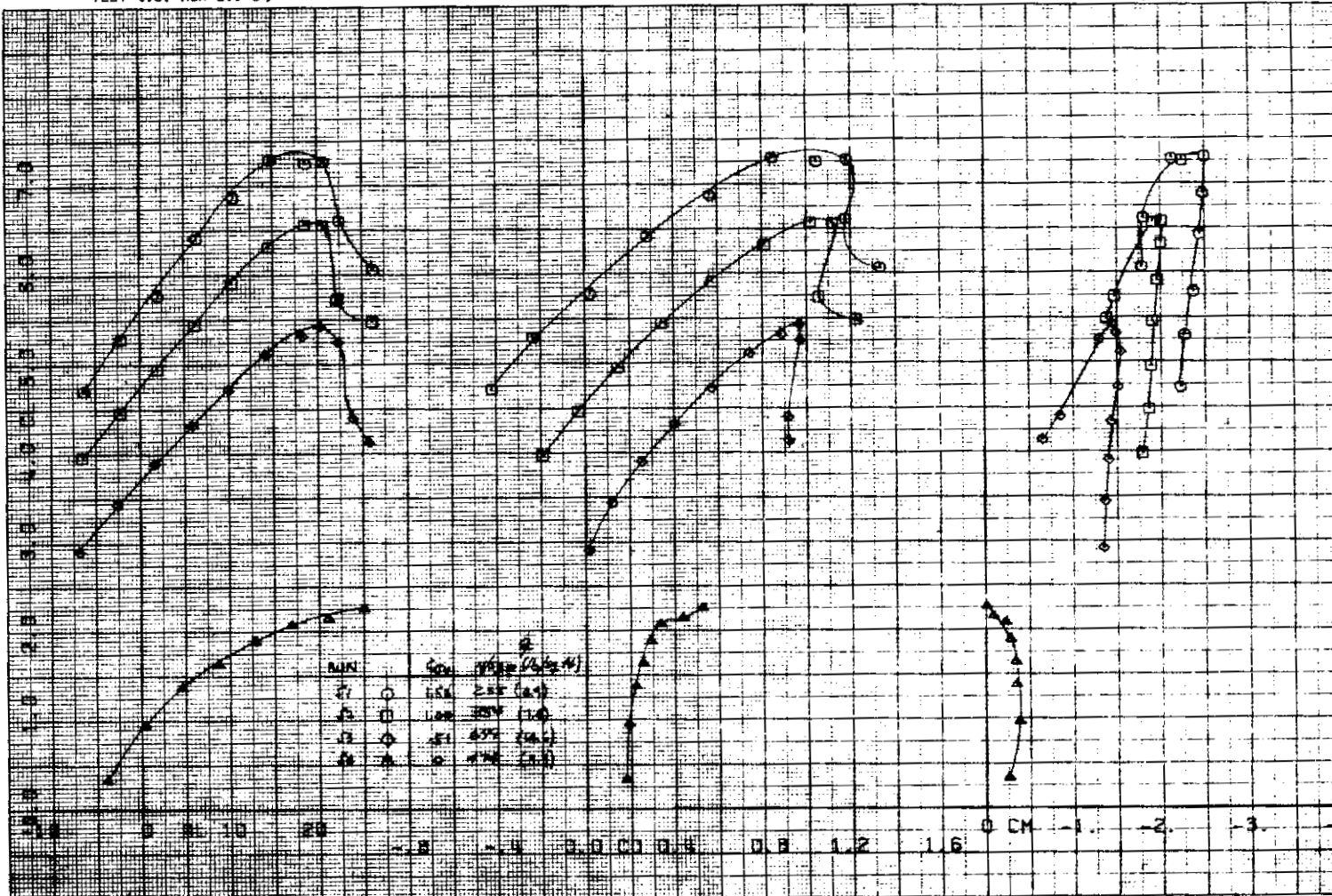
Figure 15. - Continued.

TEST 415. RUN 51.-54

COMPLET®

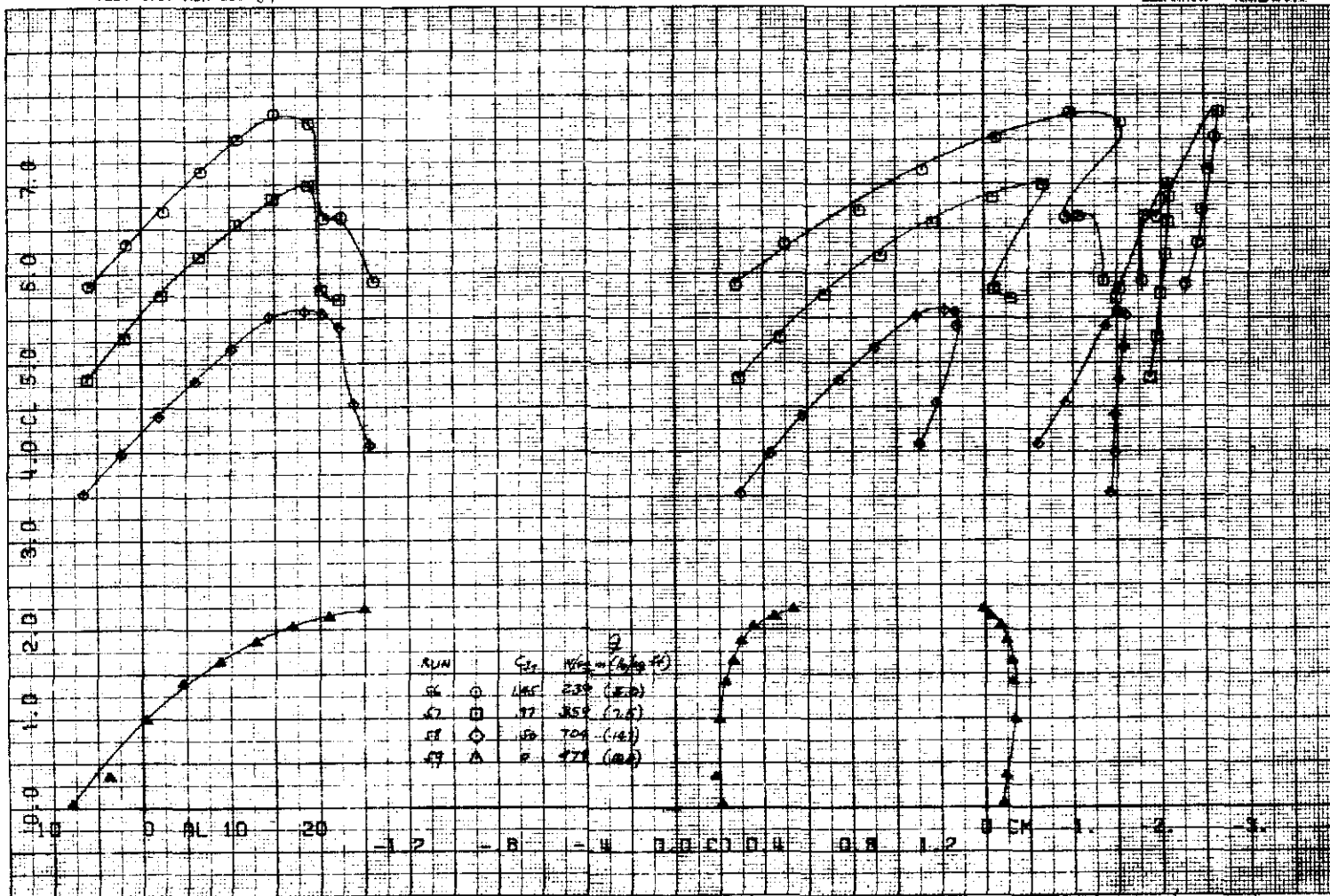
OMNIGRAPHIC®

HOUSTON INSTRUMENT
 BELLAMY YEARS
 CHART NO. PC-30 PRINTED IN U.S.A.



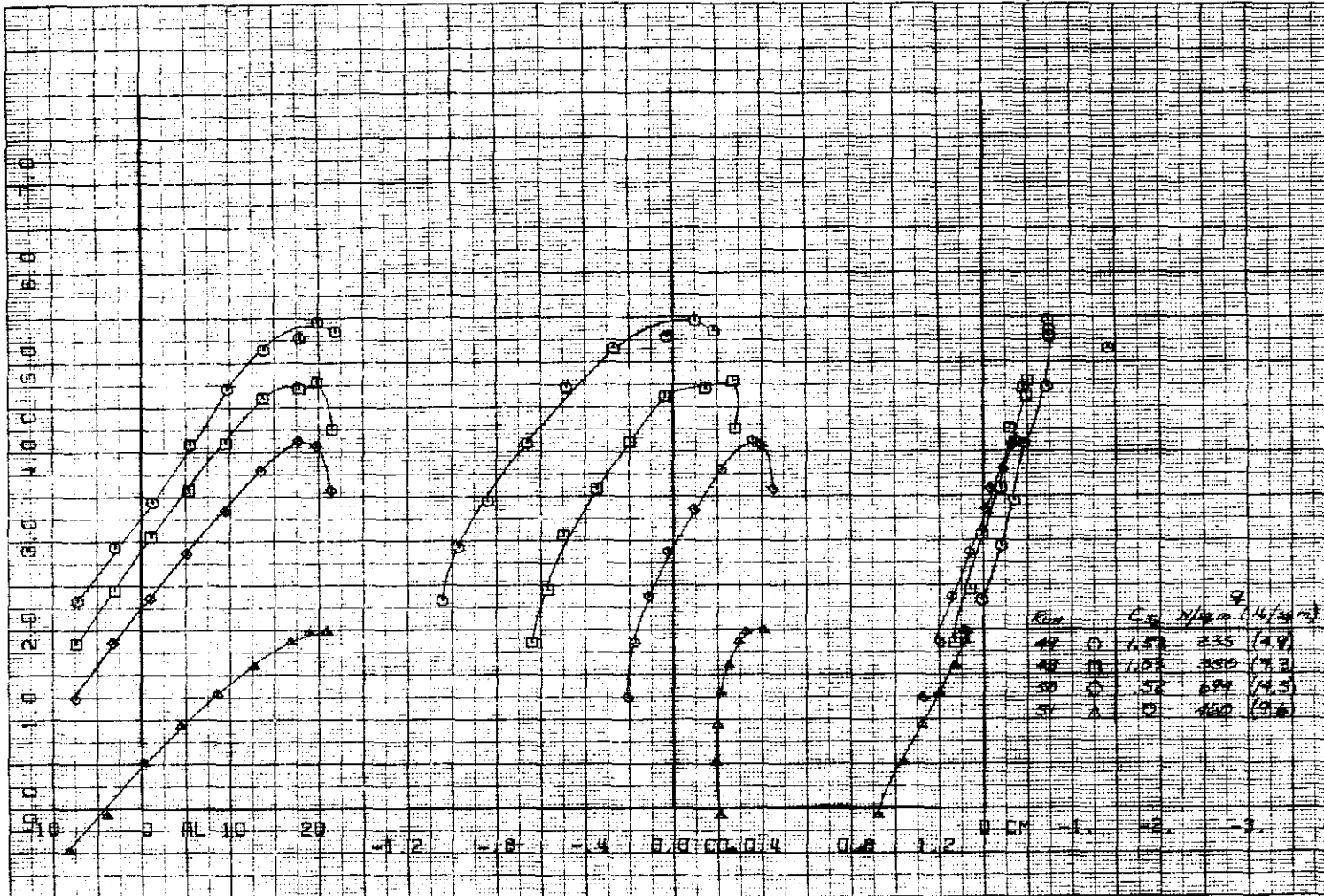
(c) $\delta_c = 30^\circ$, $\delta_{s1} = 60^\circ$.

Figure 15. - Continued.



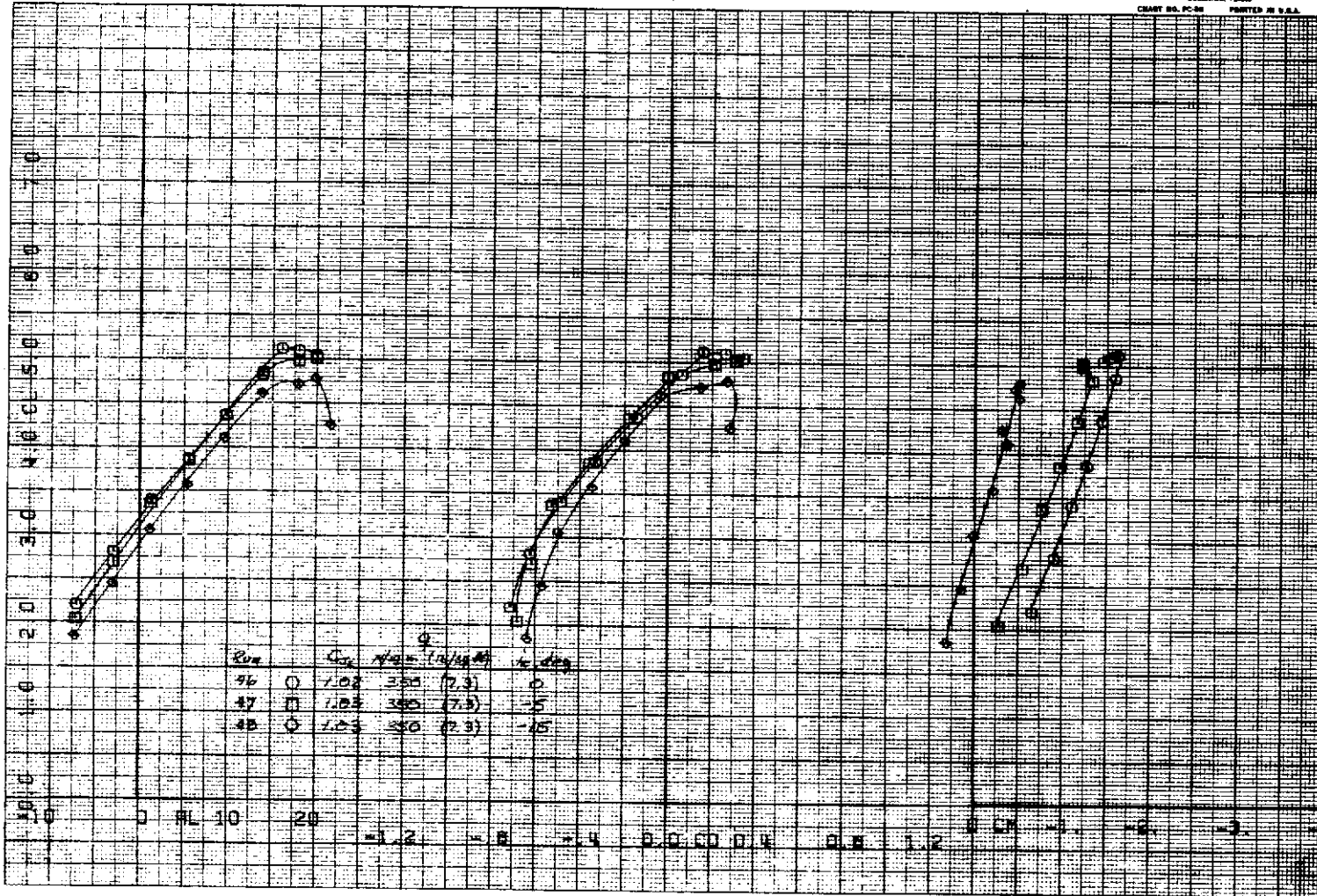
(d) $\delta_c = 50^\circ$, $\delta_{s_1} = 60^\circ$.

Figure 15. - Concluded.



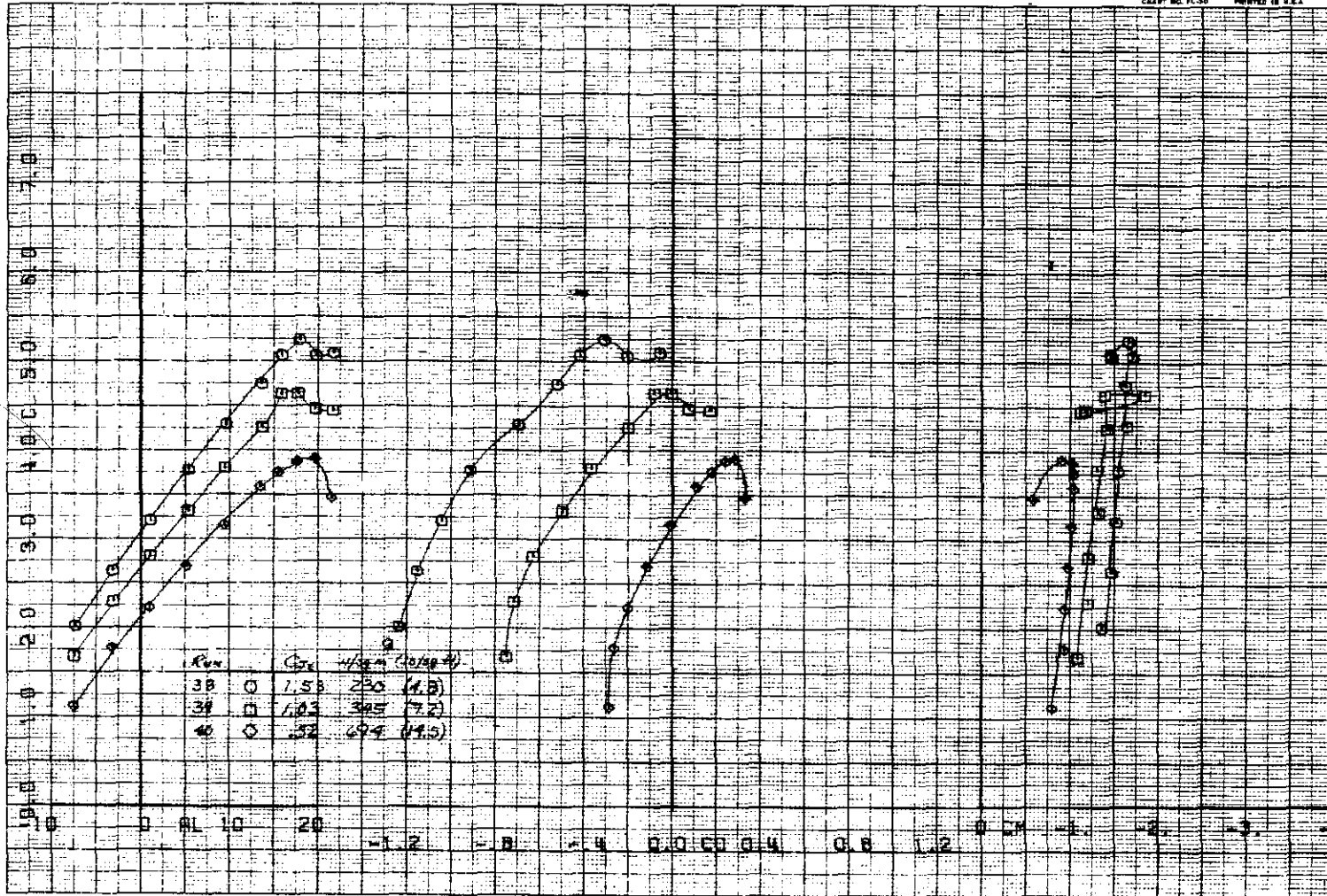
(a) Effect of C_{J_I} ; $i_t = -15$.

Figure 16. — Longitudinal characteristics of the model with the horizontal tail installed; part-span flap, $\delta_f = 30^\circ$, $\delta_a = 30^\circ$, $\delta_c = 0^\circ$, $\delta_{s_2} = 60^\circ$.



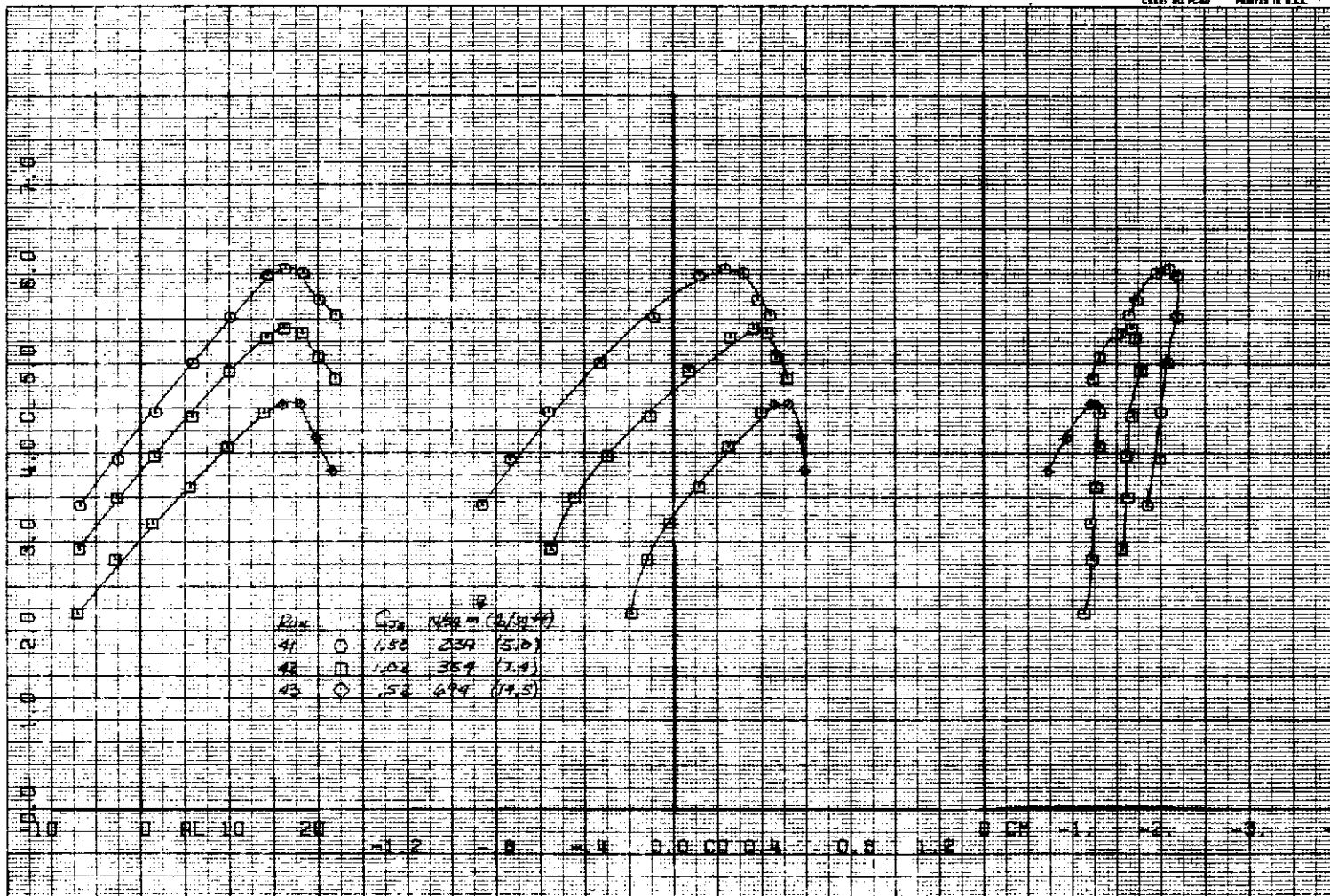
(b) Effect of i_t .

Figure 16. — Concluded.



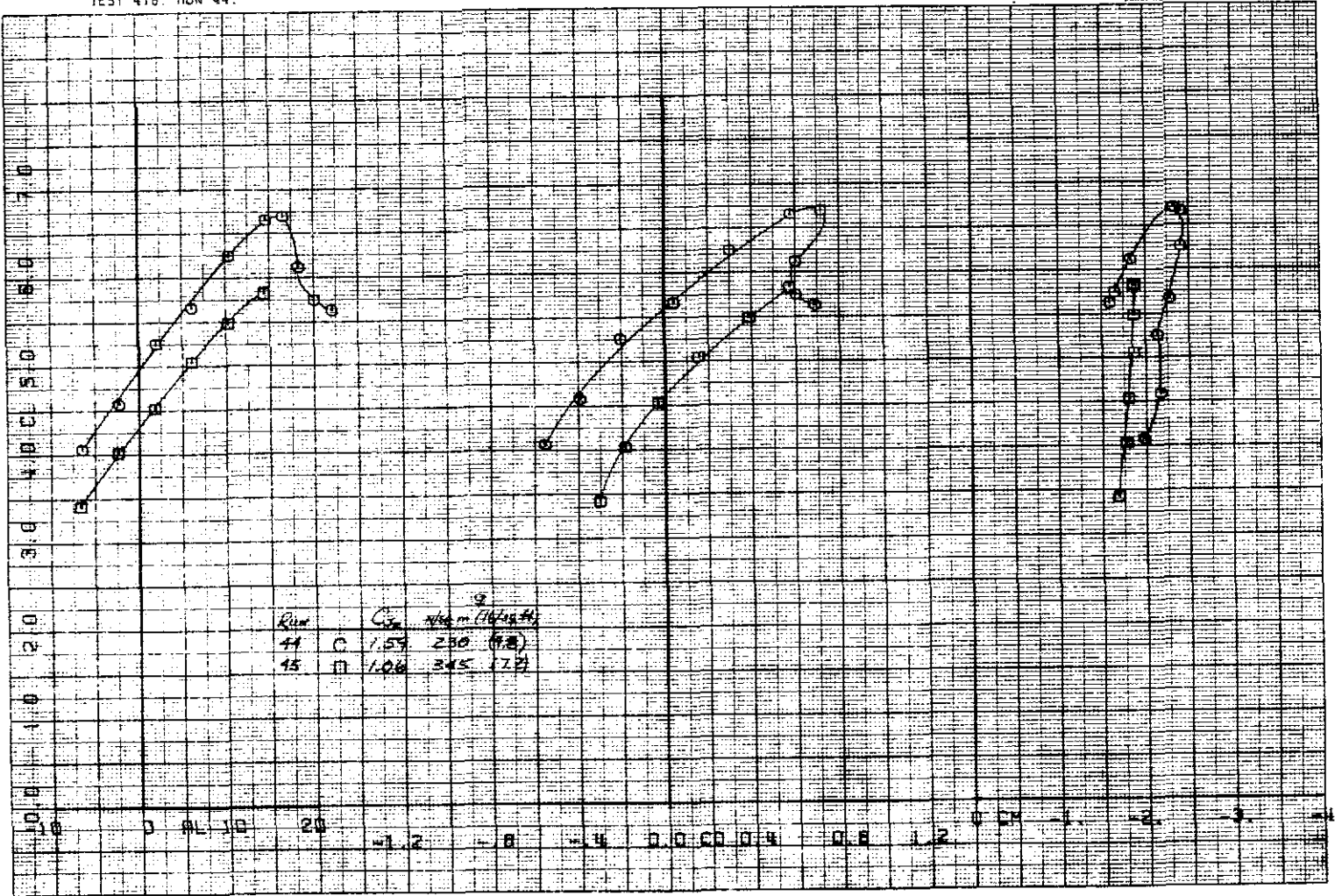
(a) $\delta_c = 0^\circ/-20^\circ$.

Figure 17. — The effect of C_{jI} on the longitudinal characteristics of the model; part-span flap, $\delta_f = 30^\circ$, $\delta_a = 30^\circ$, $\delta_{s2} = 60^\circ$, horizontal tail off.



(b) $\delta_c = 0^\circ/20^\circ$.

Figure 17. - Continued.



(c) $\delta_c = 0^\circ/40^\circ$.

Figure 17. - Concluded.

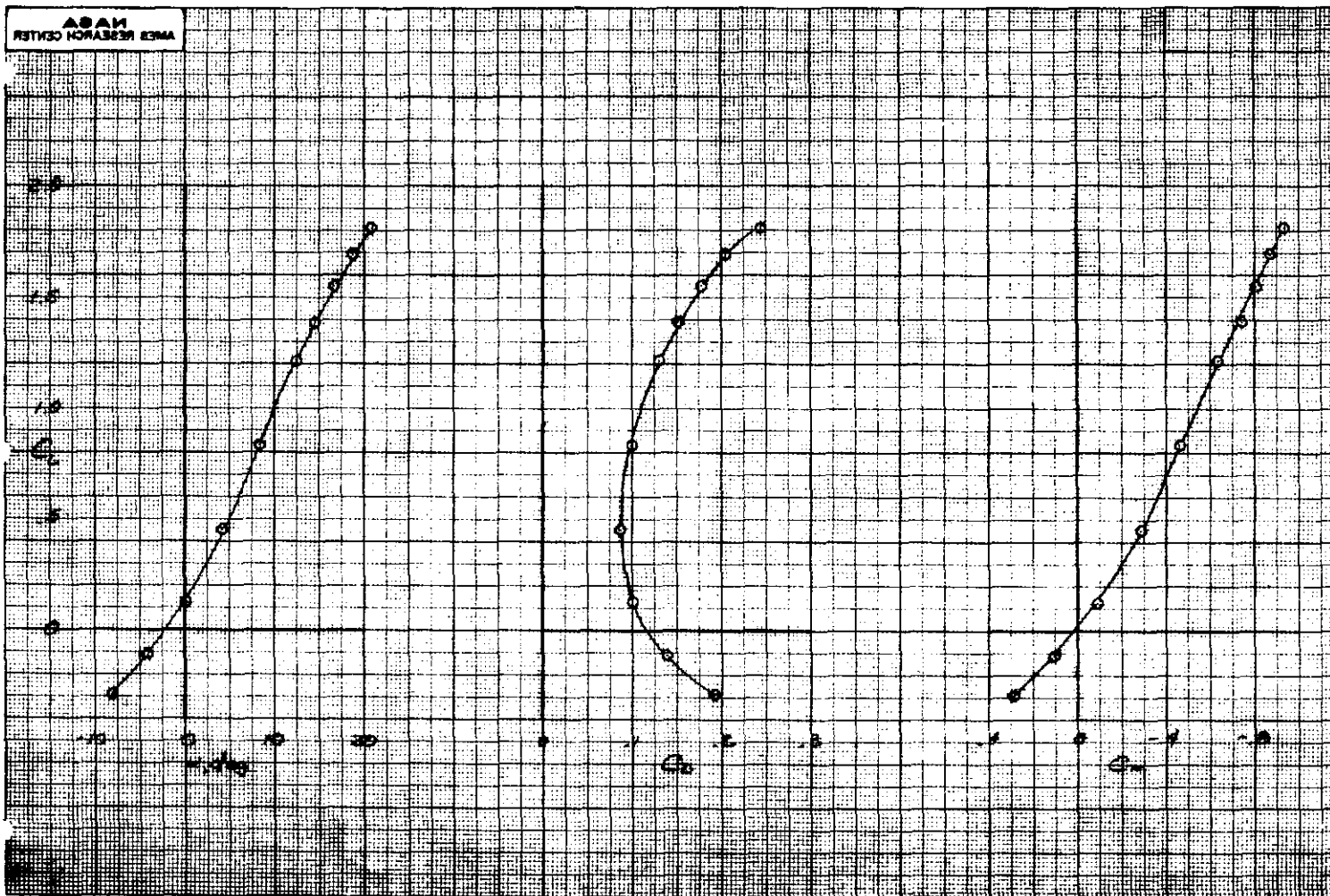


Figure 18. - Longitudinal characteristics of the model with the nose fairing and horizontal tail installed; $\delta_f = 0^\circ$, $\delta_c = 0^\circ$, $\delta_{s_2} = 60^\circ$, $i_t = 0^\circ$, tail slot off, $C_{j_I} = 0$.

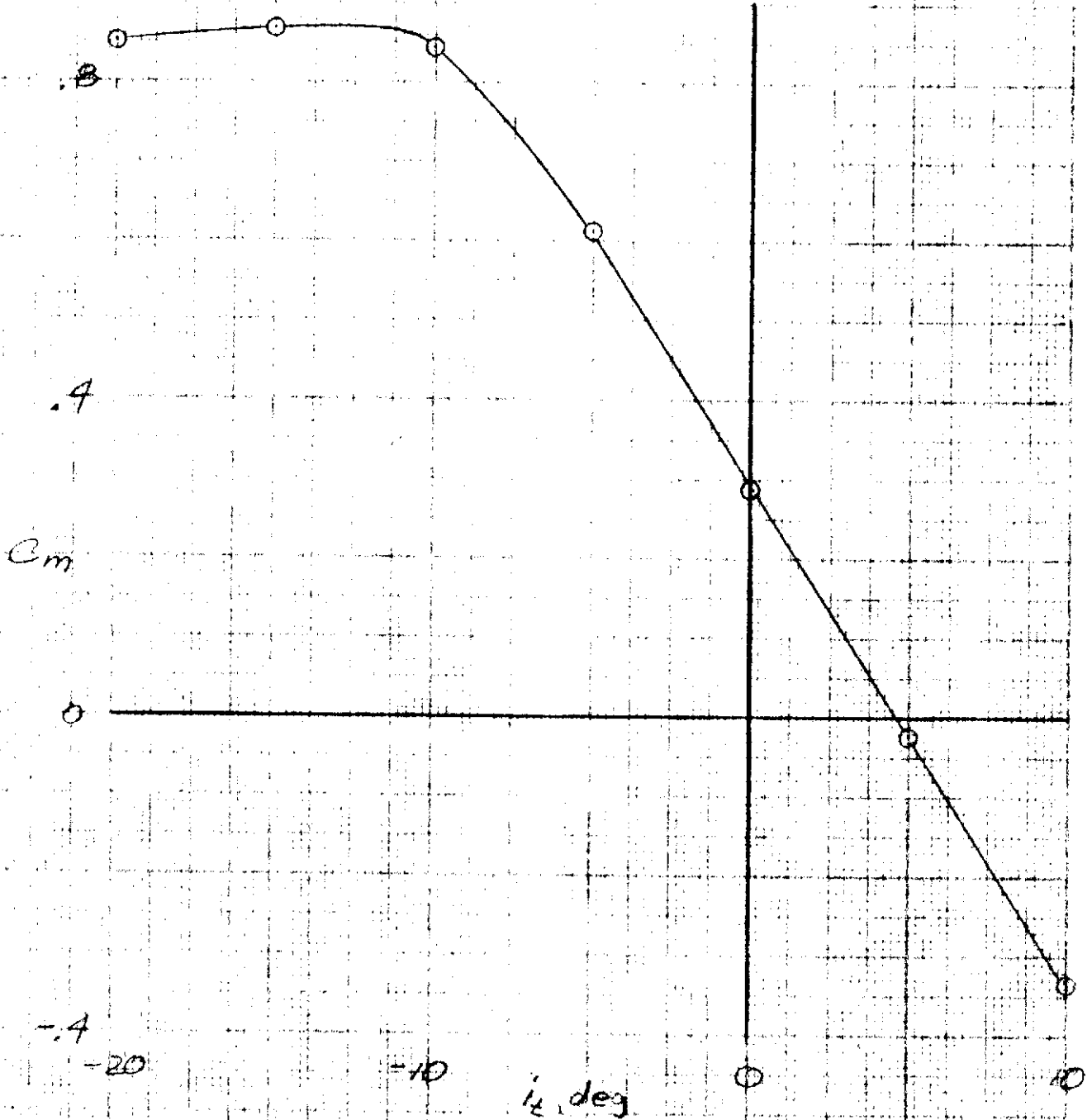
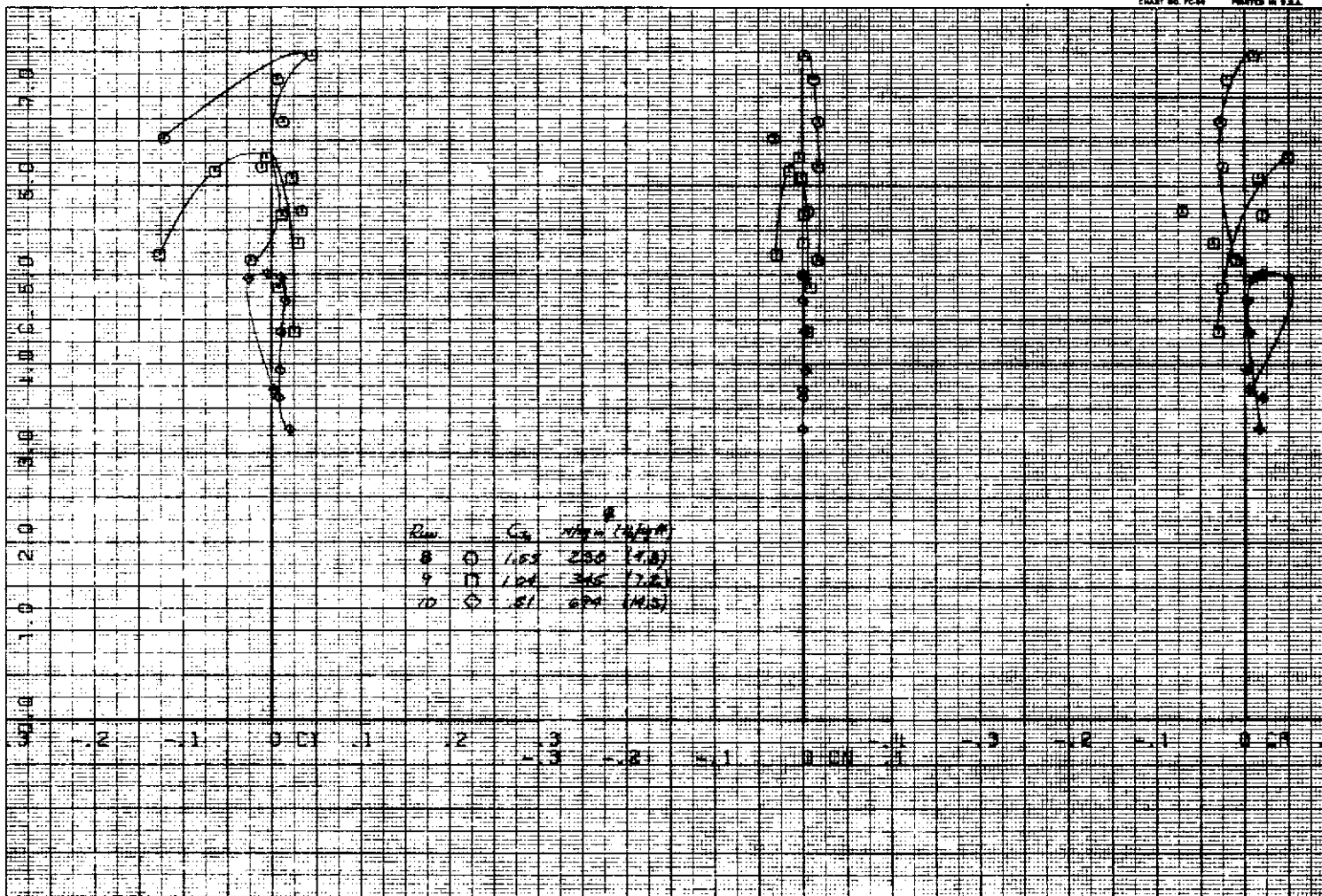


Figure 19. — The effect of tail incidence, i_t , on the model pitching moment, nose fairing and horizontal tail installed; $\delta_f = 0^\circ$, $\delta_c = 0^\circ$, $\delta_{s_2} = 60^\circ$, tail slot off.



(a) $\delta_c = 0^\circ$.

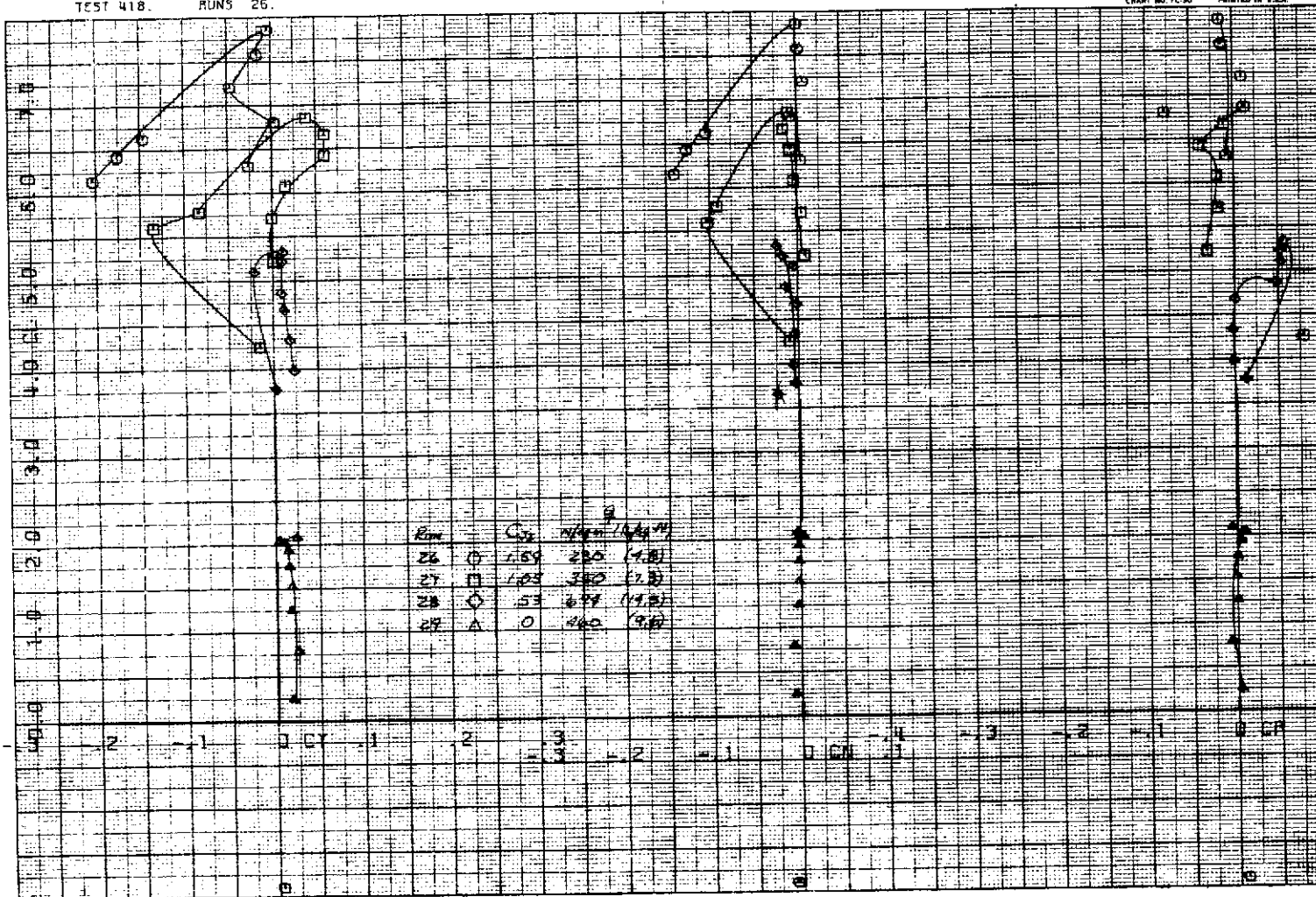
Figure 20. - The effect of C_{J_I} on the lateral-directional characteristics of the model; part-span flap, $\delta_f = 60^\circ$, $\delta_a = 30^\circ$, $\delta_{s2} = 60^\circ$, horizontal tail off, $C_{J_I} = 0$.

TEST 418. RUNS 26.

COMPLLOT

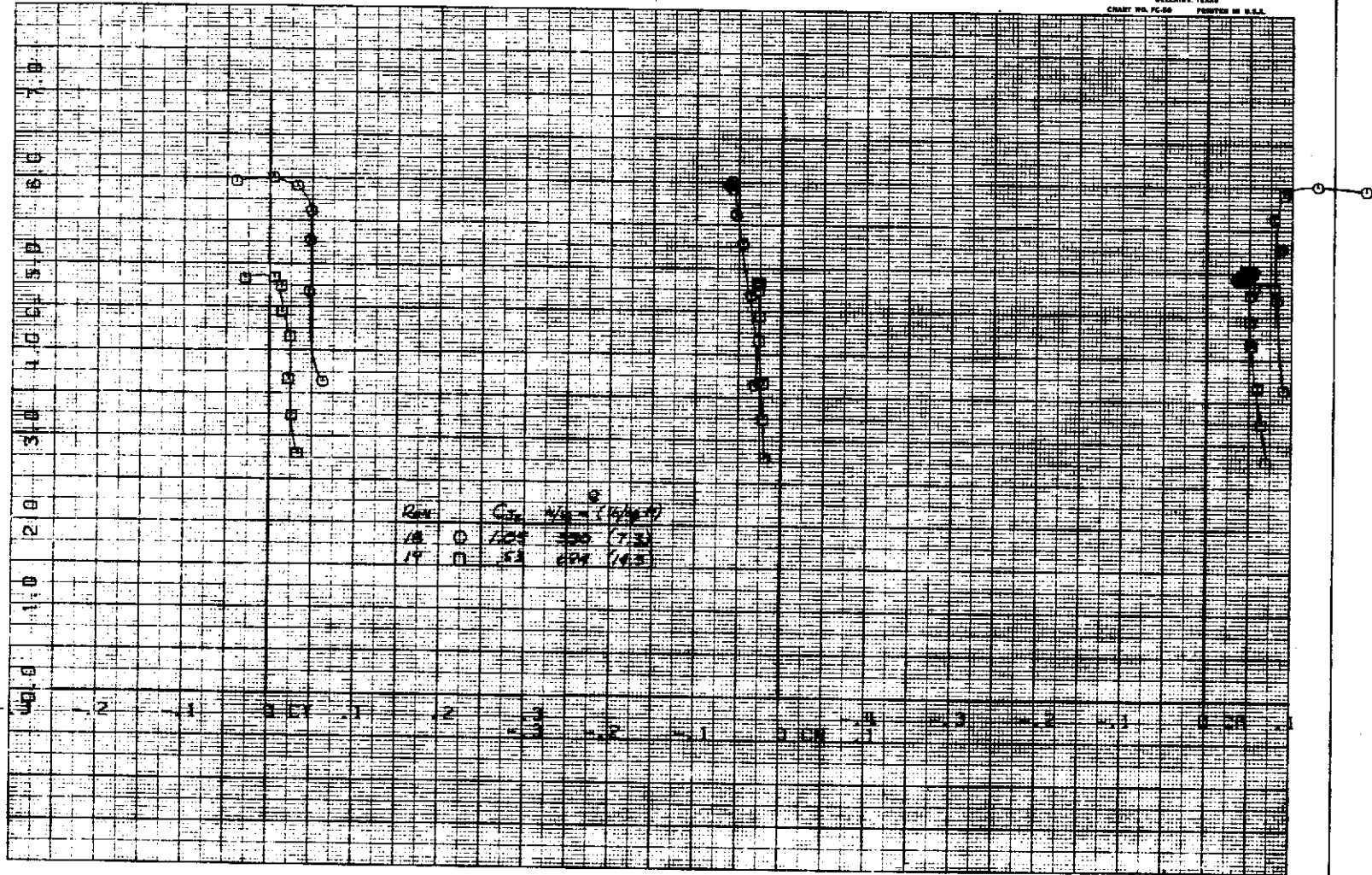
OMNIGRAPHIC

HOUSTON INSTRUMENT
DIVISION OF HONEYWELL
 BELLAIRE, TEXAS
 CHART NO. FC-80 PRINTED IN U.S.A.



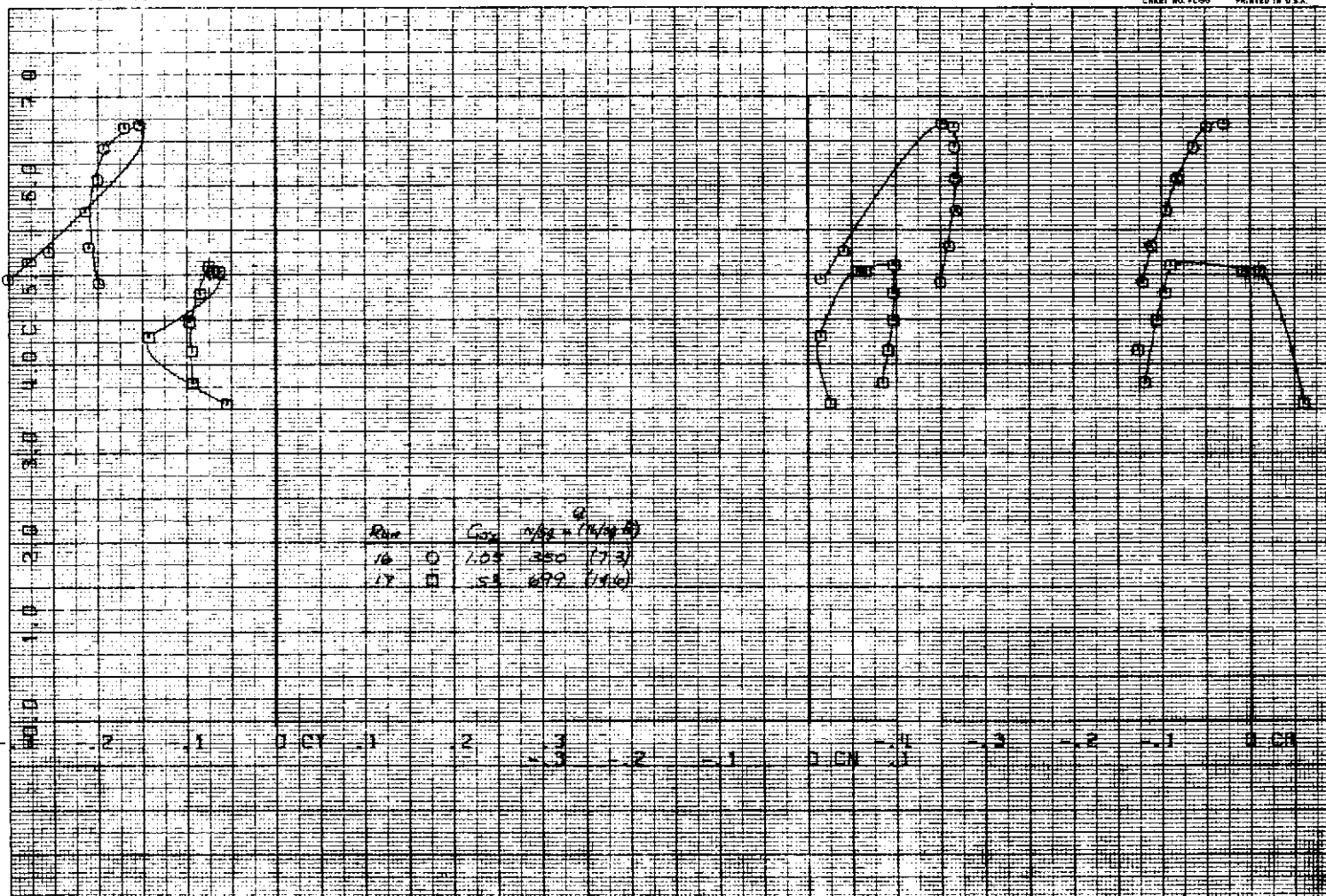
(b) $\delta_c = 20^\circ$.

Figure 20. -- Continued.



(c) $\delta_c = 0^\circ/-20^\circ$.

Figure 20. - Continued.



(d) $\delta_c = 0^\circ/40^\circ$.

Figure 20. - Concluded.

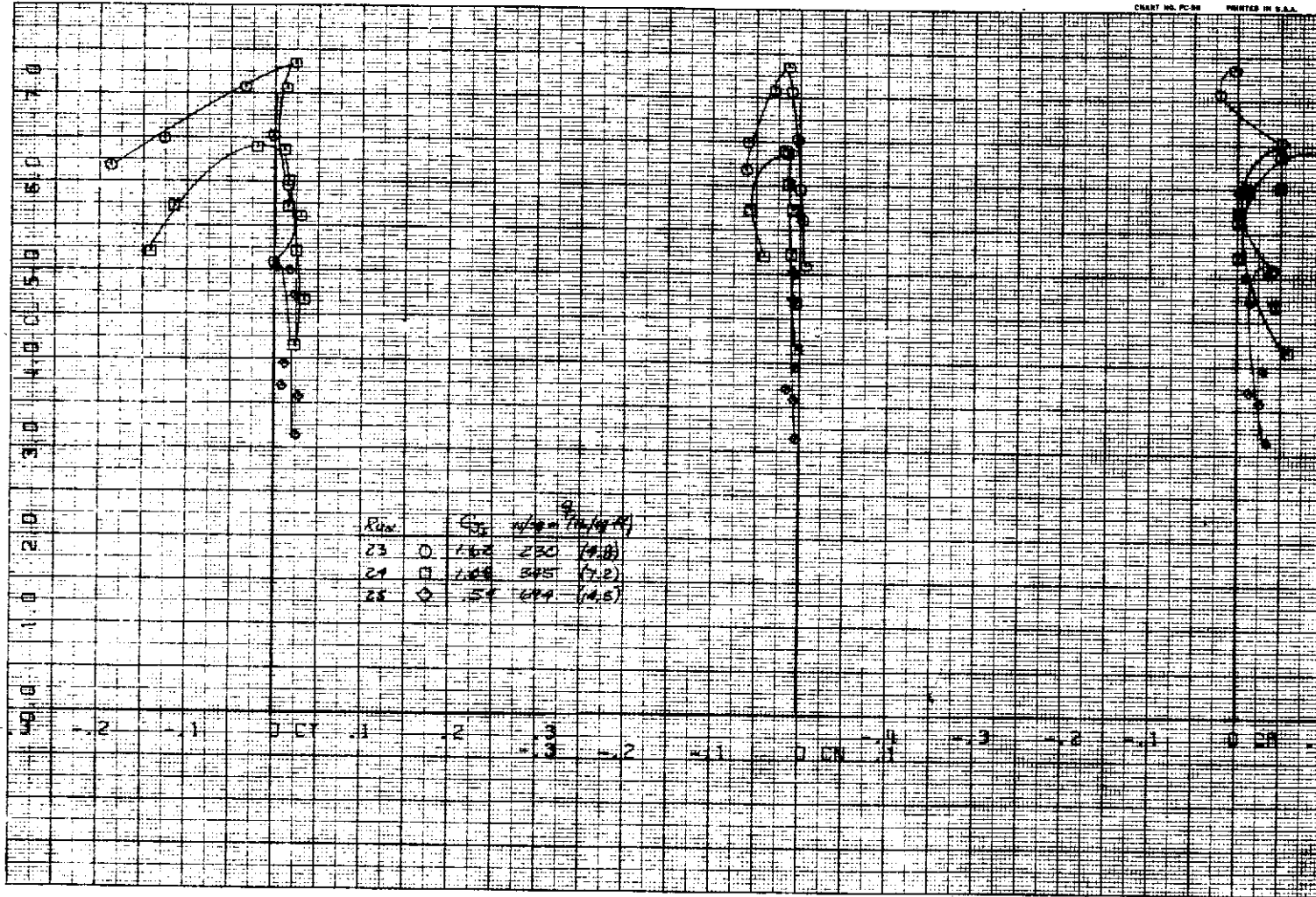
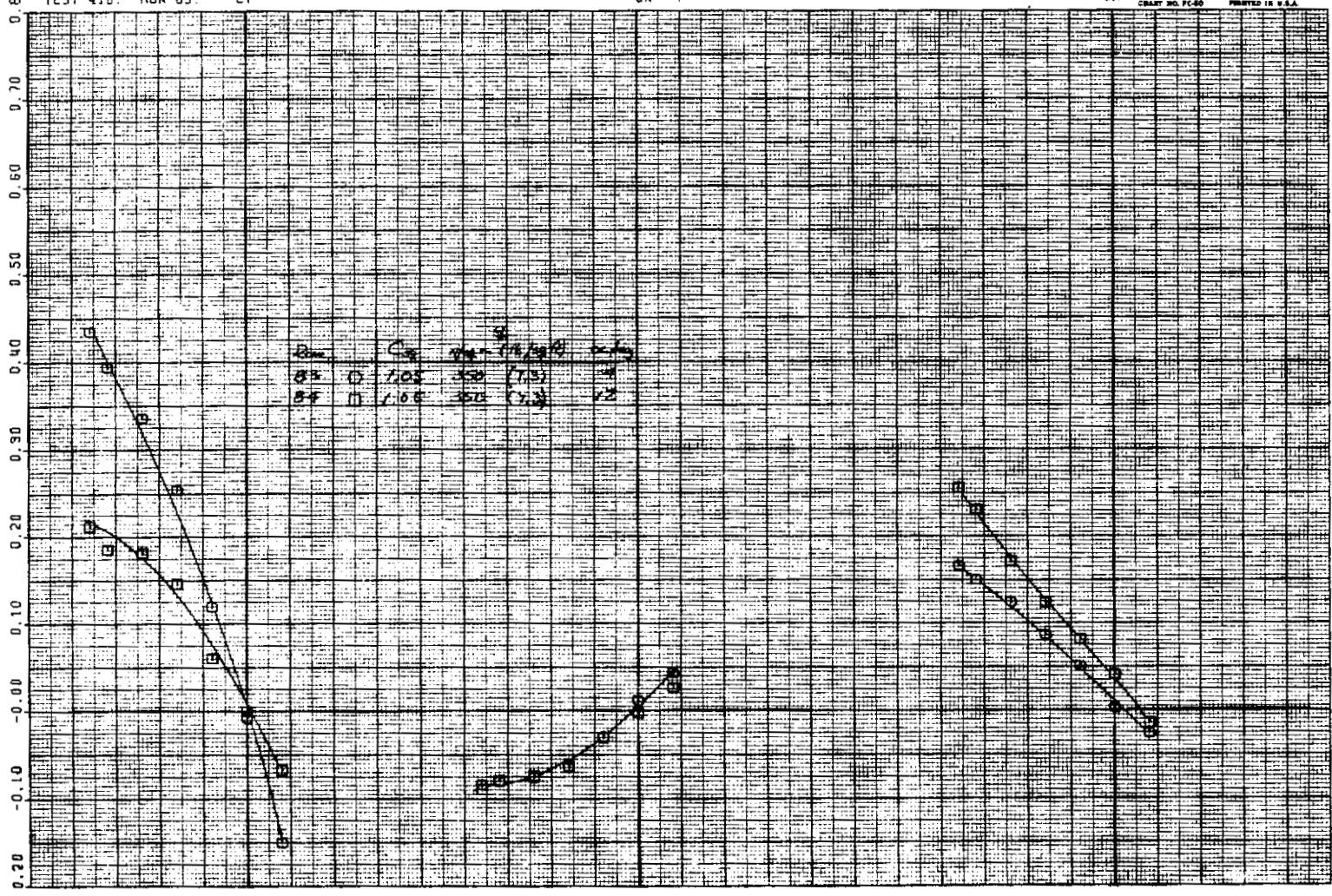
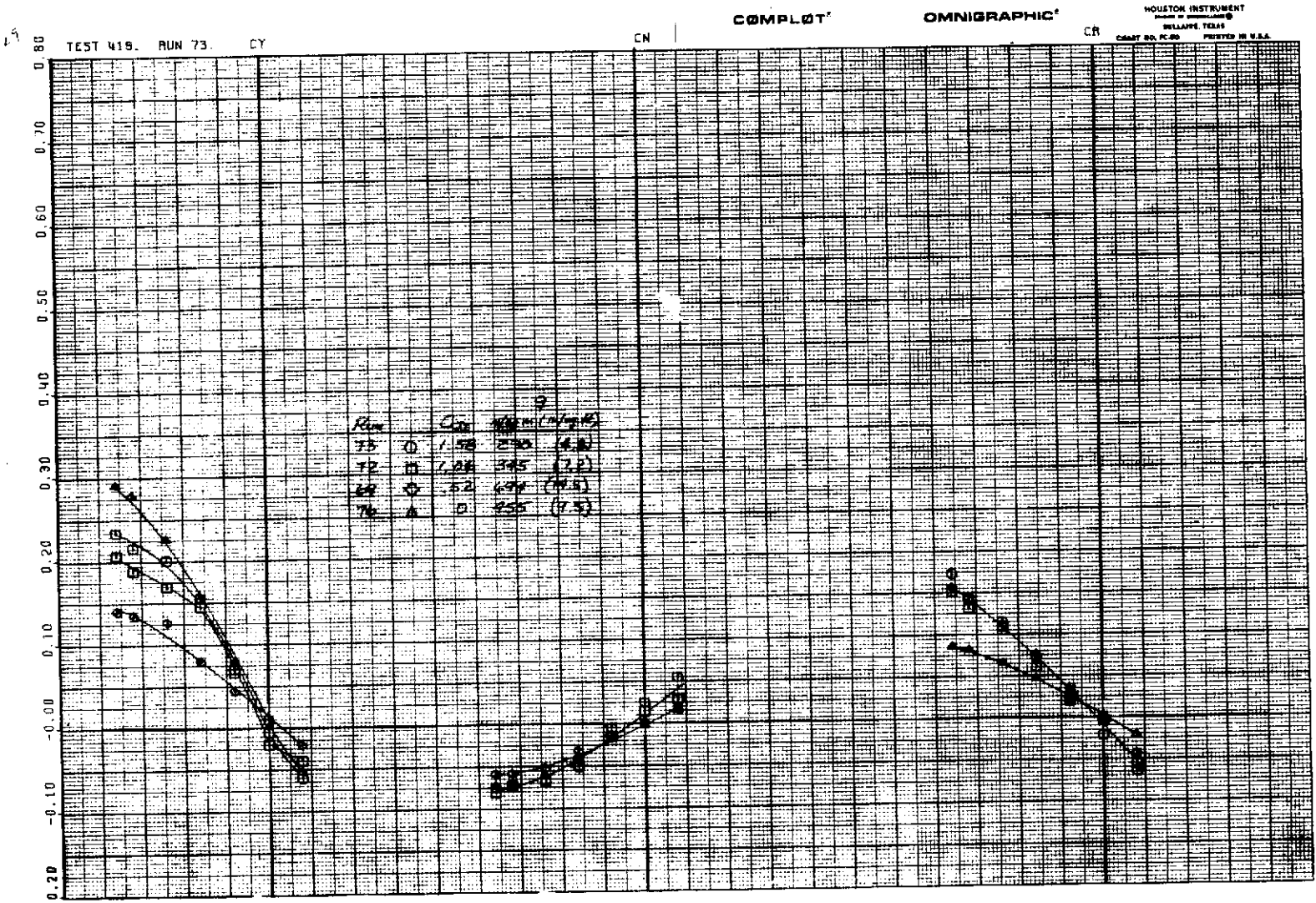


Figure 21. -- The effect of C_{J_I} on the lateral-directional characteristics of the model; part-span flap, $\delta_f = 60^\circ$, $\delta_a = 30^\circ/10^\circ$, $\delta_c = 0^\circ$, $\delta_{s_2} = 60^\circ$, horizontal tail off.



(a) Effect of α , $\delta_c = 0^\circ$.

Figure 22. - Lateral-directional characteristics of the model in sideslip; part-span flap, $\delta_f = 60^\circ$, $\delta_a = 30^\circ$, $\delta_{s2} = 60^\circ$, $i_t = 10^\circ$.



(b) Effect of C_{J_I} , $\alpha = 4^\circ$, $\delta_C = 20^\circ$.
Figure 22. - Continued.

Plot 40

TEST 418. RUN 74. CY

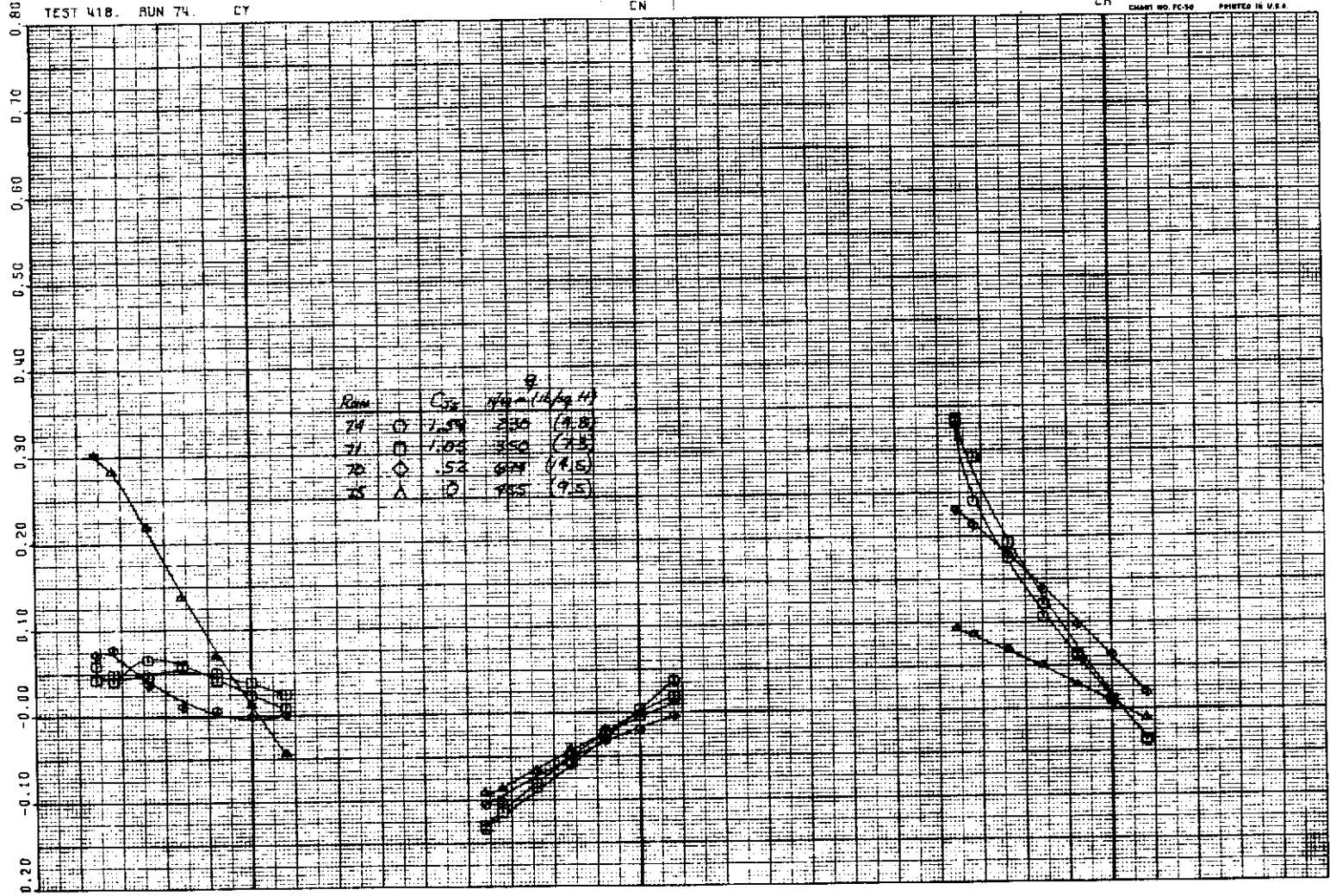
CN

COMPLLOT®

OMNIGRAPHIC®

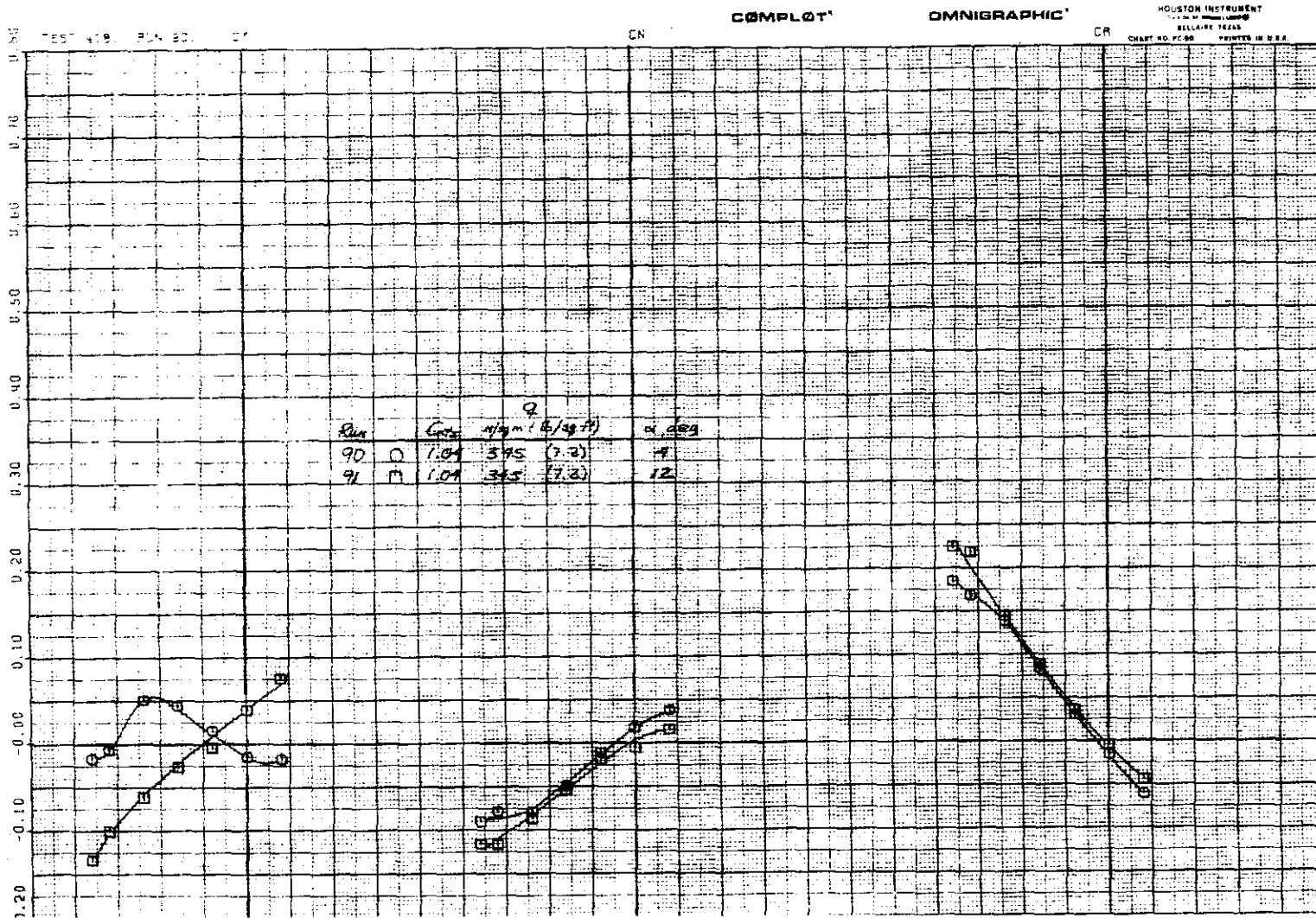
HOUSTON INSTRUMENT
DALLAS, TEXAS
CHART NO. FC-50 PRINTED IN U.S.A.

CR



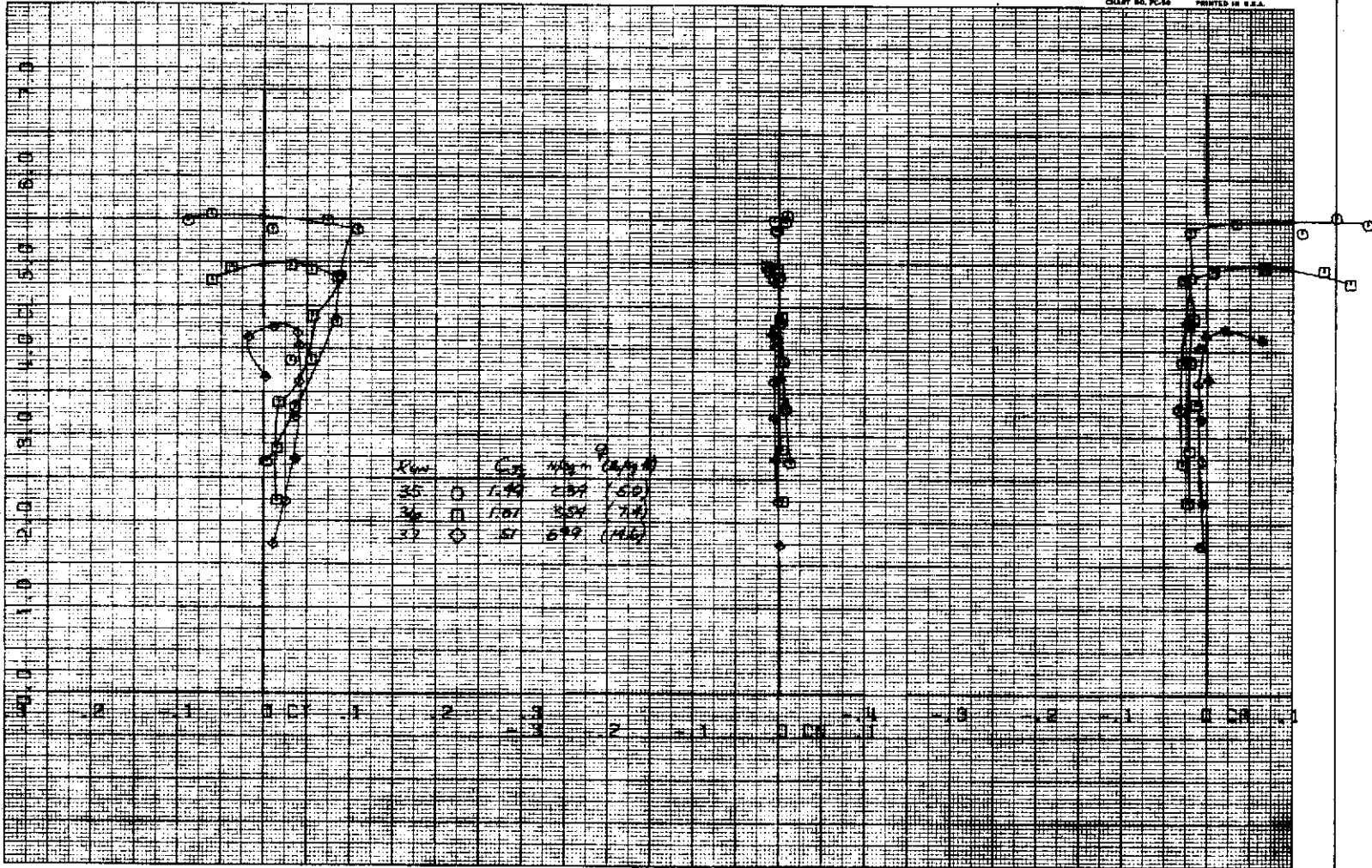
(c) Effect of C_{J_I} , $\alpha = 12^\circ$, $\delta_c = 20^\circ$.

Figure 22. - Continued.



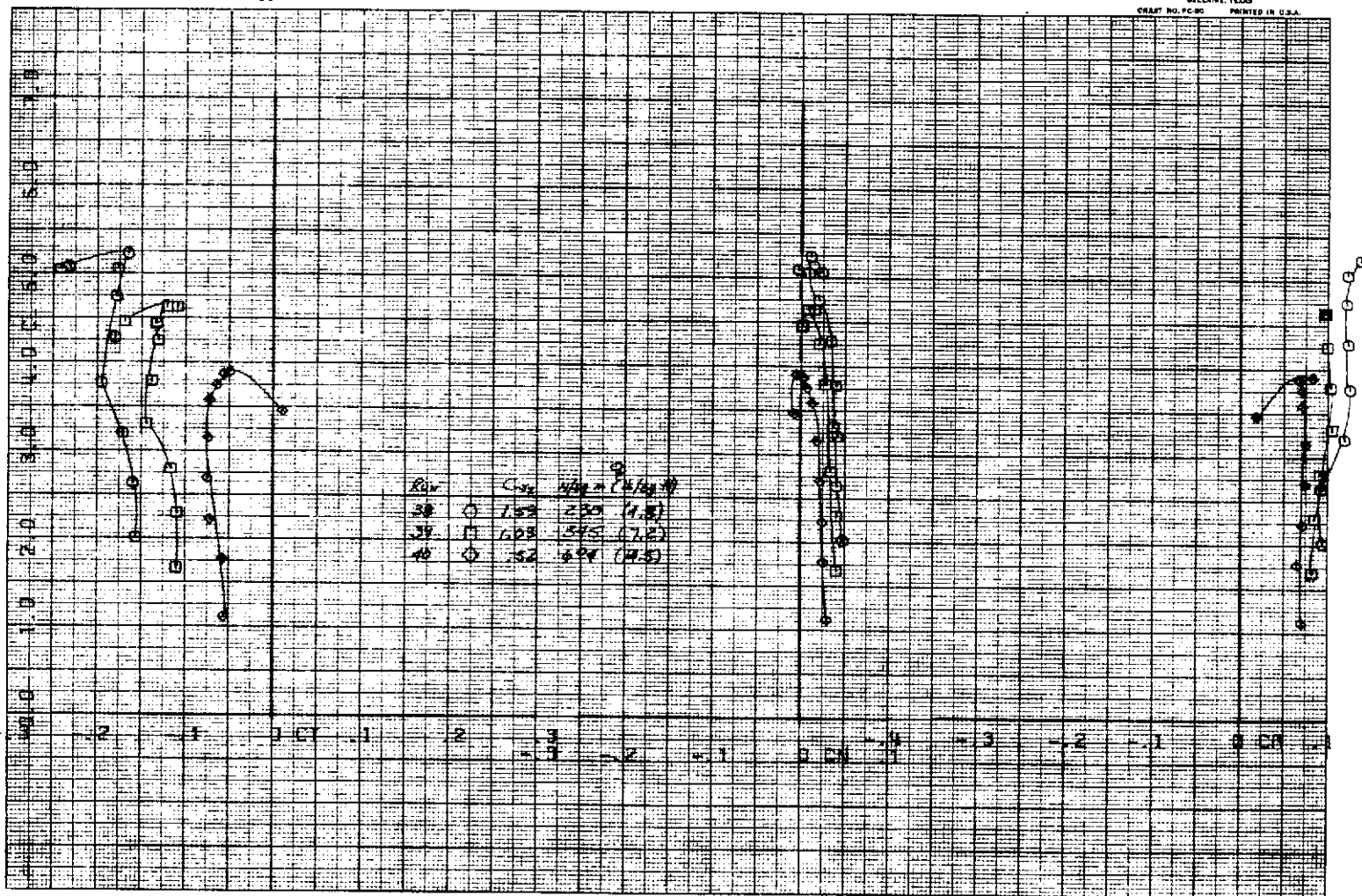
(d) Effect of α , $\delta_c = 40^\circ$.

Figure 22. - Concluded.



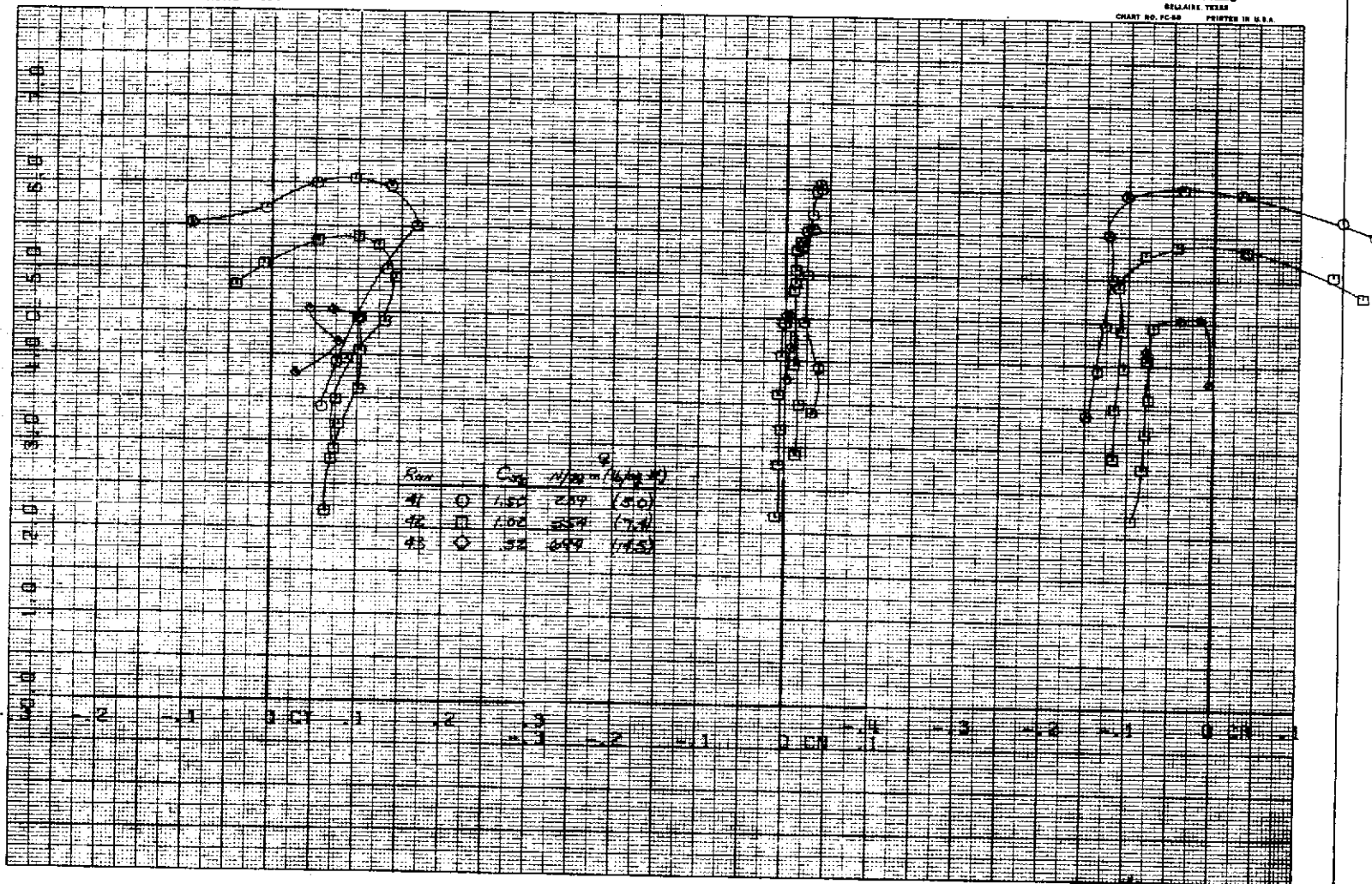
(a) $\delta_c = 0^\circ$.

Figure 23. - The effect of C_{J_I} on the lateral-direction characteristics of the model, part-span flap, $\delta_f = 30^\circ$, $\delta_a = 30^\circ$, $\delta_{s_2} = 60^\circ$, horizontal tail off.



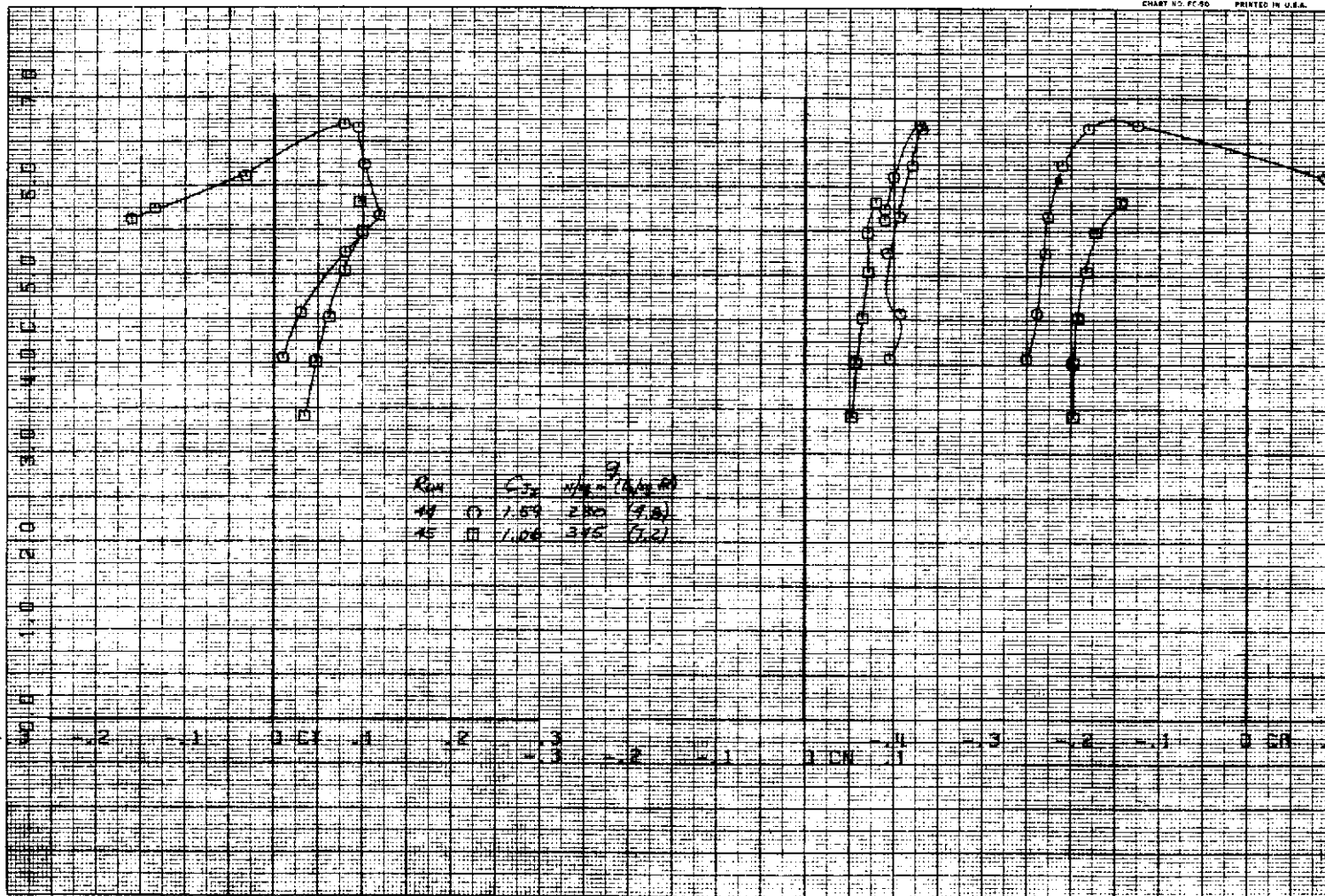
(b) $\delta_c = 0^\circ/-20^\circ$.

Figure 23. — Continued.



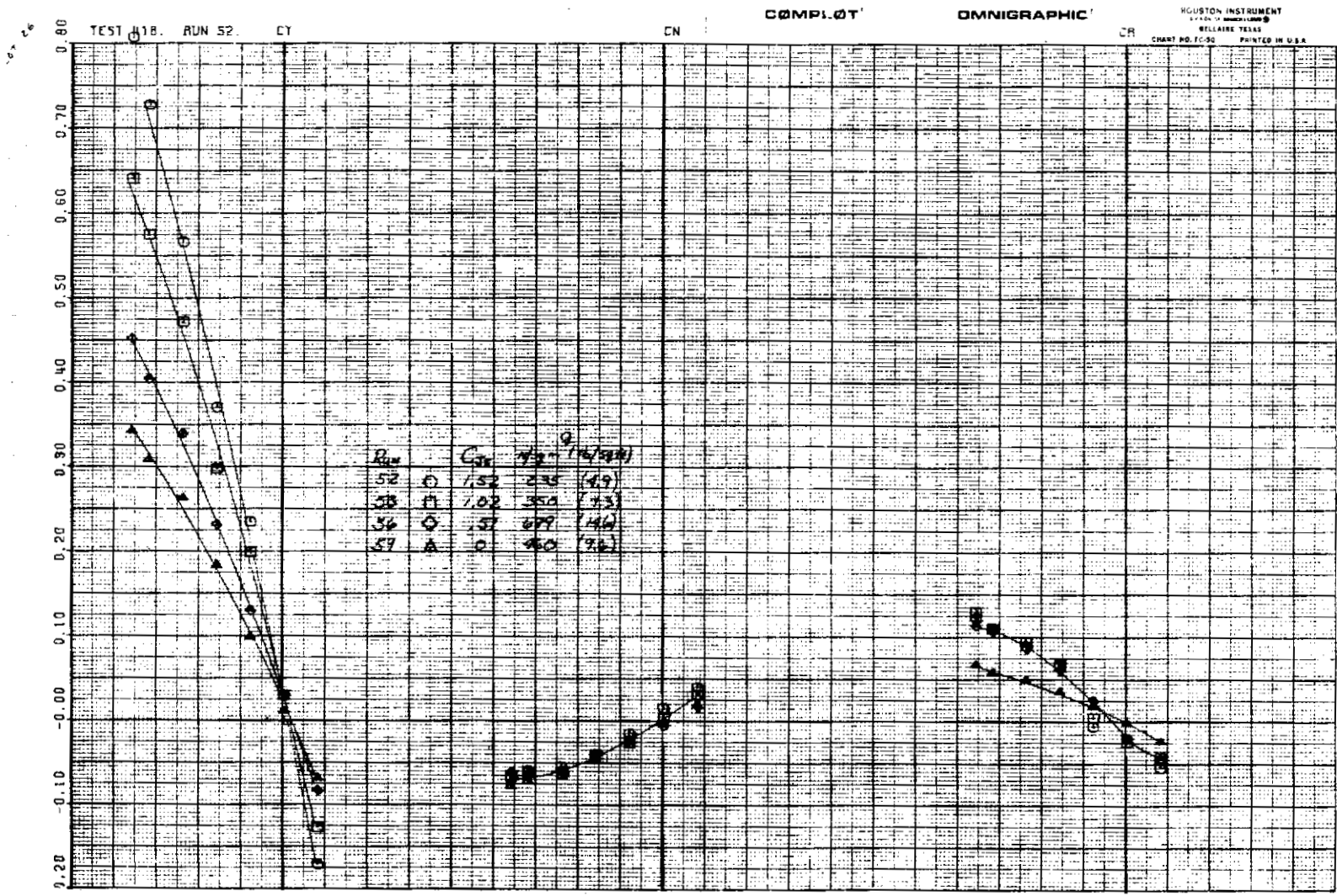
(c) $\delta_c = 0^\circ/20^\circ$.

Figure 23. - Continued.



(d) $\delta_c = 0^\circ/40^\circ$.

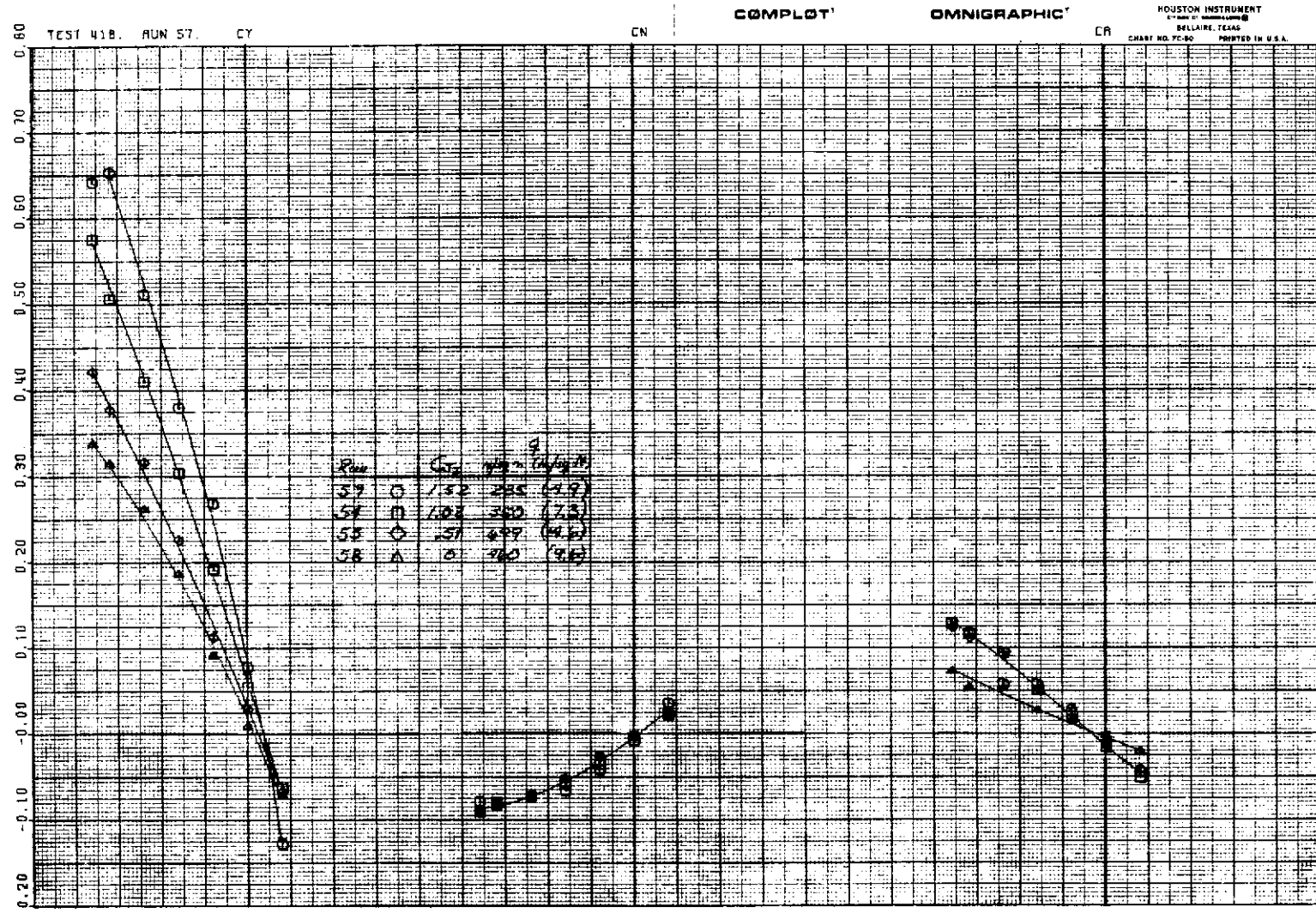
Figure 23. - Concluded.



(a) $\alpha = 4^\circ$.

Figure 24. — The effect of C_{J_I} on the lateral-directional characteristics of the model in sideslip; part-span flap, $\delta_f = 30^\circ$, $\delta_a = 30^\circ$, $\delta_c = 0^\circ$, $\delta_{s_2} = 60^\circ$, $i_t = -15^\circ$.

Page 27



(b) $\alpha = 12^\circ$.
Figure 24. - Concluded.